

# NOTE TO USERS

This reproduction is the best copy available.

**UMI**<sup>®</sup>



# **Analysis and implementation of a two-dimensional wavelength-time optical code-division multiple-access system**

Rhys Allan Adams

Photonic Systems Group  
Department of Electrical and Computer Engineering  
McGill University  
Montréal, Québec, Canada  
October 2004

A thesis submitted to the Faculty of Graduate Studies and Research in partial fulfillment of the requirements of the degree of Master of Engineering

© Rhys Allan Adams, 2004



Library and  
Archives Canada

Bibliothèque et  
Archives Canada

Published Heritage  
Branch

Direction du  
Patrimoine de l'édition

395 Wellington Street  
Ottawa ON K1A 0N4  
Canada

395, rue Wellington  
Ottawa ON K1A 0N4  
Canada

*Your file* *Votre référence*  
*ISBN: 0-494-12572-1*  
*Our file* *Notre référence*  
*ISBN: 0-494-12572-1*

#### NOTICE:

The author has granted a non-exclusive license allowing Library and Archives Canada to reproduce, publish, archive, preserve, conserve, communicate to the public by telecommunication or on the Internet, loan, distribute and sell theses worldwide, for commercial or non-commercial purposes, in microform, paper, electronic and/or any other formats.

The author retains copyright ownership and moral rights in this thesis. Neither the thesis nor substantial extracts from it may be printed or otherwise reproduced without the author's permission.

#### AVIS:

L'auteur a accordé une licence non exclusive permettant à la Bibliothèque et Archives Canada de reproduire, publier, archiver, sauvegarder, conserver, transmettre au public par télécommunication ou par l'Internet, prêter, distribuer et vendre des thèses partout dans le monde, à des fins commerciales ou autres, sur support microforme, papier, électronique et/ou autres formats.

L'auteur conserve la propriété du droit d'auteur et des droits moraux qui protègent cette thèse. Ni la thèse ni des extraits substantiels de celle-ci ne doivent être imprimés ou autrement reproduits sans son autorisation.

---

In compliance with the Canadian Privacy Act some supporting forms may have been removed from this thesis.

Conformément à la loi canadienne sur la protection de la vie privée, quelques formulaires secondaires ont été enlevés de cette thèse.

While these forms may be included in the document page count, their removal does not represent any loss of content from the thesis.

Bien que ces formulaires aient inclus dans la pagination, il n'y aura aucun contenu manquant.

  
**Canada**

## ABSTRACT

The development and growth of new communication services and emerging applications requires high-performance access networks capable of providing high-bandwidth interconnections to end-users. In recent years, optical code-division multiple-access (OCDMA) has been proposed as a means for providing flexible access to high-bandwidth applications and offering different levels of quality of service. This thesis explores the impact of encoder/decoder mismatch on system performance for 2 dimensional wavelength-time (2D  $\lambda$ -t) OCDMA and the implementation of a multi-user 2D  $\lambda$ -t OCDMA direct detection demonstrator system. Our analysis and experimental demonstrations are based on depth-first search codes (DFSCs) which have previously been shown to be attractive in OCDMA applications. We have developed an OCDMA system simulation model that quantifies the BER performance as wavelength and/or time misalignments (which cause mismatch in the encoder/decoder) increase. Furthermore, we have succeeded in encoding and decoding DFSCs as well as in demonstrating a 4-user system which has been implemented using standard commercially available off-the-shelf optical components.

## SOMMAIRE

Le développement et la croissance de nouveaux services de communication et d'applications émergentes exigent des réseaux d'accès de qualité supérieure capables de fournir des connexions de grande largeur de bande aux utilisateurs finaux. Récemment, le CDMA (accès multiples à répartition des codes) optique a été proposé comme moyen pour fournir un accès flexible aux applications de grande largeur de bande et offrir divers niveaux de qualité de service. Cette thèse explore les impacts d'erreur d'assortiment de encodeur/décodeur sur la performance de systèmes de CDMA optique bidimensionnel basés sur la longueur d'onde et le temps (2D  $\lambda$ -t), et l'implémentation d'un système démonstrateur CDMA optique 2D  $\lambda$ -t à utilisateurs multiples basé sur les codes de recherche en profondeur (DFSCs). Il fut précédemment démontré que ces codes puissent être attrayants pour les applications de CDMA optique. Nous avons créé un modèle de simulation d'un système CDMA optique qui prend en considération les déviations de longueur d'onde et/ou de temps et nous quantifions la performance du système en relation avec l'augmentation de ces déviations. De plus, nous avons réussi à encoder et décoder les codes DFSCs et nous sommes arrivés à implémenter un système à 4-utilisateurs à l'aide de composants optiques disponibles commercialement.

## ACKNOWLEDGEMENTS / REMERCIEMENTS

The past years being a student at McGill University, and specifically being a member of the Photonic Systems Group, would not have been as enjoyable and successful without the help, encouragement and presence of many. It is with great pleasure that I thank the following people for this rewarding experience:

First I would like to thank my supervisor, Professor Lawrence Chen. Thank you Lawrence for all your guidance throughout my M.Eng., for your support, for all early morning and late afternoon discussions about everything possible, for your sense of humor, and your friendship. The last two years were a thrill and it was a pleasure working with you.

Many thanks are deserved for those who contributed to the OCDMA project. Merci à Julien Faucher pour ton aide, surtout dans le laboratoire, et pour m'expliquer les subtilités du CDR. Thank you Luay Thomas, Reuven Gordon, Paul Kamel, Noha Kheder and Professor Dave Plant for your lab help, simulations and constructive ideas.

I want to extend my thanks to the many people I worked with since being a summer student with PSG. Your help with course projects, lab setups, explanations, brainstorming, and simple chats about photonics, politics, sports, music and the meaning of life are appreciated! Merci à Frédéric Lacroix et Michael Ayliffe pour m'avoir introduit à l'optique et la photonique en été 2000. Ce fut un grand plaisir de travailler et d'apprendre avec vous deux. Merci aussi à / Many thanks to Frédéric Thomas Dupuis, Eric Bisailon, Madeleine Mony, Michaël Ménard, Jean-Philippe Thibodeau, Cristina Marinescu, Patrick Sabourin, Samuel Brien, Marc Châteauneuf, Dominik Pudo, Alan Li, Roberto Rotili, and Professor Andrew Kirk. Special thanks to the guru Chris Rolston et le lab manger Nicolas Bélanger. Thanks for all your help... I (and most of us here) would be loss without you both.

Thanks to the ITF technical staff for allowing me to use their resources in performing length measurements on all power splitters/combiners. Special thanks to Pierre Poirier who assisted me with these measurements.

Merci au Professeure Sophie LaRochelle et à ses étudiants du Centre d'Optique Photonique et Laser (COPL) de l'Université Laval pour leur aide avec les mesures des WDMs et des lignes de délais optique.

Thanks to all my friends and coworkers at ONI Systems. I learned so much and had a fulfilling experience during my summer 2001 internship.

In addition to the names already mentioned, I would like to thank all my friends that have made these years in Montréal so enjoyable. Merci à tous mes amis qui ont rendu mes années à Montréal si plaisantes: Marco Fournier, Justin Furlotte, Martin Kraënzell, Xavier Jaques Bédard, Maxime Johnson, Maxime Fortin, Matt Beutel, Karl Lerbscher, Réjean et France, all my hockey buddies, IoP and GG.

Merci à ma famille, surtout à mes parents, qui m'ont soutenu et encouragé, à l'intérieur et aussi à l'extérieur du milieu universitaire, pendant toute ma vie. My accomplishments would not have been possible without you two.

Finalement, merci à ma meilleure amie, Annie. Merci pour tout ton amour, encouragement et support pendant les six dernières années.

Ce travail a été soutenu financièrement par *le Fonds québécois de la recherche sur la nature et les technologies*.

# TABLE OF CONTENTS

<b>1. INTRODUCTION .....</b>	<b>1</b>
1.1 MOTIVATION .....	1
1.2 THESIS OBJECTIVES AND CONTRIBUTIONS.....	3
1.3 THESIS OUTLINE .....	5
<b>2. OVERVIEW OF OCDMA .....</b>	<b>6</b>
2.1 FUNDAMENTALS OF OCDMA.....	6
2.2 HYBRID ENCODING APPROACHES TO OCDMA .....	8
2.3 2D WAVELENGTH-TIME DEPTH-FIRST SEARCH CODES .....	11
2.4 CHALLENGES IN OCDMA .....	14
<b>3. EFFECTS OF ENCODER/DECODER MISMATCH ON BER PERFORMANCE .....</b>	<b>16</b>
3.1 INTRODUCTION .....	16
3.2 DESCRIPTION OF WAVELENGTH AND TIME CHIP MISALIGNMENTS .....	16
3.3 SIMULATION PROCEDURE.....	18
3.4 RESULTS .....	20
3.4.1 Wavelength misalignment.....	20
3.4.2 Time chip misalignment.....	26
3.4.3 Wavelength and time chip misalignments.....	28
3.5 SUMMARY.....	31
<b>4. DEMONSTRATION OF A 4-USER OCDMA SYSTEM.....</b>	<b>32</b>
4.1 INTRODUCTION .....	32
4.2 IMPLEMENTATION OF THE 4-USER OCDMA SYSTEM.....	32
4.2.1 Description of the demonstration setup.....	32
4.2.2 Building and characterization of encoders and decoder.....	36
4.2.3 Testing of encoders and decoder .....	39
4.2.3.1 Desired encoder and decoder.....	39
4.2.3.2 User 2 encoder .....	44

4.2.3.3 User 3 encoder .....	48
4.2.3.4 User 4 encoder .....	51
4.3 TESTING OF FULL SYSTEM.....	54
4.3.1 Sending a “1” bit and an arbitrary bit pattern.....	54
4.3.2 Effects of chromatic dispersion .....	58
4.3.3 Eye diagrams and BER measurements.....	60
4.3.4 Clock and data recovery .....	64
4.4 SUMMARY.....	67
<b>5. CONCLUSION .....</b>	<b>69</b>
5.1 SUMMARY AND CONCLUSIONS .....	69
5.2 FUTURE DIRECTIONS .....	70
<b>6. REFERENCES .....</b>	<b>73</b>
<b>APPENDIX A: RESULTS OF ENCODER/DECODER MISMATCH SIMULATIONS.....</b>	<b>82</b>
<b>APPENDIX B: ENCODERS AND DECODER MEASUREMENTS .....</b>	<b>90</b>
<b>APPENDIX C: PICTURES OF THE OCDMA SETUP.....</b>	<b>91</b>
<b>APPENDIX D: PUBLICATIONS ACCEPTED FOR CONFERENCES .....</b>	<b>94</b>

## LIST OF FIGURES

Fig. 1.1	WDMA, TDMA, and CDMA .....	2
Fig. 1.2	A local access network employing CDMA [3] .....	2
Fig. 2.1	Schematic of an OCDMA system .....	6
Fig. 2.2	Wavelength-view and time-view of a 2D $\lambda$ -t code.....	9
Fig. 2.3	DWDM (de)multiplexer and optical delay line based 2D $\lambda$ -t OCDMA encoder.	10
Fig. 2.4	Fiber Bragg grating based 2D $\lambda$ -t OCDMA encoder .....	11
Fig. 2.5	BER as a function of the number of simultaneous active users for (a) $n=16$ , $w=6$ , and $m$ as a parameter; (b) $m=16$ , $w=6$ , and $n$ as a parameter; (c) $m=32$ , $n=16$ , and $w$ as a parameter [4].....	13
Fig. 2.6	Comparing the BER as a function of the number of simultaneous active users between different 2D codes [4] .....	14
Fig. 3.1	Example of a code using 6 wavelengths, 6 time chips, and weight 6; (a) ideal situation; pulse at position $(\lambda_2, t_4)$ suffers (b) a wavelength misalignment, (c) a time chip misalignment, (d) both a wavelength and time chip misalignment.....	17
Fig. 3.2	Flow chart of simulation methodology .....	19
Fig. 3.3	BER histogram of a 12 user, (32, 16, 6) DFSCs, “IPP” situation with only a wavelength misalignment of variance 0.05 .....	20
Fig. 3.4	(a) Average BER and (b) standard deviation of BER as a function of the variance of the Gaussian distribution for the wavelength misalignment; 12 simultaneous users with (32, 16, 6) DFSCs .....	21
Fig. 3.5	Average BER as a function of the variance of the Gaussian distribution for the wavelength misalignment; 8 simultaneous users with (32, 16, 6) DFSCs .....	23
Fig. 3.6	Average BER as a function of the variance of the Gaussian distribution for the wavelength misalignment; 12 simultaneous users with (16, 32, 6) DFSCs .....	24
Fig. 3.7	BER as a function of the number of simultaneous users with (32, 16, 6) DFSCs; variance of the Gaussian distribution for the wavelength misalignment is 0.1 .....	25
Fig. 3.8	Average BER as a function of the variance of the Gaussian distribution for the time chip misalignment; 12 simultaneous users with (32, 16, 6) DFSCs.....	27

Fig. 3.9 BER as a function of the number of simultaneous users with (32, 16, 6) DFSCs; variance of the Gaussian distribution for the time chip misalignment is 0.1 .....	28
Fig. 3.10 Contour plot of the average BER as a function of the variance of the Gaussian distributions of both the wavelength and time chip misalignments for case “IPP”; 12 simultaneous users with (32, 16, 6) DFSCs.....	29
Fig. 3.11 Contour plot of the average BER as a function of the variance of the Gaussian distributions of both the wavelength and time chip misalignments for case “PPI”; 12 simultaneous users with (32, 16, 6) DFSCs.....	30
Fig. 4.1 The four codes used in the demonstration setup .....	33
Fig. 4.2 Block diagram of the 4-user system .....	33
Fig. 4.3 Block diagram of an encoder (e.g. desired encoder).....	34
Fig. 4.4 (a) Desired; (b) User 2; (c) User 3; (d) User 4 codes before and after decoding .	35
Fig. 4.5 Components used in building each encoder and decoder .....	37
Fig. 4.6 Picture of encoders and decoder.....	38
Fig. 4.7 Time characteristics of an un-coded input pulse .....	39
Fig. 4.8 Wavelength characteristics of desired encoder and decoder.....	40
Fig. 4.9 Time characteristics of (a) the desired user, and (b) the decoder.....	41
Fig. 4.10 The desired encoded code with (a) $\lambda_1$ ; (b) $\lambda_3$ ; (c) $\lambda_6$ ; (d) $\lambda_7$ missing .....	42
Fig. 4.11 (a) Wavelength characteristics and (b) time characteristics of the desired decoded signal .....	43
Fig. 4.12 (a) Wavelength characteristics and (b) time characteristics of user 2.....	45
Fig. 4.13 User 2 encoded code with (a) $\lambda_2$ ; (b) $\lambda_2$ and $\lambda_6$ ; (c) $\lambda_3$ ; (d) $\lambda_4$ missing .....	46
Fig. 4.14 (a) Wavelength characteristics and (b) time characteristics of the user 2 decoded signal.....	47
Fig. 4.15 (a) Wavelength characteristics and (b) time characteristics of user 3.....	48
Fig. 4.16 User 3 encoded code with (a) $\lambda_3$ ; (b) $\lambda_3$ and $\lambda_5$ missing .....	49
Fig. 4.17 (a) Wavelength characteristics and (b) time characteristics of the user 3 decoded signal.....	50
Fig. 4.18 (a) Wavelength characteristics and (b) time characteristics of user 4.....	51
Fig. 4.19 User 4 encoded code with (a) $\lambda_3$ ; (b) $\lambda_5$ ; (c) $\lambda_7$ ; (d) $\lambda_8$ missing .....	52

Fig. 4.20 (a) Wavelength characteristics and (b) time characteristics of the user 4 decoded signal.....53

Fig. 4.21 Wavelength characteristics of all codes multiplexed together (top) before and (bottom) after the decoder .....55

Fig. 4.22 Time characteristics of all codes multiplexed together (a) before and (b) after the decoder for a “1” bit .....56

Fig. 4.23 Time characteristics of all codes multiplexed together (a) before and (b) after the decoder for a repeated “11010011” bit pattern.....57

Fig. 4.24 Time characteristics of all codes multiplexed together after propagating through 7.4 km of single-mode fiber (a) before and (b) after the decoder for a “1” bit .....59

Fig. 4.25 Eye diagram of decoded waveform of: (a) only the desired signal; (b) the desired signal and user 2; (c) the desired signal and user 3; (d) the desired signal and user 4; and (e) all users.....61

Fig. 4.26 BER as a function of the average optical power launched in the O/E converter; from left to right: user 1 alone; users 1 and 2; users 1 and 4; users 1 and 3; all users .....64

Fig. 4.27 CDR signals when only desired user is present .....65

Fig. 4.28 Eye diagram of CDR signals (a) desired user only; (b) desired user and user 3; (c) desired user and users 3 and 4.....66

## LIST OF TABLES

Table 4.1 Demonstration setup parameters .....	33
Table A.1 Average BER and the standard deviation for simulating wavelength misalignment; (32, 16, 6) DFSCs; K = 8 active users .....	82
Table A.2 Average BER and the standard deviation for simulating wavelength misalignment; (32, 16, 6) DFSCs; K = 12 active users .....	83
Table A.3 Average BER and the standard deviation for simulating wavelength misalignment; (16, 32, 6) DFSCs; K = 8 active users .....	84
Table A.4 Average BER and the standard deviation for simulating wavelength misalignment; (16, 32, 6) DFSCs; K = 12 active users .....	85
Table A.5 Average BER and the standard deviation for simulating time misalignment; (32, 16, 6) DFSCs; K = 8 active users .....	86
Table A.6 Average BER and the standard deviation for simulating time misalignment; (32, 16, 6) DFSCs; K = 12 active users .....	87
Table A.7 Average BER and the standard deviation for simulating time misalignment; (16, 32, 6) DFSCs; K = 8 active users .....	88
Table A.8 Average BER and the standard deviation for simulating time misalignment; (16, 32, 6) DFSCs; K = 12 active users .....	89
Table A.9 Insertion loss, OPL and ODL measurements for all encoders and decoder .....	90

# 1. Introduction

## 1.1 Motivation

Long gone are the days of fire signal based optical communications. Albeit clever for eighth century B.C., it is cumbersome for transmitting voice, images, music and video. These days we depend on more sophisticated technologies to satisfy our data fix. Vast improvements in computing and telecommunications have enabled us to exchange information worldwide with a simple “click”. Terabits of data flow through low-cost long-haul fiber optic communication systems each second, yet non-fiber optic based communication systems limit the data throughput of local access networks. Wanting to accommodate growth in bandwidth demand, we must ask the following question, “How can we decongest the local area domain?” Given the aspiration to curtail optical-to-electrical and electrical-to-optical conversions, the ideal solution is to employ an all-photonics technology.

Hence, optical fiber must be brought in to the local access networks (LAN). Furthermore, efficient multiple access schemes are required to manage simultaneous transmission of multiple users over a common transmission medium. The three multiple access schemes most often considered, as presented in Fig. 1.1, are time-division multiple access (TDMA), wavelength-division multiple access (WDMA), and code-division multiple access (CDMA). TDMA separates a time frame into distinct time slots and WDMA divides the optical bandwidth into distinct wavelength channels, all of which are used concurrently by different users. In CDMA, all channels occupy the same wavelength/frequency and time space, and are distinguishable by unique channel specific codes. Fig. 1.2 depicts a LAN employing CDMA. Optical CDMA (OCDMA) can be viewed as a technology that combines aspects of both TDMA and WDMA: each bit is divided into time chips and each time chip may or may not have a pulse of a certain wavelength [1, 2].

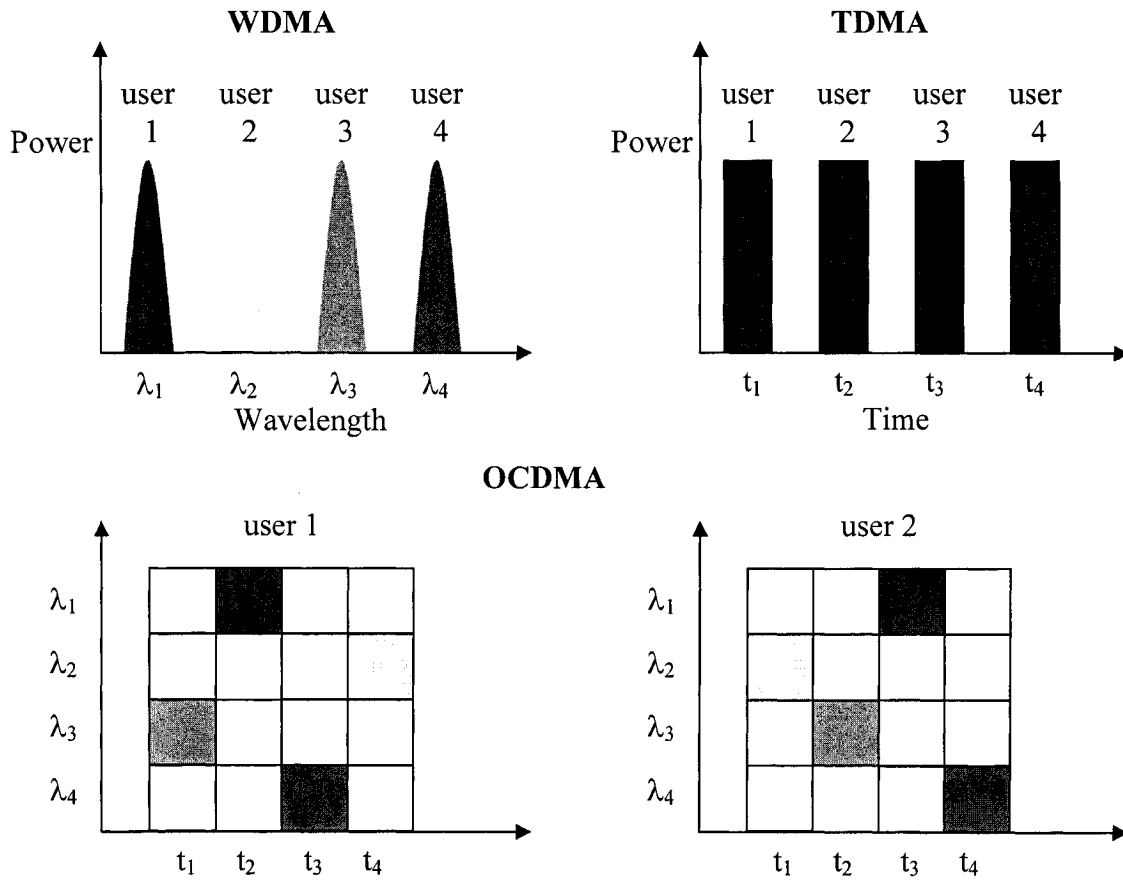


Fig. 1.1 WDMA, TDMA, and CDMA

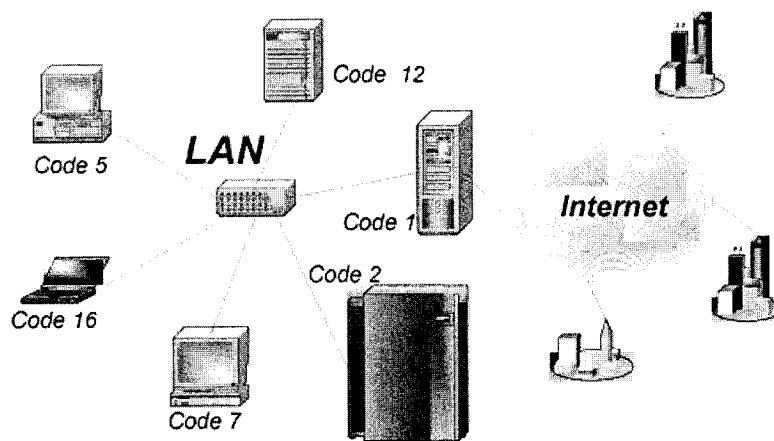


Fig. 1.2 A local access network employing CDMA [3]

TDMA is limited by the time-serial nature of the technology, and requires strong centralized control, which introduces additional overhead and latency. Furthermore, this technique does not fully exploit statistical multiplexing gain, which may be important for bursty traffic. WDMA requires a significant amount of dynamic coordination between nodes which wastes bandwidth, and similar to TDMA, also introduces additional overhead and latency. Moreover, the maximum capacity for both TDMA and WDMA is hard limited by the total number of slots or wavelengths used [1].

OCDMA exploits the large bandwidth of the fiber medium with the flexibility of the CDMA technique to realize high speed connectivity. The advantages are many and include [1]:

- eliminating time and wavelength management at all nodes,
- supporting a large number of active users in an asynchronous environment without centralized control,
- accommodating simultaneous information exchange among users on the same medium,
- embedding destination and source addresses in the code, and
- allowing for flexible network design since the bit error rate (BER) depends on the number of active users.

It is not surprising that OCDMA has been proposed as a means for providing flexible access to high-bandwidth applications and offering different levels of quality of service (QoS). Although we are still years away from commercial release, today's research will lay the foundation for future optical local access networks.

## ***1.2 Thesis objectives and contributions***

The two main objectives of this thesis are to characterize the effects of encoder/decoder mismatch on BER performance for 2 dimensional (2D) wavelength-time ( $\lambda$ -t) OCDMA and to build a multi-user 2D  $\lambda$ -t OCDMA direct detection demonstrator system. In this work, we focus on the 2D  $\lambda$ -t depth-first search codes (DFSCs) developed in [3, 4] since they have the following advantages over other possible 2D codes [4]:

- the codes can be designed with fewer time chips and thus are able to support higher data rates,
- more codes can be generated for a given code dimension, and
- the codes can fully exploit the gain provided by forward error correction (FEC) to allow a large number of simultaneous users operating with good BER performance.

Previous work on these DFSCs was focused on theoretical BER performance considering only multi-access interference (MAI) and ideal encoding/decoding of user codes (i.e. no time delays nor wavelength mismatch between the desired and interfering encoders and decoder). Knowing that an ideal implementation is impossible, we first investigate the impact that time and/or wavelength mismatch between desired and interfering encoders and decoder can have on the BER performance. Next, we demonstrate successful encoding and decoding of 2D  $\lambda$ -t DFSCs and successful implementation of a 4-user system. We use commercially available (off-the-shelf) optical components including wavelength multiplexers/demultiplexers (MUX/DEMUX) and power splitters/combiners; time delays are obtained by splicing appropriate lengths of fiber. Finally, we conduct appropriate test measurements to evaluate multi-user system performance.

The original research contributions of this thesis have been reported in the following journals and conferences:

- The analysis of time and/or wavelength mismatch occurring between desired and interfering encoders and decoder has been presented at the *Conference on Lasers and Electro-Optics (CLEO) 2004* under the title “Effects of encoder/decoder mismatch on BER performance for 2-D wavelength-time OCDMA” [5] (see Appendix D), and forms the basis of the following manuscript, “Impact of encoder/decoder mismatch due to wavelength and time misalignments on system performance of 2D wavelength-time optical CDMA systems” submitted to *Applied Optics* [6].

- The demonstration of a 2D  $\lambda$ -t OCDMA system using DFSCs has been presented at the *IEEE Laser and Electro-Optics Society (LEOS) Annual Meeting 2004* under the title, “Demonstration of a 4-user 2-D wavelength-time OCDMA system employing depth-first search codes” [7] (see Appendix D).
- Clock and data signal recovery (CDR) from an optically decoded 2D  $\lambda$ -t OCDMA signal was achieved using a novel OCDMA receiver, designed by Julien Faucher. Results on the demonstration system, including CDR, receiver design, and testing, form the basis of the following manuscripts: “Multi-user OCDMA system demonstrator with full CDR using a novel OCDMA receiver” submitted to *IEEE Photonics Technology Letters* [8] and “Performance of a multi-user OCDMA system demonstrator with full clock and data recovery” submitted for the *Conference on Lasers and Electro-Optics (CLEO) 2005* [9].

### **1.3 Thesis Outline**

The remainder of this thesis is organized as follows. In chapter 2, we present an overview of OCDMA, including fundamentals and recent progress. We discuss 2D approaches, and in particular,  $\lambda$ -t DFSCs. Finally, we highlight the various challenges associated with OCDMA technology. In chapter 3, we describe the impact of encoder/decoder mismatch on system performance. We give the methodology for our simulations and show the effects of wavelength, time, and combined wavelength and time misalignments in the encoders/decoder on the BER performance. In chapter 4, we demonstrate a 4-user 2D  $\lambda$ -t OCDMA system employing DFSCs. We describe the implementation and characterization of the encoders and decoder. We then demonstrate the successful encoding/decoding of a “1” bit, as well as rejection of an undesired transmitter. Experiments involving an arbitrary bit pattern clearly show that the desired user’s bit can be distinguished from the MAI. We also present eye diagrams, BER measurements, and an explanation of CDR. Finally, in chapter 5, we summarize the main results of the thesis and propose possible future directions for 2D  $\lambda$ -t OCDMA research.

## 2. Overview of OCDMA

### 2.1 Fundamentals of OCDMA

OCDMA operates as a multi access channel (MAC) where all the users transmit and receive encoded signals on the same fiber. As depicted in Fig. 2.1, bits of data from each user are encoded optically, and all unique encoded signals are multiplexed together before transmitting on the same fiber and being broadcasted to all decoders. Each decoder is matched to a specific encoded signal, and is designed to maximize the auto-correlation of the desired signal whilst minimizing the cross-correlation of all interfering signals. If among the received signals the desired signal is present, an auto-correlation peak should be detectable over the MAI and other noise sources. If the desired signal is not present, then the decoded waveform should be a low level of MAI and other noise sources. Hence, a threshold must be set in order to decide whether the received signal is a “1” or a “0” bit [10-13].

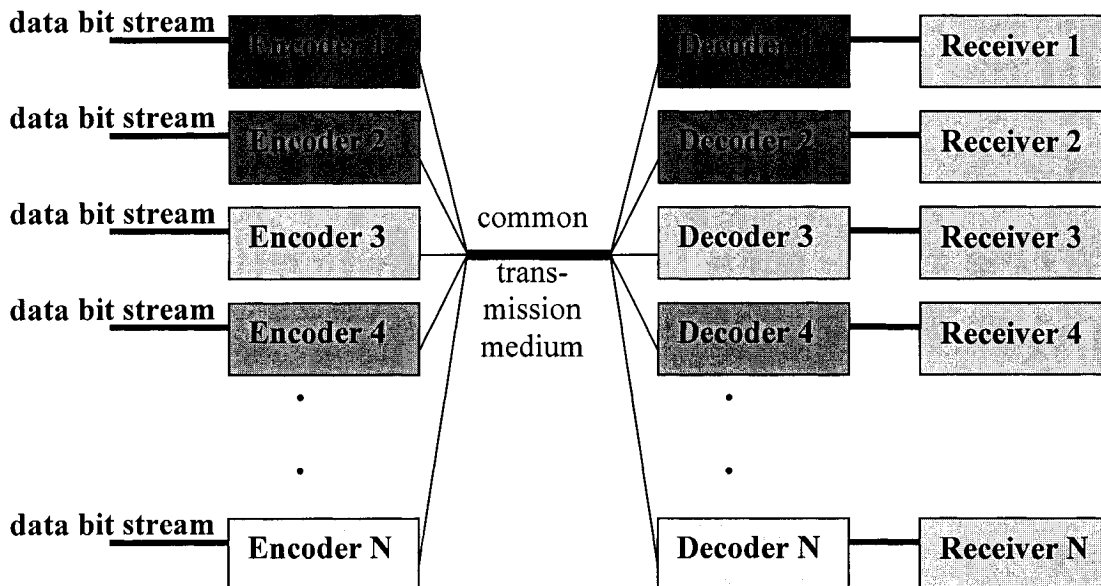


Fig. 2.1 Schematic of an OCDMA system

The past two decades have seen many different approaches to OCDMA systems. The different tactics may be incoherent (the phase of the optical signals is unimportant) or coherent, employ unipolar or bipolar coding schemes with optical orthogonal codes (OOCs) or truly orthogonal codes, and use direct or differential detection [14-17]. The schemes can be broadly divided as follows [17]:

- 1D temporal encoding (spread spectrum)
- 1D spectral encoding (spread time)
  - Spectral phase
  - Spectral amplitude
- 2D spatial encoding (spread space)
- Hybrid encoding
  - Multi-dimensional approaches involving a combination of space, wavelength, time, and polarization

Temporal encoding separates a bit window into many time chips where each time chip may or may not have a pulse of light (note that the short pulse used occupies the duration of a time chip). All user pairs are given a unique OOC pulse pattern. The dimension of the codes can rise rapidly and become cumbersome if many users with low cross-correlation are to be accommodated [12, 18].

Spectral phase encoding manipulates the phases of the spectral content of a coherent ultrashort pulse. A pulse spectral shaper, usually based on a  $4f$  grating-phase mask system, is used to manipulate the phases of the input pulse, and create a pseudorandom noise burst in time, whereas decoding involves a conjugate phase mask to recover the desired original pulse. Improperly decoded signals remain as pseudorandom noise bursts [19-21].

Spectral amplitude encoding is very similar to temporal encoding except that the temporal and spectral domains are interchanged: the frequency components of a broadband source are separated into spectral slots (synonymous to a bit window being divided into time chips) and each component is either “on” or “off” for a given code [22].

Spatial encoding uses multiple fibers to create parallel communication channels to create optical orthogonal signature patterns (OOSPs). This approach may be attractive for image transmission [23, 24].

## 2.2 Hybrid encoding approaches to OCDMA

There are several catalysts that have led to hybrid approaches to OCDMA systems. Performance wise, lengthy 1D temporal codes limit data rates, and spectral phase encoding schemes suffer from transmission impairments or require precise techniques for their proper compensation. Second, technological advances in dense wavelength division multiplexing/demultiplexing (DWDM) techniques, filtering and fiber Bragg gratings (FBGs), the introduction of affordable single mode lasers and short pulse lasers, and reliable optical delay lines, can potentially reduce system complexity [7, 25, 26].

Simultaneous exploitation of two dimensions provides greater flexibility in code design that can allow for minimal cross-correlation between users, increase the number of simultaneous users and increase potential data throughput [4, 27]. Early work on hybrid techniques was presented in [27, 28] and discussed 2D space-time techniques. In this technique, pulses travel in multiple fibers and each fiber introduces a different time delay. A matched decoder is one that has complementary time delays and then combines the power of all fibers to produce an auto-correlation peak. Experimental results were positive when compared to 1D temporal OCDMA systems: higher data rates were achieved, the link suffered less power loss, the auto-correlation peak had no side-lobes, and the 2D design provided good scalability to accommodate more users.

Since this achievement, much of the focus for future OCDMA systems has been on 2D hybrid techniques (we note, though, that 1D spectral phase encoding techniques still attract considerable interest [29]). While multi-dimensional approaches involve space-wavelength [30] and space-wavelength-time [31], there is much effort concentrated towards 2D  $\lambda$ -t techniques.

In 2D  $\lambda$ -t OCDMA, a user code is defined by multiple wavelengths, each delayed by a multiple of a time chip (with respect to a reference value). Fig. 2.2 presents a wavelength-view and a time-view of a 2D  $\lambda$ -t code. What differentiates the different 2D  $\lambda$ -t approaches are the code family design and technology. Expanding on existing 1D  $\lambda$ -t approaches and designing new algorithms led to, among others, the following families of codes:

- prime-hop (PH) codes [32] and variations [33],
- fast-frequency-hop (FFH) codes [34, 35],
- codes based on mapping of 1D sequences to 2D (YP codes) [36],
- matrix codes [37, 38],
- prime/OOC (POOC) codes [39], and
- depth-first search codes (DFSCs) [3, 4].

The designs follow different auto- and cross-correlation constraints, and allow for a combination of either “single pulse per row or column” (SPPR/C) or “multiple pulses per row or column” (MPPR/C).

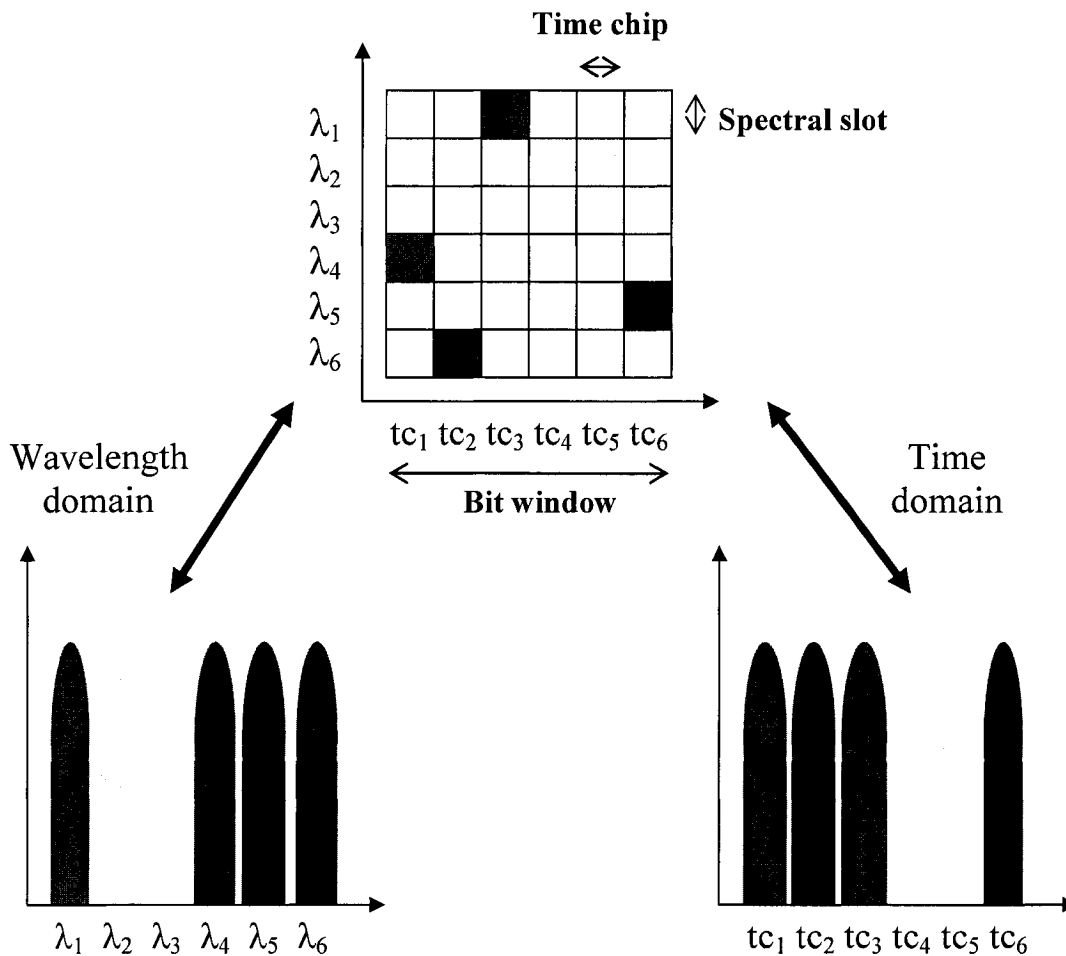


Fig. 2.2 Wavelength-view and time-view of a 2D  $\lambda$ -t code

Furthermore, the technological aspect has an obvious influence on code design and implementation. Improvements in arrayed waveguide grating (AWG) technology have led to their exploitation in dense-wavelength-division-multiplexing (DWDM) (de)multiplexers. Fig. 2.3 displays their use for generating 2D  $\lambda$ -t code where a BBS is demultiplexed into individual wavelength channels, and time delays are induced to each of the desired wavelengths before they are recombined [7, 25, 38, 40-42].

FBGs have also had a significant impact and have been proposed in many of the approaches [34-36, 39, 43-49]. In an FBG, multiple gratings can be written serially or be superimposed, thus appropriately delaying the desired reflected wavelengths from a broadband source (BBS), as shown in Fig. 2.4.

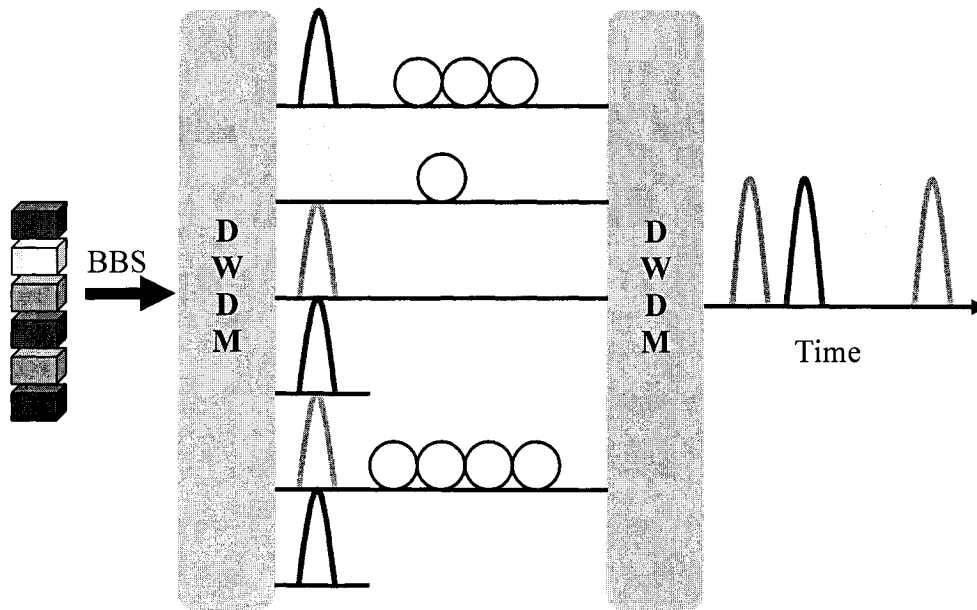


Fig. 2.3 DWDM (de)multiplexer and optical delay line based 2D  $\lambda$ -t OCDMA encoder

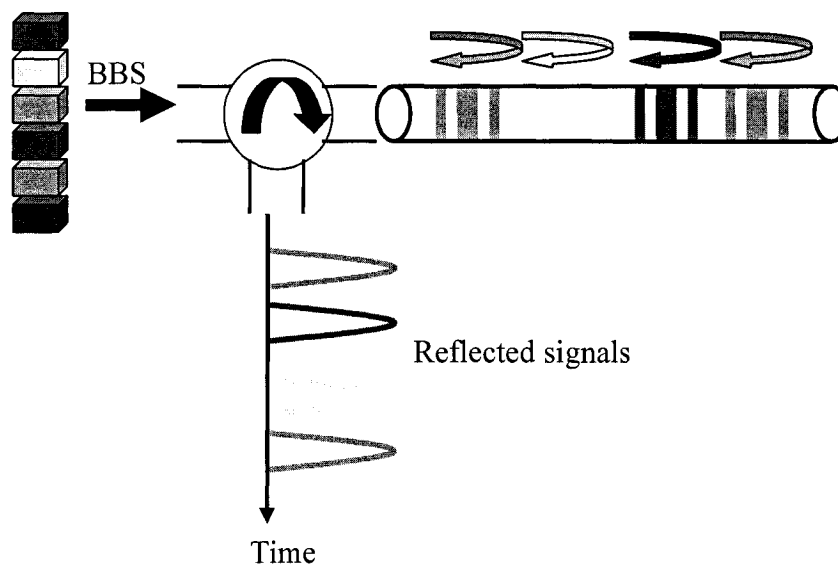


Fig. 2.4 Fiber Bragg grating based 2D  $\lambda$ -t OCDMA encoder

### 2.3 2D wavelength-time depth-first search codes

The previous section discussed 2D  $\lambda$ -t OCDMA and listed some existing code families. The codes are all similar in the sense that the optically encoded signals comprise pulses at different wavelengths positioned in specific time chips. However, each of these code families is generated with different constraints that spread the wavelengths differently. Among the many types of existing 2D  $\lambda$ -t codes, we focus on DFSCs in this thesis. We now provide a brief review of 2D  $\lambda$ -t DFSCs and their advantages.

The depth first search algorithm is an effective means for generating 2D  $\lambda$ -t codes of “ $m$ ” wavelengths, “ $n$ ” time chips, and constant weight “ $w$ ”, denoted  $(m, n, w)$ , satisfying the following constraints [3, 4]:

- the cross-correlation between different codes is less than or equal to one for any arbitrary time shift, and
- the auto-correlation sidelobe for all codes is less than or equal to one.

Moreover, the algorithm allows for MPPR and MPPC so that several pulses of different wavelengths can appear within the same time chip, or a pulse at a given wavelength can occupy multiple time chips within the bit period.

To analyze the BER performance of the codes, the following assumptions are made:

- perfect synchronization of time chips between all interfering users,
- ideal rectangular-shaped temporal pulses and spectral slices for the encoded and decoded signals,
- incoherent superposition of MAI,
- absence of channel noise and receiver noise, and
- no encoder/decoder mismatch.

For a large number of active users, a Gaussian distribution with mean  $\mu$  and variance  $\sigma^2$  can be used to approximate the MAI from the active users. To optimize the BER, the bit detection threshold must be set to  $\mu + w/2$ . This yields a probability of error given in terms of the signal-to-interference ratio (SIR) as:

$$BER = Q\left(\frac{\sqrt{SIR}}{2}\right) = Q\left(\frac{1}{2}\sqrt{\frac{w^2}{(K-1)\sigma_{pq}^2}}\right) \quad (2.1)$$

where  $w$  is the code weight,  $K$  is the number of simultaneous active users,  $\sigma_{pq}^2$  is the average variance of the Hamming aperiodic cross-correlation between every  $p$  and  $q$  code pairs due to the  $2n$  possible relative time shifts, and

$$Q(x) = \frac{1}{\sqrt{2\pi}} \int_x^{\infty} \exp(-t^2/2) dt \quad (2.2)$$

As described in [3, 4], for a given number  $K$  of simultaneous active users, a Monte Carlo simulation is used in which  $K$  codes are randomly chosen from all possible codes to evaluate  $\sigma_{pq}^2$  and calculate the resulting BER. Fig 2.5 presents the BER as a function of the number of simultaneous active users for different values of  $m$ ,  $n$ , and  $w$ .

The effect on the BER of increasing either  $m$  or  $n$  is the same, but increasing  $m$  generates more codes than increasing  $n$ . Increasing  $w$  has negligible effect on the BER, but does reduce the number of codes that can be generated. Therefore, if it is desired to support many codes, it is best to use more wavelengths than time chips and to keep the weight low. Additionally, permitting MPPR and MPPC adds flexibility to the code design and allows for more codes to be generated when compared to PH [32], YP [36] and FFH [34] codes of similar dimensions.

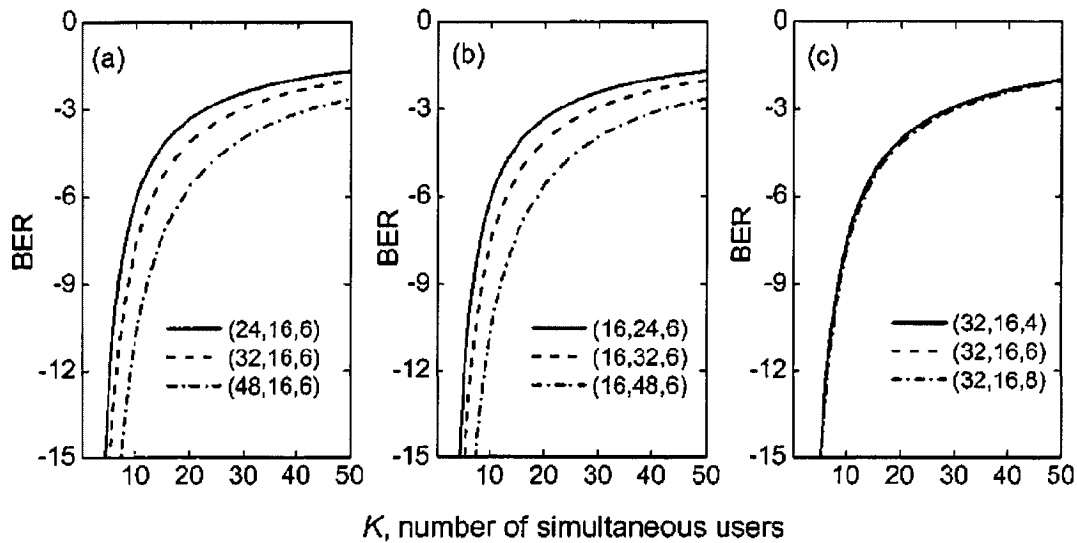


Fig. 2.5 BER as a function of the number of simultaneous active users for (a)  $n=16$ ,  $w=6$ , and  $m$  as a parameter; (b)  $m=16$ ,  $w=6$ , and  $n$  as a parameter; (c)  $m=32$ ,  $n=16$ , and  $w$  as a parameter [4]

Fig. 2.6 compares the BER performance of DFSC, YP, and FFH codes. The performance of DFSC and YP codes is similar; however there are subtle differences. Besides being able to generate more codes for a comparable code dimension, DFSCs can be designed with much fewer time chips (e.g. 16 instead of 67, and 63 instead of 127); hence they can support higher data rates. When compared to FFH codes, the BER performance is similar and both can generate codes with few time chips. The advantages of DFSCs are that many more codes can be generated and that the maximum number of codes generated is not limited by the number of wavelengths used. The significance of generating and supporting many codes is that when FEC is used, a greater number of simultaneous active users can operate at a given BER. If the maximum number of codes

for a code family is low, then it cannot exploit the gain that FEC provides [4, 50]. It is because of these advantages that DFSCs are considered in this thesis.

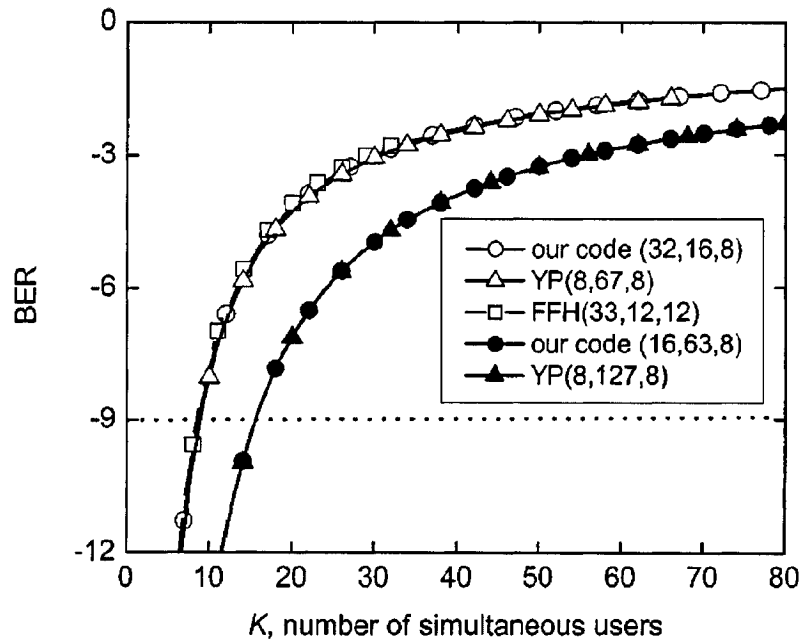


Fig. 2.6 Comparing the BER as a function of the number of simultaneous active users between different 2D codes [4]

## 2.4 Challenges in OCDMA

The first challenge with OCDMA is code design. Ideally, an OCDMA system should support up to hundreds of simultaneous users operating with a BER below  $10^{-9}$ . Furthermore, the encoder and decoder structures should be simple. These criteria place a burden on the code design since the former may require large code dimensions, whereas the latter may require smaller code dimensions. The code design is also dependent on technology since current optical components may limit the complexity and scalability of potential code families.

Second, overcoming the limitations of optics is a challenge. Most OCDMA systems are based on unipolar signaling which use direct detection. Yet, BER performance would improve if bipolar signaling were to be used. To enable bipolar

signaling, differential detection must be used, which increases the complexity of the decoder and receiver structures.

Assessing the impact of device limitations and transmission impairments on BER performance is also a challenge. Most theoretical works on OCDMA present results assuming ideal situations. While effects of encoder/decoder mismatch, dispersion, and additive noise may be minimized in real-life systems, they can not be entirely eliminated. Thus, these effects must be investigated and assessed.

Last, there is difficulty in implementing OCDMA. Technology demonstrators with few simultaneous users have been reported, but there has yet to be a technology demonstrator with a modest or substantial number of simultaneous users. Even once an implementation of modest size is functional, performing appropriate test measurements to evaluate its performance pose a challenge.

## **3. Effects of encoder/decoder mismatch on BER performance**

### **3.1 Introduction**

The BER performance of OCDMA systems is one vital aspect used to assess its viability as an optical transport technology. Moreover, system limitations must be determined. Within the context of 2D  $\lambda$ -t OCDMA, limitations due to chromatic dispersion and beat noise have been studied [51-55]. However, there have been no studies on the limitations imposed by encoder/decoder mismatch. This chapter presents the impact of encoder and decoder mismatch on BER performance for 2D  $\lambda$ -t OCDMA. The simulation model that we have developed can be applied to any 2D  $\lambda$ -t codes, yet, as discussed previously, our focus will be on DFSCs. The remainder of this chapter is organized as follows. Section 3.2 quickly reviews the ideal situations and explains what are meant by wavelength and time chip misalignments. Section 3.3 describes the simulation methodology and results are presented in section 3.4.

### **3.2 Description of wavelength and time chip misalignments**

The ideal situation is part of the focus of chapter 3 of [3] and has been discussed in section 2.3 of this thesis. To reiterate, an *ideal situation* refers to the following: perfect synchronization of time chips between all interfering users, ideal rectangular-shaped temporal pulses and spectral slices for the encoded and decoded signals, incoherent superposition of MAI, absence of channel noise and receiver noise, and no encoder/decoder mismatch. BER plots for different code families (size and weight) as a function of the number of simultaneous active users are shown in Fig. 2.5.

With respect to encoder/decoder mismatch and wavelength and/or time chip misalignment, an ideal situation is depicted in Fig 3.1 (a). For the encoder, all of the optical power of each encoded pulse is entirely contained in its time chip and in its

allotted wavelength slot. An ideal decoder would have wavelength selective filters that are perfectly matched to those of the encoder and complementary time delays to re-order the wavelength components so that all of the optical power of the encoded signal is detected in one time chip by the receiver.

Wavelength misalignments, as shown in Fig 3.1 (b), can occur due to wavelength drift in lasers or due to filters with a bandwidth which is detuned from the desired center wavelength. Time chip misalignments, as shown in Fig. 3.1 (c), can occur due to time delays that are not perfectly matched. Fig 3.1 (d) presents an encoded pulse suffering from both a wavelength and time chip misalignment. As a result of these misalignments, less optical power is received at the receiver or cross-talk is induced, thereby altering the MAI, and ultimately, affecting the BER.

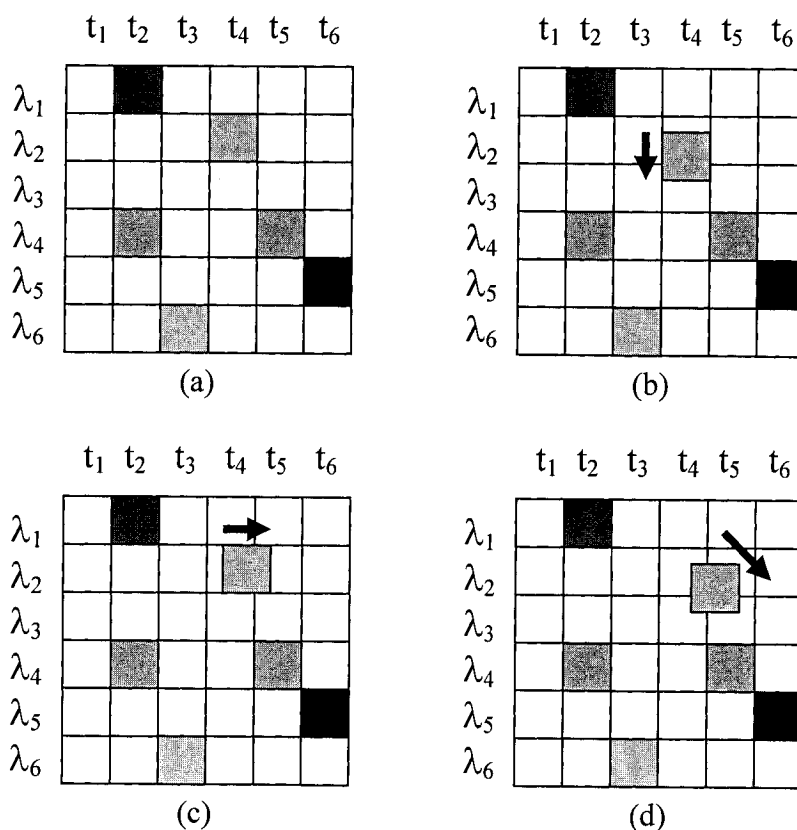


**Fig. 3.1 Example of a code using 6 wavelengths, 6 time chips, and weight 6; (a) ideal situation; pulse at position  $(\lambda_2, t_4)$  suffers (b) a wavelength misalignment, (c) a time chip misalignment, (d) both a wavelength and time chip misalignment**

### 3.3 Simulation procedure

The simulations were performed using MATLAB<sup>TM</sup>. A family of (32, 16, 6) DFSCs, yielding a total of 350 possible codes, and (16, 32, 6) DFSCs, yielding a total of 178 possible codes were used. We consider  $K = 12$  active users (i.e. 1 desired user and 11 interferers) or 8 active users (i.e. 1 desired user and 7 interferers).

Each simulation is described by a 3 letter set indicating whether the desired user encoder, interferer encoders, and desired user decoder are perfect (ideal) “P”, or imperfect (non-ideal) “I”. For example, “PPP” describes the situation when the three components are perfect, where as “PPI” describes the situation when only the desired user decoder is imperfect.

We assume the probability distribution of wavelength and/or time chip misalignment is Gaussian with zero mean (i.e. no misalignment) and with variances  $\sigma^2 = 0, 0.001, 0.005, 0.01, 0.05, \text{ or } 0.1$  in units of a wavelength slot or time chip.

We perform a Monte Carlo simulation in which all pulses in a code (set by the weight) can exhibit different wavelength and/or time chip misalignments, but all with the same probability distribution. Furthermore, if the interferer encoders are imperfect, then each interferer encoder exhibits different wavelength and/or time chip misalignments. The BER performance is evaluated as described in [3], and accounts only for MAI. 100,000 iterations are performed; in each, 8 or 12 of the 350 (or of the 178) codes are chosen randomly. Finally, we calculate the average BER and the standard deviation of all 100,000 iterations. Figure 3.2 summarizes the simulation process in the form of a flowchart.

As mentioned in section 2.3, the Gaussian approximation used to describe the MAI from active users is increasingly valid for a large number of active users. Section 3.3.2 of [3] examines the validity of the Gaussian approximation by comparing it to binary statistics. The conclusion of the analysis is that when the number of active users exceeds 80, the Gaussian approximation holds with less than 5% difference compared to binary statistics. However, for simplicity, our simulation procedure uses the Gaussian approximation to calculate the BER. We expect the trends to be similar if we use binary statistics as opposed to the Gaussian approximation.

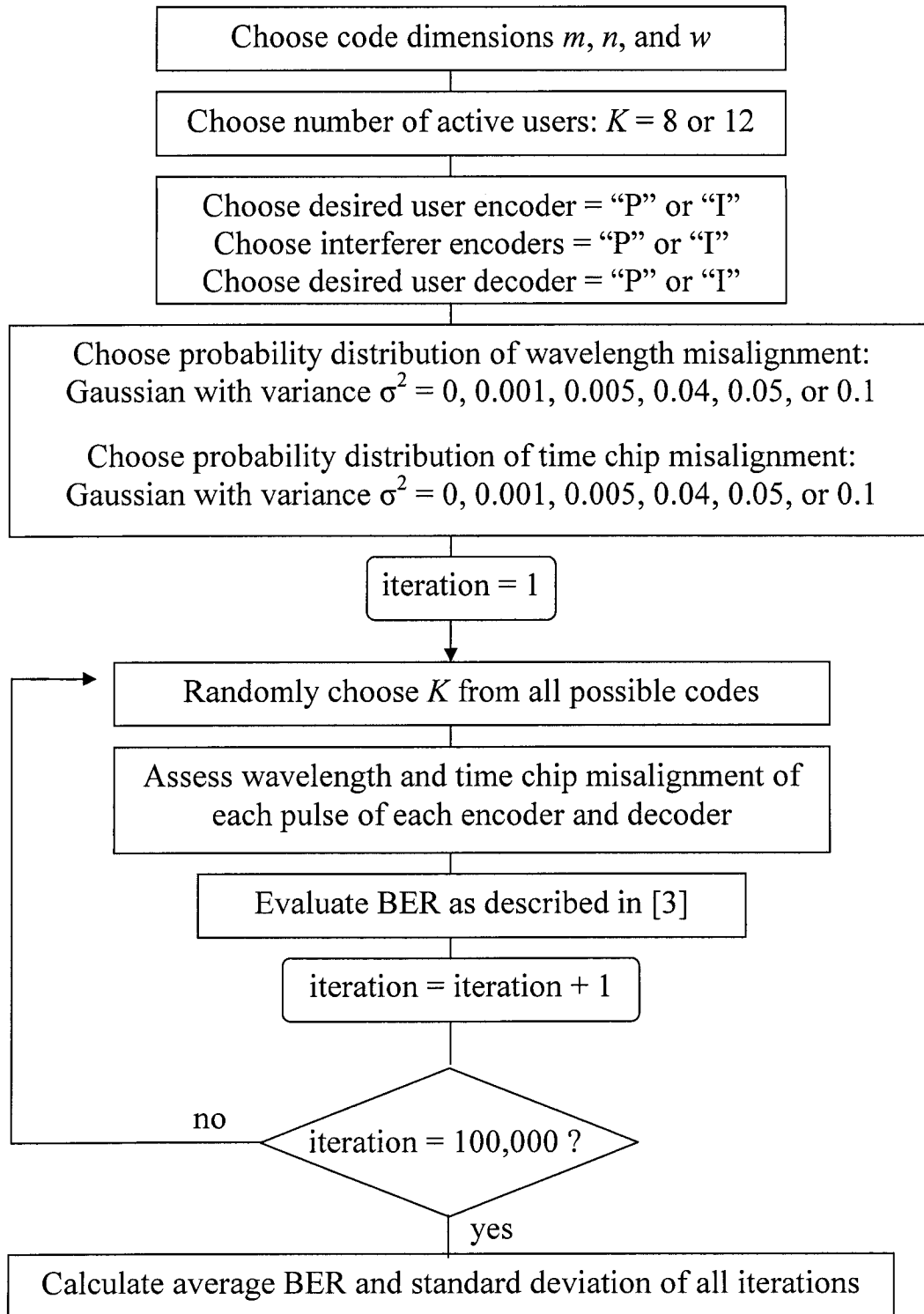
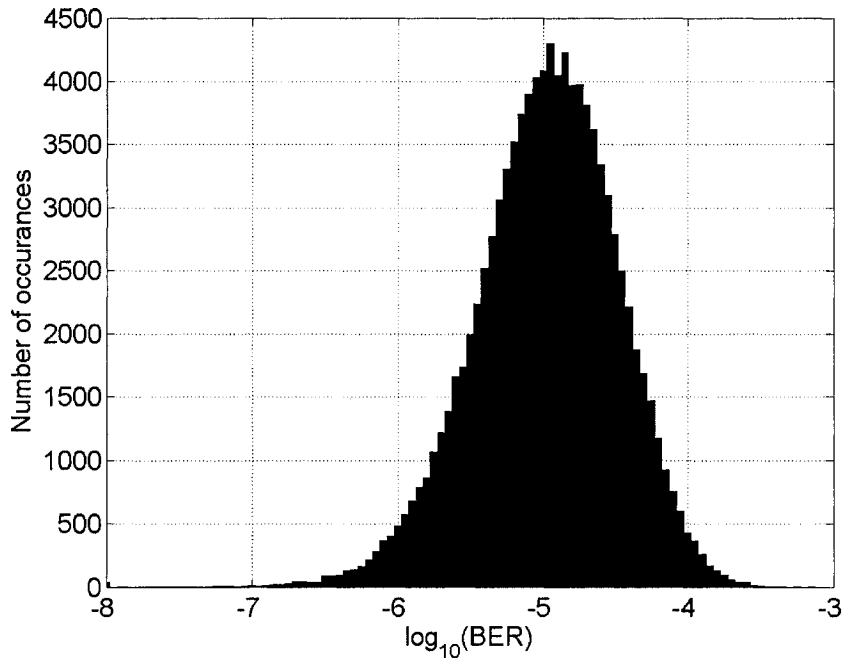


Fig. 3.2 Flow chart of simulation methodology

### 3.4 Results

#### 3.4.1 Wavelength misalignment

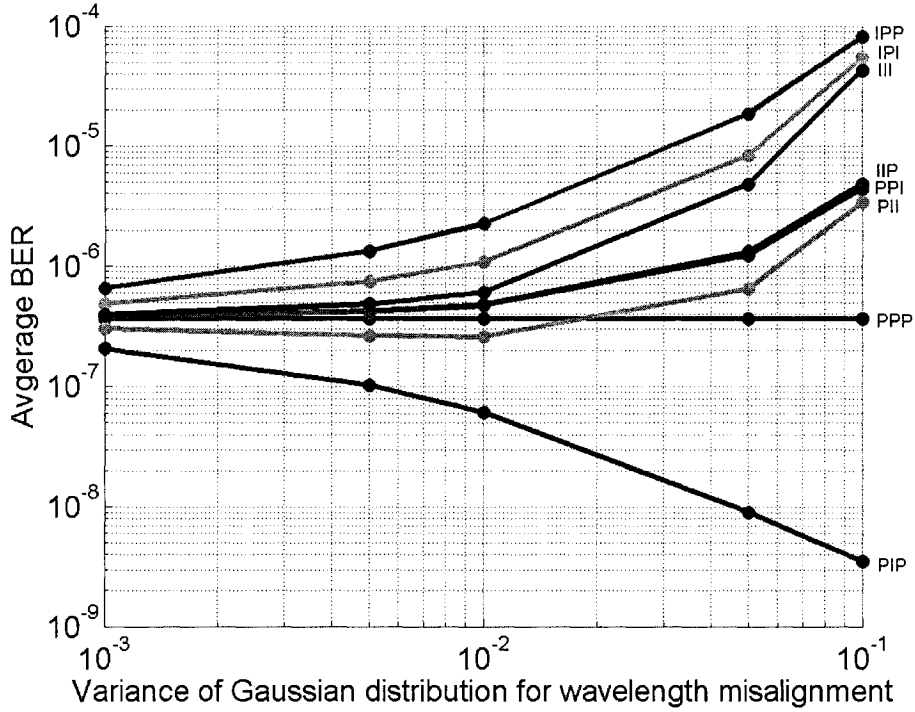
The results of the Monte Carlo simulation involving 100,000 trials for a given misalignment can be summarized in a BER histogram. Fig. 3.3 presents a typical BER histogram of an “IPP” situation with only a wavelength misalignment of variance 0.05 for 12 active users with (32, 16, 6) DFSCs. In this example, the average BER is  $1.86 \times 10^{-5}$  and the standard deviation is  $2.32 \times 10^{-5}$ . The average BER and the standard deviation of all the wavelength misalignment simulations are given in Appendix A.



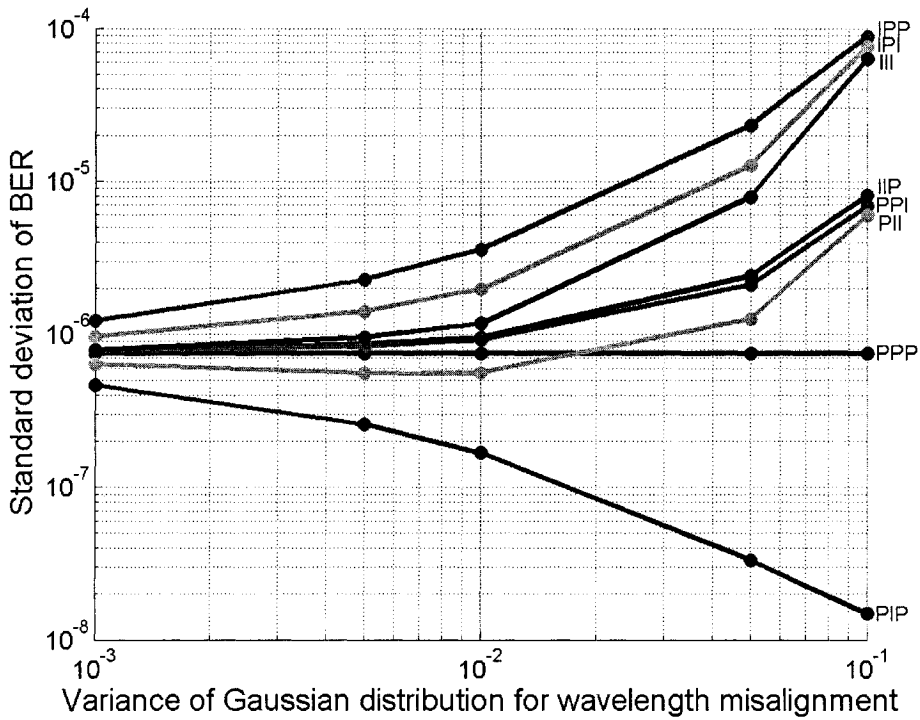
**Fig. 3.3 BER histogram of a 12 user, (32, 16, 6) DFSCs, “IPP” situation with only a wavelength misalignment of variance 0.05**

We first present results for codes employing more wavelengths than time chips. Figs. 3.4 (a) and 3.4 (b) respectively show the average BER, and the standard deviation, as a function of the variance of the Gaussian distribution for the wavelength misalignment. 12 simultaneous users with (32, 16, 6) DFSCs are used with all 8 possible cases, “PPP”, “IPP”, “IPI”, “III”, “IIP”, “PPI”, “PII”, and “PIP”.

3. Effects of encoder/decoder mismatch on BER performance



(a)



(b)

Fig. 3.4 (a) Average BER and (b) standard deviation of BER as a function of the variance of the Gaussian distribution for the wavelength misalignment; 12 simultaneous users with (32, 16, 6) DFSCs

As expected, for almost all cases, the BER worsens as the variance of the Gaussian distribution increases. Intuition may have led us to believe that the worst case would be “III”, however, the worst case occurs when only the desired encoder is imperfect (“IPP”), since only the desired user signal power is degraded, i.e. the signal-to-interference ratio (SIR) decreases. When only the desired decoder is imperfect (“PPI”), the decrease in desired user signal power is offset by a greater decrease in power from the interferers, thus resulting in a smaller BER penalty. By the same argument, it follows that when there is only an interferer encoder/desired decoder mismatch (“PIP”), the BER improves compared to “PPP”.

Fittingly, both the “IPI” and “III” curves are slightly better than the “IPP” curve, yet worse than the “PPI” curve. Again, for “IPI”, the desired user signal power is degraded while each interferer emits its maximum power. Yet, by chance, both the desired user encoder and decoder can have complementary misalignments, thus allowing more power to be received, thereby being slightly better than “IPP”. As for “III”, the same explanation as the “IPI” case follows, but since the interferers are not ideal, less interfering power is received, resulting in a better performance than “IPI”.

It is also simple to understand that “IIP” and “PPI” have nearly identical curves. In the two cases, all encoders, the desired and the interferers, are mismatched with the decoder. Finally, since for “PII” all interferes are mismatched with the decoder, there is less received interferer power, and therefore, “PII” is somewhat better than both “IIP” and “PPI”. In fact, up to a wavelength misalignment of variance of 0.01, “PPI” is slightly better than “PPP”.

Note that as the variance of the wavelength misalignment increases, all BER curves tend to  $\frac{1}{2}$  (which is expected for equiprobable “1” and “0” bits), except for “PIP”, which tends towards zero since there would be no interfering power (and give infinite SIR). We also conclude that for the most probable scenario of “III”, in order to keep the degradation in the BER to be less than one order of magnitude relative to “PPP”, the variance of the wavelength misalignment distribution must remain below 0.01.

We now investigate the impact when the number of simultaneous active users is reduced to 8. Fig. 3.5 illustrates the average BER as a function of the variance of the Gaussian distribution for the wavelength misalignment with (32, 16, 6) DFSCs.

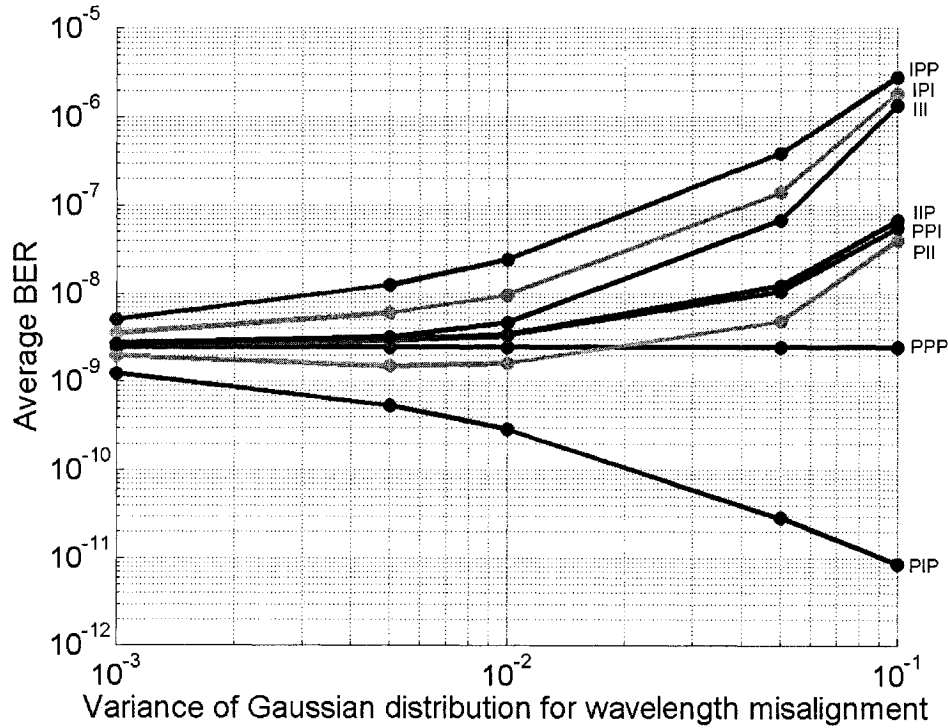


**Fig. 3.5 Average BER as a function of the variance of the Gaussian distribution for the wavelength misalignment; 8 simultaneous users with (32, 16, 6) DFSCs**

Because there are less active users, the BER values on Fig. 3.5 are superior to those on Fig. 3.4. In addition, the difference between the best case and worst case average BER for a given wavelength misalignment variance is greater for 8 simultaneous users compared to 12 simultaneous users. Yet, the curves are of very similar form, and the analysis and conclusions drawn earlier also apply.

Next, we consider codes in which the number of time chips is greater than the number of wavelengths. Fig. 3.6 displays the average BER as a function of the variance of the Gaussian distribution for the wavelength misalignment with 12 simultaneous users with (16, 32, 6) DFSCs.

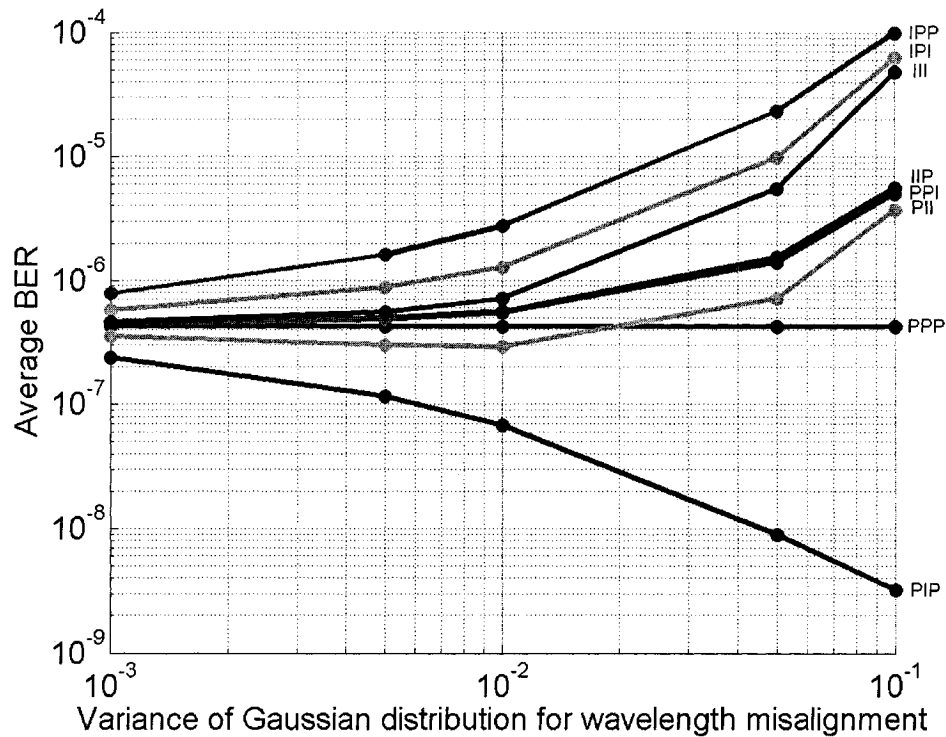


**Fig. 3.6 Average BER as a function of the variance of the Gaussian distribution for the wavelength misalignment; 12 simultaneous users with (16, 32, 6) DFSCs**

Even though (16, 32, 6) DFSCs yield fewer possible codes than their (32, 16, 6) counterparts (178 instead of 350), simulations yield similar results. Thus, wavelength misalignments have the same impact on BER system performance, regardless of whether the code family comprises more wavelengths than time chips. Since (32, 16, 6) DFSCs generate more codes and support higher data rates than (16, 32, 6) DFSCs, it is advantageous to use DFSCs that employ more wavelengths than time chips.

When the number of simultaneous active users is reduced to 8, the curves for the average BER as a function of the variance of the Gaussian distribution for the wavelength misalignment are almost identical to those shown in Fig. 3.5. The curves are thus omitted; again, the analysis and conclusions from Fig. 3.4 hold for these two cases.

The previous figures illustrate how the average BER varies as the wavelength misalignment increases for a given number of simultaneous users. It is also interesting to examine how the BER worsens as the number of active users increase when the variance of the Gaussian distribution for wavelength misalignment is fixed, and to compare the plots to the ideal situation. Fig. 3.7 shows the BER as a function of the number of

simultaneous active users for a wavelength misalignment variance of 0.1. We use (32, 16, 6) DFSCs; but since the conclusions derived for (32, 16, 6) and (16, 32, 6) DFSCs are the same, the BER curves as a function of the number of simultaneous users for a wavelength misalignment variance of 0.1 with (16, 32, 6) DFSCs are similar. Only “IPP”, “PPI”, and “PIP” are presented along side “PPP”. For a wavelength misalignment variance of 0.1, “IPI” and “III” have similar curves to “IPP”; and “IIP” and “PII” have similar curves to “PPI”, and are thus omitted from the following figure. The simulations were completed as described in section 3.3; however, only 1,500 iterations were used for each number  $K$  of simultaneous active users.

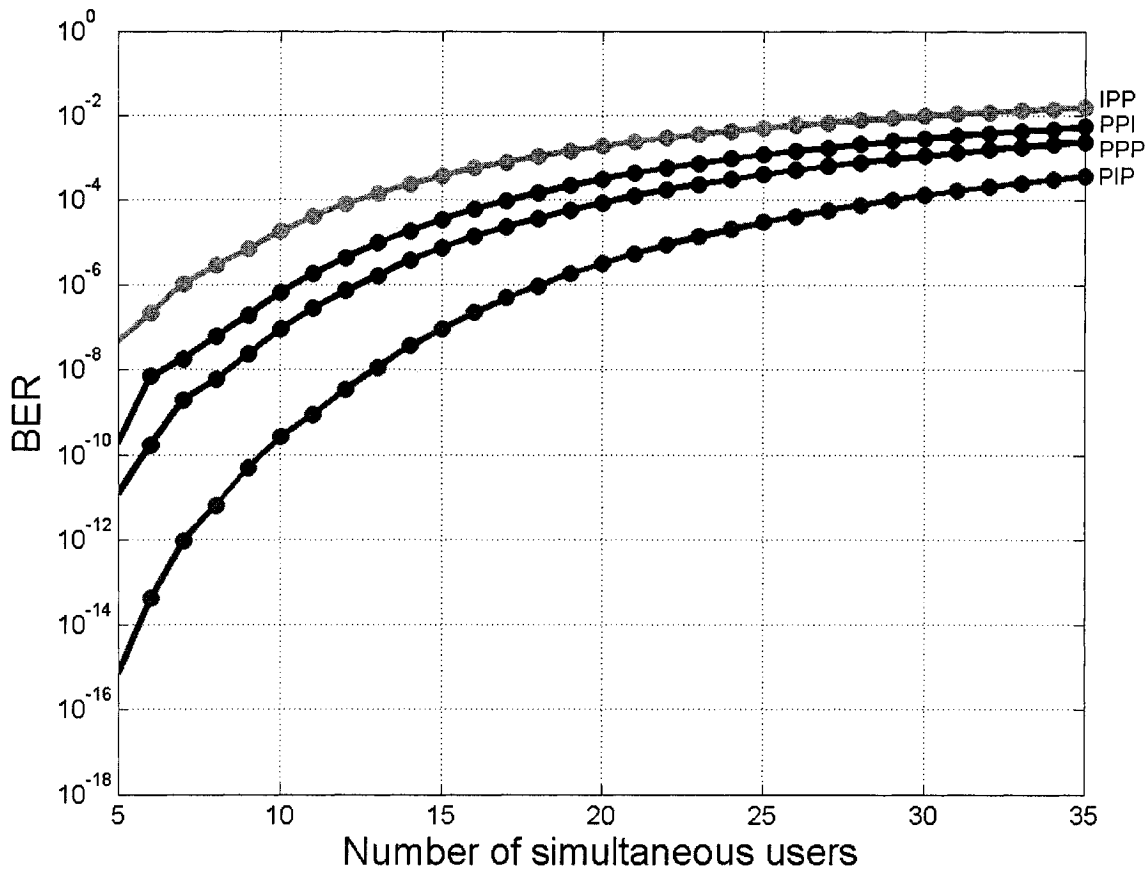


**Fig. 3.7** BER as a function of the number of simultaneous users with (32, 16, 6) DFSCs; variance of the Gaussian distribution for the wavelength misalignment is 0.1

A keen eye will notice that all BER values for 8 and 12 simultaneous users on Fig. 3.7 are almost exact to those on Figs. 3.4 and 3.6 for a wavelength misalignment

variance of 0.1. This reassures that using only 1,500 iterations instead of 100,000 does not skew the results. Moreover, as the number of simultaneous users increases, the non-ideal BER curves approach that of the ideal situation. Hence, an OCDMA system running with many simultaneous users suffers from a smaller BER penalty due to encoder and decoder mismatch than when it is running with fewer users. When 35 users are active, the BER worsens by one order of magnitude. Recall that when 12 users are active, the variance of the wavelength misalignment must be below 0.01 in order to keep BER penalty less than one order of magnitude.

#### 3.4.2 Time chip misalignment

Intuitively, whether the misalignment happens with wavelength or time chip, the effects should be similar, and indeed, this is the situation. A typical BER histogram generated from a 100,000 trial Monte Carlo time chip misalignment simulation has the same form as that presented in Fig. 3.3. The average BER and the standard deviation of all the time chip misalignment simulations are given in Appendix A.

Fig. 3.8 displays the average BER of as a function of the variance of the Gaussian distribution for the time chip misalignment for 12 simultaneous users with (32, 16, 6) DFSCs for all 8 possible cases, “PPP”, “IPP”, “IPI”, “III”, “IIP”, “PPI”, “PII”, and “PIP”.

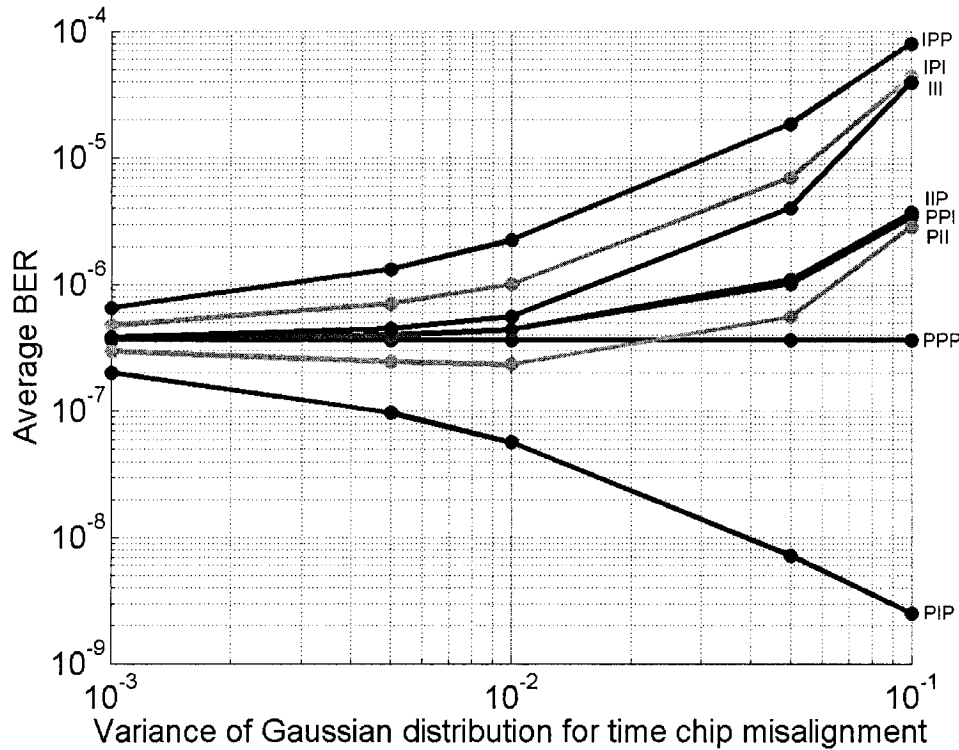


**Fig. 3.8 Average BER as a function of the variance of the Gaussian distribution for the time chip misalignment; 12 simultaneous users with (32, 16, 6) DFSCs**

The 8 curves for time chip misalignment are almost indistinguishable to those for wavelength misalignment, as shown in Fig. 3.4. Similarly, all the average BER curves as a function of the variance of the Gaussian distribution for the time chip misalignment are virtually indistinguishable from those for wavelength misalignment. For this reason, with the exception of Fig. 3.8, the time chip misalignment curves for 8 and 12 simultaneous users with (32, 16, 6) and (16, 32, 6) DFSCs are omitted. For all 4 separate time chip misalignment scenarios, the analysis provided and conclusions derived follow those from their wavelength misalignment counterparts. Thus, with time chip misalignments, the impact on BER system performance is independent of the number of time chips. Since (32, 16, 6) DFSCs generate more codes and support higher data rates than (16, 32, 6) DFSCs, again we conclude that it is more advantageous to use DFSCs that employ more wavelengths than time chips.

Fig. 3.9 presents the BER as a function of the number of simultaneous users for a time chip misalignment variance of 0.1 using (32, 16, 6) DFSCs. The simulations are

completed as described for Fig. 3.7, and displayed are the “IPP”, “PPI”, and “PIP” curves along side “PPP”.

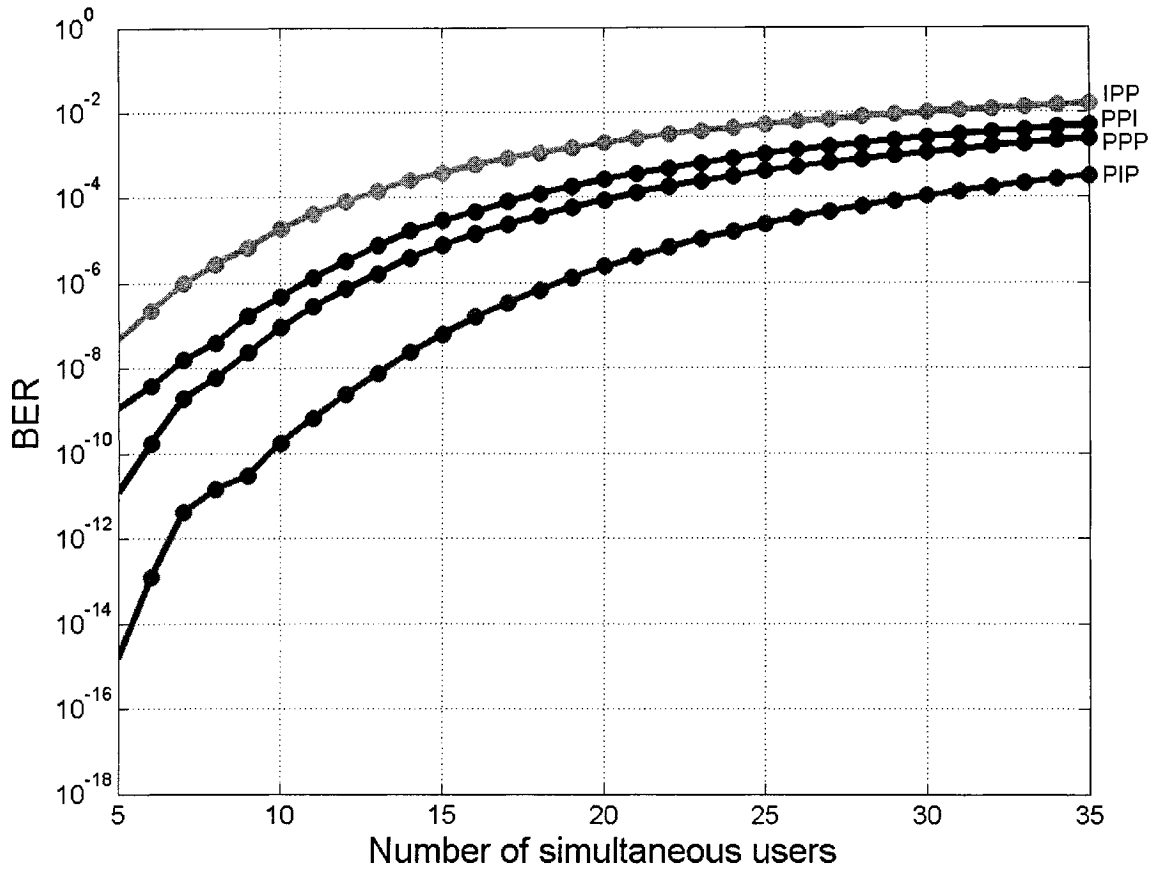


Fig. 3.9 BER as a function of the number of simultaneous users with (32, 16, 6) DFSCs; variance of the Gaussian distribution for the time chip misalignment is 0.1

Once again, Fig. 3.9 is very similar to Fig. 3.7, and consequently, the analysis and conclusions put forward for wavelength misalignment all hold for time chip misalignment.

### 3.4.3 Wavelength and time chip misalignments

Simulating the combined effects of both wavelength and time chip misalignments is slightly more complex and demands more computer processing power than simulating one misalignment alone. Since a thorough analysis was performed for both cases of

wavelength and time chip misalignments, we consider only two cases: “IPP” and “PPI”. It is expected that the effects of “IPI” and “III” follow that of “IPP”; that the effects of “IIP” and “PII” follow that of “PPI”; and that “PIP” improves the BER. Simulations were completed using 12 simultaneous users with both (32, 16, 6) and (16, 32, 6) DFSCs, but since the plots are almost identical, only those using (32, 16, 6) DFSCs are presented.

Figs. 3.10 and 3.11 display contour plots of the average BER as a function of the variance of the Gaussian distributions of both the wavelength and time chip misalignments for “IPP” and “PPI” cases, respectively. Recall that for the “PPP” case, the average BER is  $3.62 \times 10^{-7}$ .

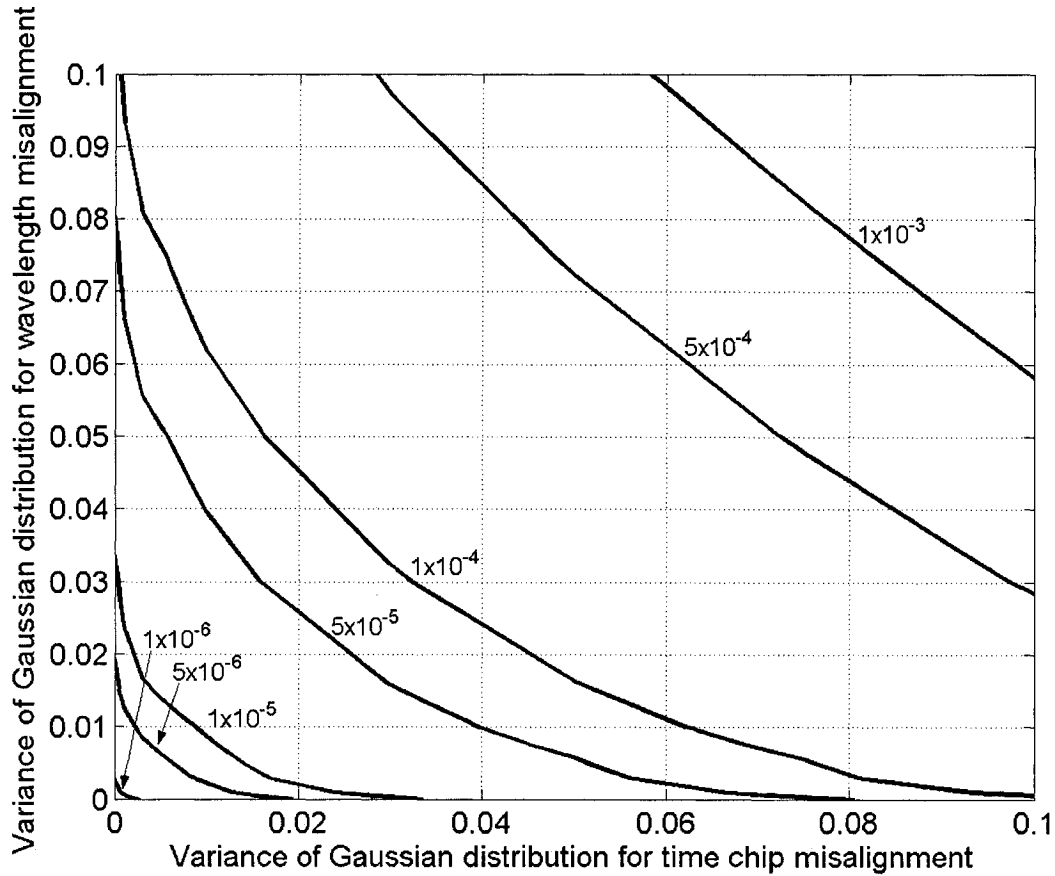


**Fig. 3.10** Contour plot of the average BER as a function of the variance of the Gaussian distributions of both the wavelength and time chip misalignments for case “IPP”; 12 simultaneous users with (32, 16, 6) DFSCs

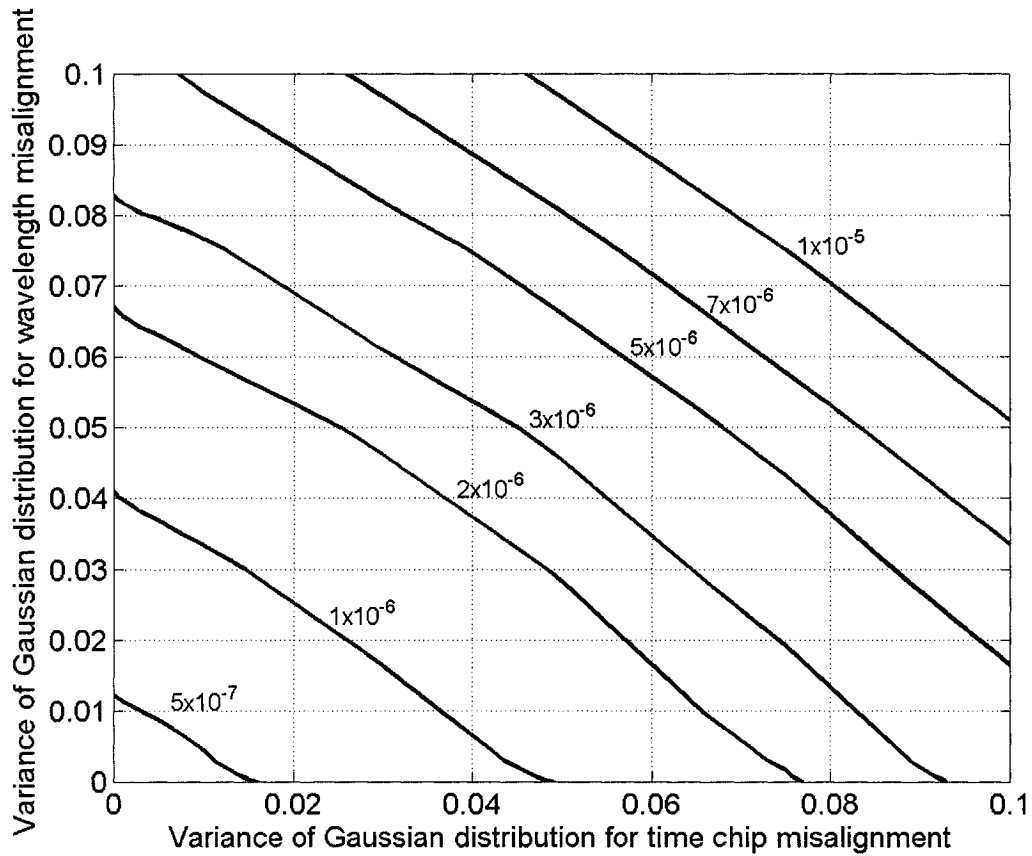


**Fig. 3.11** Contour plot of the average BER as a function of the variance of the Gaussian distributions of both the wavelength and time chip misalignments for case “PPI”; 12 simultaneous users with (32, 16, 6) DFSCs

As expected, the “IPP” case is worse than the “PPI” case. Considering “IPP”, the average BER worsens by 4 orders of magnitude when both variances of the wavelength and time chip misalignments are 0.1. On the other hand, when only wavelength or time chip misalignment exists, the average BER worsens by 2 orders of magnitude. For “PPI”, the average BER worsens by 2 orders of magnitude when both variances of the wavelength and time chip misalignments are 0.1 compared to 1 order when only wavelength or time chip misalignment exists.

### **3.5 Summary**

In this chapter, we presented the impact of encoder and decoder mismatch on BER performance for 2D  $\lambda$ -t OCDMA system employing DFSCs. This was accomplished by creating a MATLAB<sup>TM</sup> OCDMA simulation model that accounts for wavelength and/or time chip misalignments. The OCDMA model created is flexible; not only can it simulate DFSCs of various dimensions, but it can accommodate other 2D  $\lambda$ -t codes. Also, probability distributions other than Gaussian can be examined.

As expected, the simulations attest that the effects of encoder and decoder mismatch caused by wavelength and/or time chip misalignments is detrimental to the BER performance. The impact on the BER is scenario dependent; but for the worst case scenario, either using (32, 16, 6) or (16, 32, 6) DFSCs, if the variance of the Gaussian distribution for both wavelength and time chip misalignments is 0.1, the BER can degrade by 4 orders of magnitude. In order to ensure a BER penalty below 1 order of magnitude, the variance of the Gaussian distribution for both wavelength and time chip misalignments must remain below 0.01.

Also note that the BER performance as a function of wavelength and/or time chip misalignments is almost identical for both (32, 16, 6) and (16, 32, 6) DFSCs. The impact of misalignment in wavelength (or time chips) is the same regardless of the number of wavelengths (or time chips) used in the codes. Thus for a given code dimension  $m \times n$ , it is preferable to design codes with more wavelengths than time chips since (1) they can support higher data rates and (2) they can generate more codes.

While it is certain that misalignments in both wavelength and time exist in a real life systems, the results of these simulations will motivate engineers to carefully choose components, to be extremely precise in introducing optical delay lines, and to properly consider packaging issues when assembling the optical encoders and decoders required for a successful OCDMA implementation.

## **4. Demonstration of a 4-user OCDMA system**

### **4.1 Introduction**

While it is accurate to say that OCDMA is a promising technology for use in local area or access optical networks carrying bursty and asynchronous traffic, the deployment of OCDMA lies with successful implementation. There have been several 2D  $\lambda$ -t OCDMA technology demonstrators [25, 40, 49]. However, given the advantages of DFSCs over other 2D  $\lambda$ -t approaches, it is desirable to demonstrate their practicality.

In this chapter, we demonstrate successful encoding and decoding of 2D  $\lambda$ -t DFSCs as well as a successful implementation of a 4-user system. Section 4.2 discusses the building and characterization of the encoders and decoder. Section 4.3 describes the implementation of the 4-user system and examines the wavelength and time characteristics of each encoder and decoder. Finally, section 4.4 presents the testing of the 4-user system and provides eye diagrams, BER measurements and an explanation of CDR.

### **4.2 Implementation of the 4-user OCDMA system**

#### **4.2.1 Description of the demonstration setup**

In our 4-user demonstration system, we use DFSCs that are based on 8 wavelengths, 8 time chips, and a weight of 4, i.e. (8, 8, 4) DFSCs, resulting in 31 possible codes. All parameters of the demonstration setup are presented in Table 4.1. The choice of the code dimension and system parameters was based on the available equipment in our laboratory. The four codes used are illustrated in Fig. 4.1. Users 2-4 are interferers and have been chosen such that they each have 2 wavelengths in common with the desired user (User 1) thereby making the task of identifying the auto-correlation peak more difficult (this represents a worst-case scenario among the 31 codes generated by the DFS algorithm). A block diagram of the set-up is shown in Fig. 4.2.

Table 4.1 Demonstration setup parameters

Parameter	Value
Wavelength range	1547.6 nm - 1553.2 nm
Channel spacing	100 GHz (0.8 nm)
Data rate	155.52 Mb/s
Bit time	6.430 ns
Chip rate	1.244 Gb/s
Chip time	804 ps

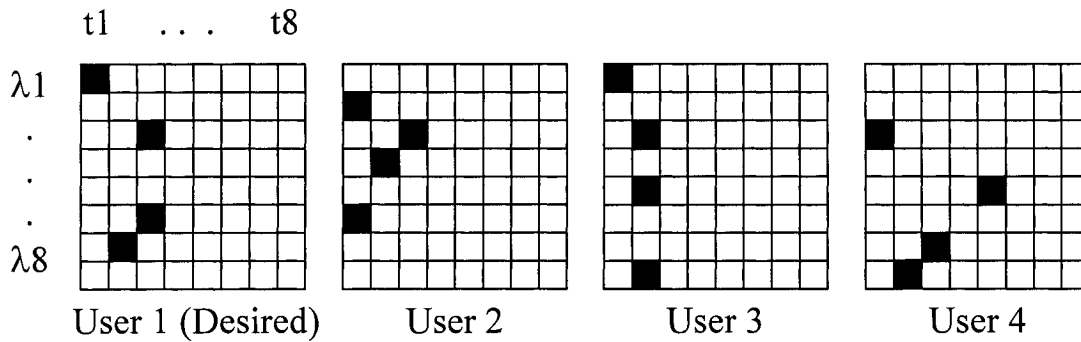


Fig. 4.1 The four codes used in the demonstration setup

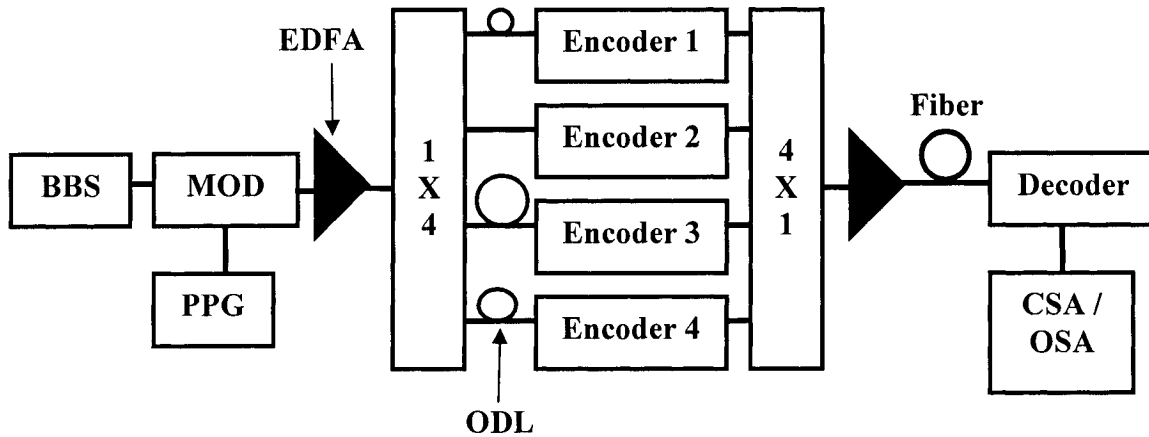


Fig. 4.2 Block diagram of the 4-user system

An electro-optic modulator (MOD), which is driven by a pulse pattern generator (PPG), generates a pulse at the chip rate from the BBS. The pulse is split into four paths (using a 1×4 power splitter) of different lengths and encoded by the four encoders before

being recombined (using a 4×1 power combiner) and propagated through fiber. Although each encoder transmits the same bit pattern, additional fiber optical delay lines (ODLs) were used to decorrelate the patterns for each user.

As depicted in Fig. 4.3, each encoder filters the BBS input, time delays are introduced for each of the 4 desired wavelengths, and finally the 4 wavelengths are recombined. The decoder performs matched filtering before detection. Fig. 4.4 illustrates each encoded signal in the time domain before and after the decoder. Because of the decoder design, 2 of the 4 interfering wavelengths of each interferer are eliminated by the decoder. Erbium doped fiber amplifiers (EDFAs) are used to amplify the signals. An optical spectrum analyzer (OSA) is used to measure the wavelength characteristics (optical power vs. wavelength), and a communication signal analyzer (CSA) is used to measure the temporal waveforms (optical power vs. time). The CSA optical sampling module comprises a photodetector having a bandwidth of 12.5 GHz.

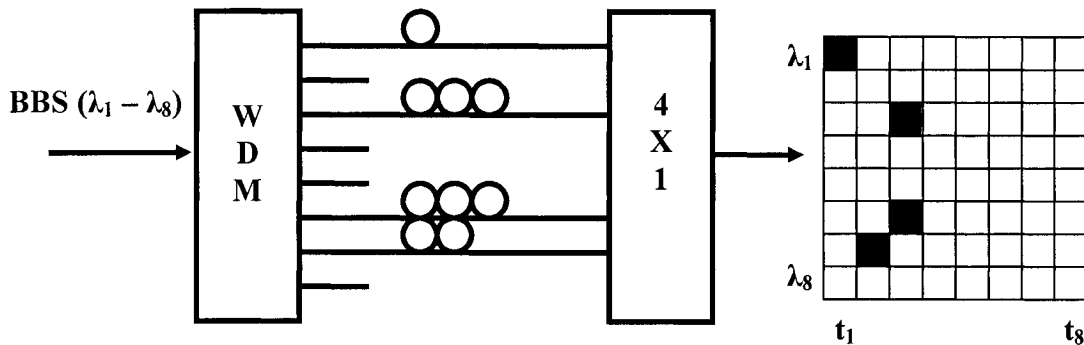


Fig. 4.3 Block diagram of an encoder (e.g. desired encoder)

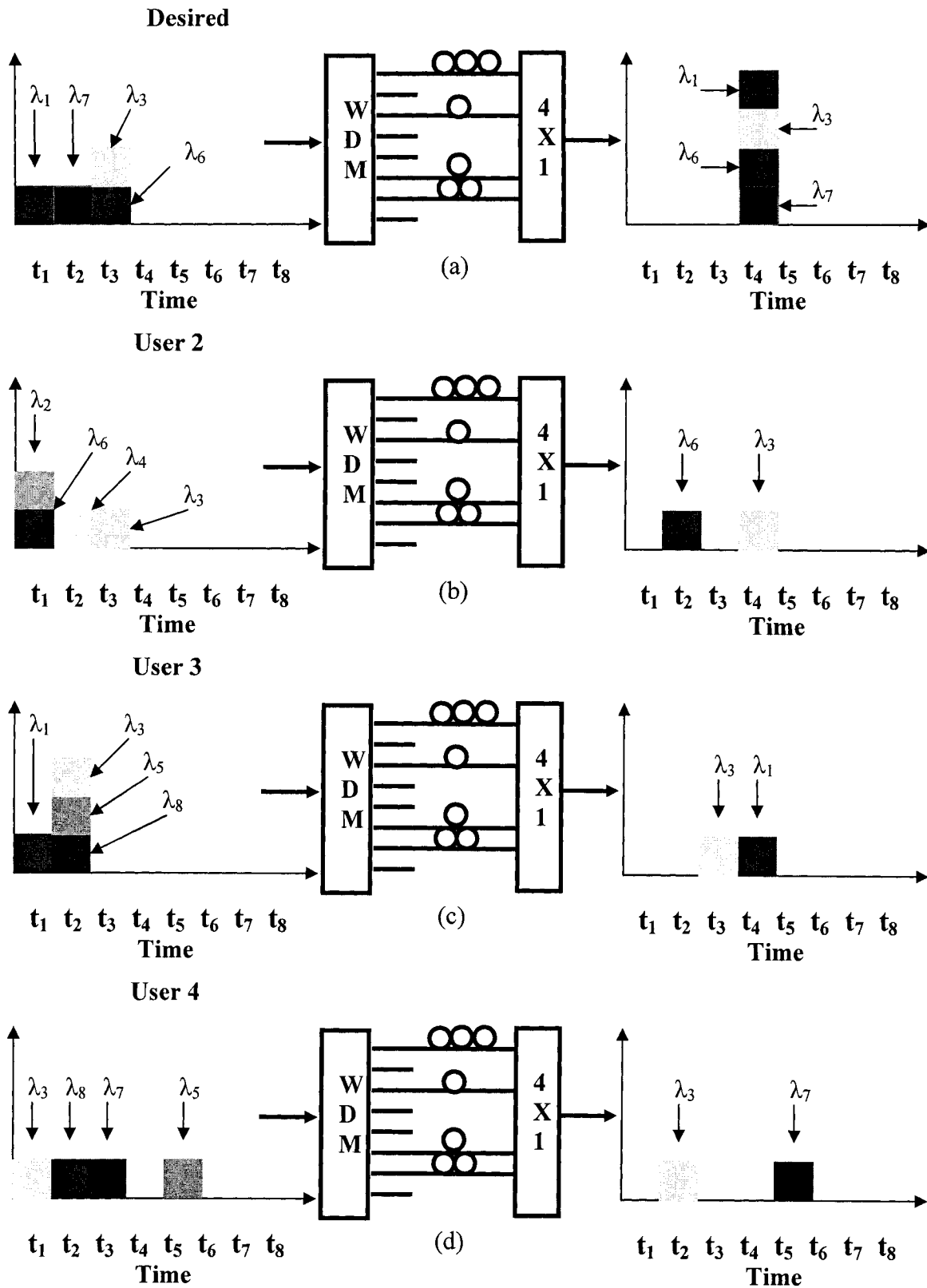


Fig. 4.4 (a) Desired; (b) User 2; (c) User 3; (d) User 4 codes before and after decoding

### 4.2.2 Building and characterization of encoders and decoder

Since the DFSCs use wavelength and time dimensions for coding, the components used for encoding and decoding must provide us with a way to manipulate each desired wavelength individually and to be able to delay the optical power of that wavelength. The approach taken is a wavelength-demultiplexing / optical delay line approach, which uses a BBS as its light source. Each of the four encoders and decoder comprise the following:

- one WDM DEMUX,
- one optical power combiner (4×1), and
- four optical delay lines (ODLs).

To begin, it is important to characterize the optical path lengths (OPLs) of the WDMs and 4×1s. A precision reflectometer is used ensure that the 4 optical paths of all the 4×1s were of equal length. White light is incident on the common port and the four reflection peaks are observed on the precision reflectometer. Each fiber pig-tail was severed so that the OPLs were equal to within 0.5 mm.

Characterizing the WDMs is different since all fiber pig-tails are packaged and we only have access to the optical ports. An optical vector analyzer is used to measure simply the OPL that each wavelength traverses. Since we do not necessarily have equal OPLs, the path differences must be considered when assembling the complete encoder/decoder.

The next step is preparing the ODLs. Each ODL comprises a nominal length of fiber, the required length to induce the required time delay, plus an additional length to compensate for the WDM OPL differences. The time/length ratio used is 50 ps time delay for each 1 cm of single-mode fiber (SMF). The duration of the time chip for the codes is 800 ps, so each delay of one time chip requires 16 cm of SMF. After the required length for an ODL is calculated, a fiber pig-tail is laid beside a measuring tape, severed at the appropriate length, and then cleaved. Finally, for each encoder and decoder, the 4 ODLs are spliced to the 4×1.

The last step is to simply enter the 4 spliced pig-tails from the 4×1 into the appropriate WDM channels. As depicted in Fig. 4.5 and described before, light from the

BBS enters the common port of the WDM and the 8 wavelengths are demultiplexed. Only 4 of the 8 wavelengths are of use for an encoder. Each of the 4 desired wavelengths enters the appropriate fiber pig-tail of the 4×1. Finally, the optical power is combined into one fiber at the common port.

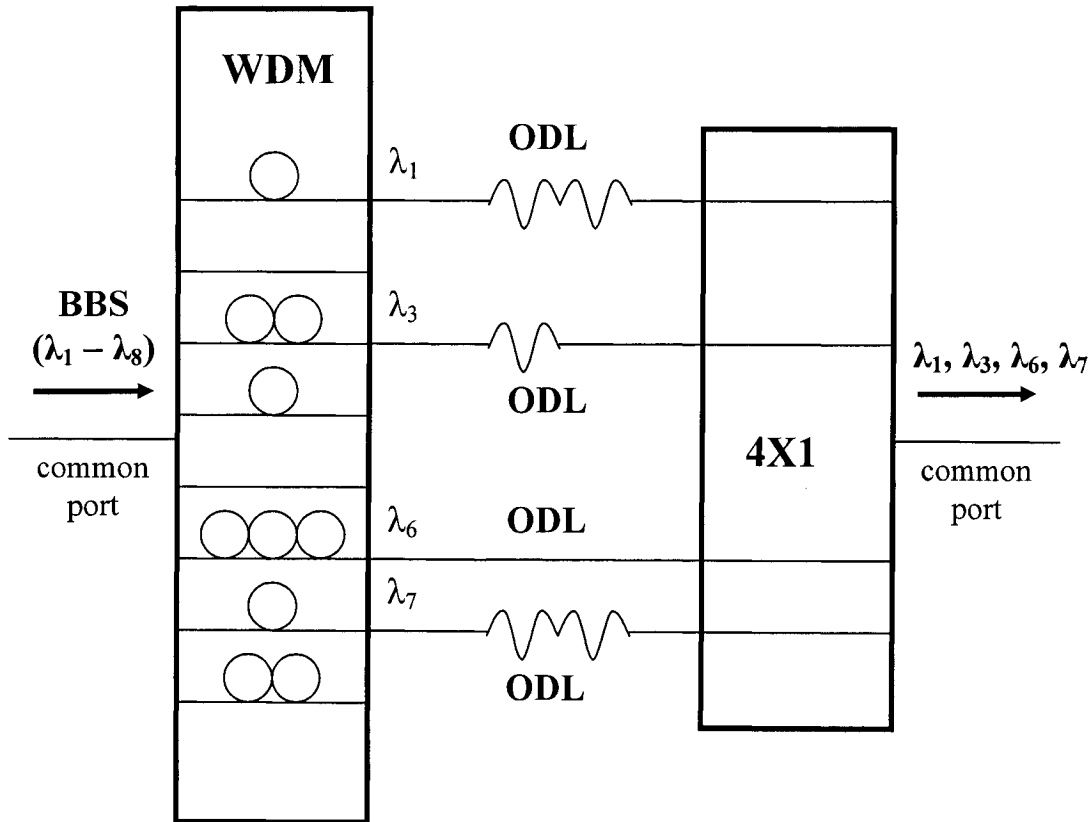


Fig. 4.5 Components used in building each encoder and decoder

After assembly, the OPLs were measured a last time to ensure that the process of splicing ODLs was done properly. The aim was to have all ODLs within  $\pm 5\%$  of a time chip error in order to minimize the effects of encoder/decoder mismatch. Since each time chip corresponds to 16 cm of SMF, the ODLs cannot be more than  $\pm 0.8$  cm off target. Fig. 4.6 illustrates a picture of the encoders and decoder.

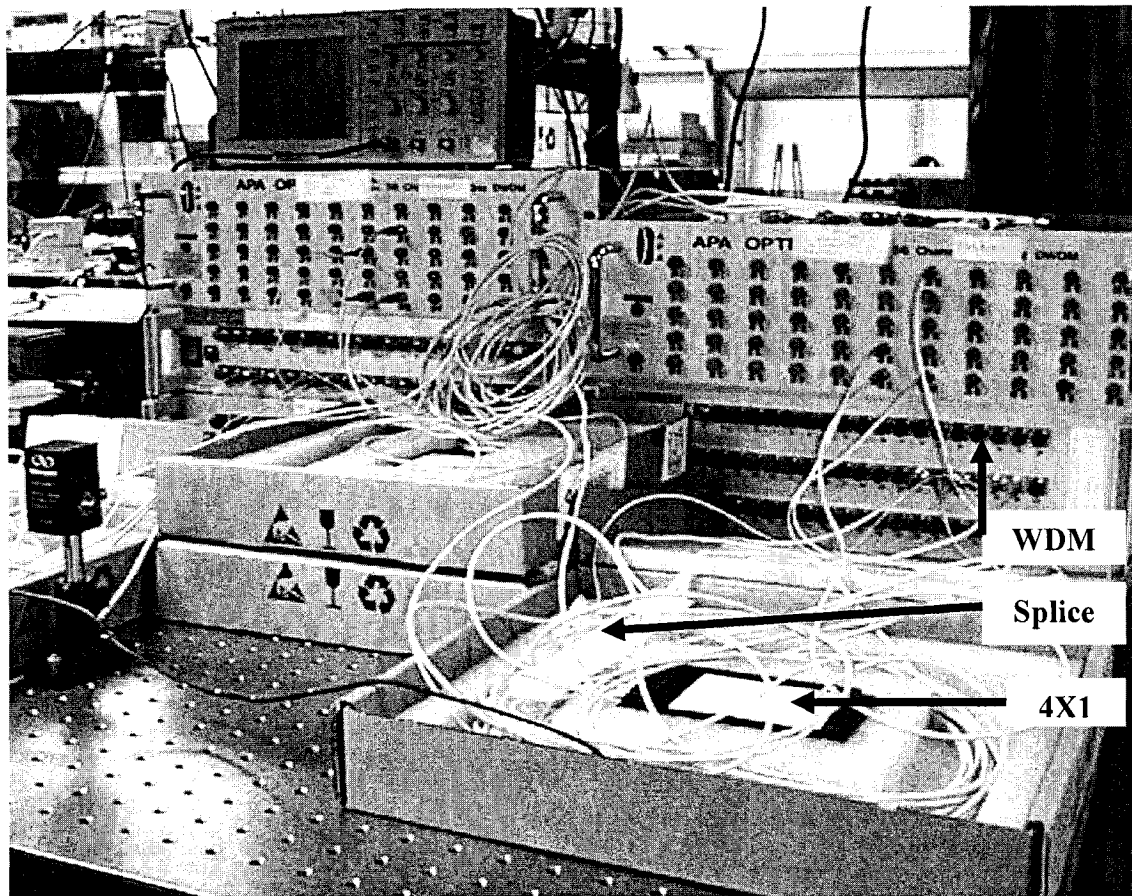


Fig. 4.6 Picture of encoders and decoder

Concerning the WDMs, the insertion losses of all channels were measured and each WDM has an insertion loss uniformity of 1 dB between channels. In addition, the center wavelength of each channel was measured. The two WDMs with the best matching center wavelength values (and which also had the least insertion losses) were chosen for the desired encoder and decoder in order to minimize wavelength misalignments. The remaining three WDMs selected to act as interferers all have center wavelengths that are within 0.1 nm of the desired center wavelength. Thus minimal wavelength misalignment exists between the interferer encoders and desired user decoder. All insertion losses and OPL measurements of the components used are included in Appendix B.

### 4.2.3 Testing of encoders and decoder

To begin, we must ensure that the wavelength and time characteristics of each encoder and decoder are correct, and that the optical power out of each encoder is approximately the same. To do so, we send a “1” bit and observe the corresponding encoding/decoding of that “1” bit. Fig. 4.7 shows the temporal waveform of the input broadband pulse. The full-width half maximum (FWHM) of the pulse is 810 ps and the extinction is 3.7 dB. For the remainder of chapter 4, unless otherwise stated, all temporal waveforms presented are averaged traces from the CSA.

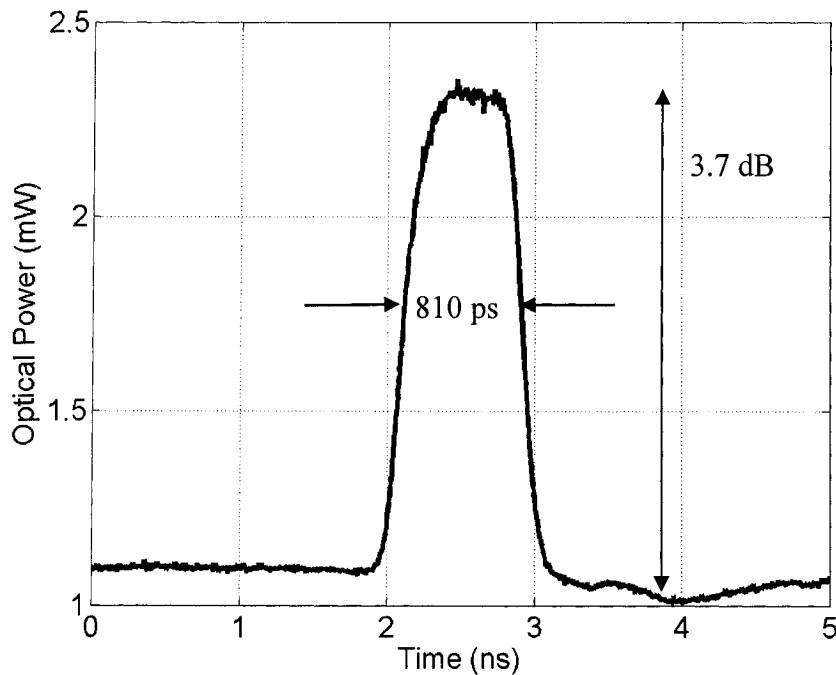


Fig. 4.7 Time characteristics of an un-coded input pulse

#### 4.2.3.1 Desired encoder and decoder

The desired encoder (or user 1) and the decoder are examined together since they are to have identical spectral characteristics and complementary time delays in order to reconstruct the auto-correlation peak. Fig. 4.8 illustrates the wavelength characteristics

of both the desired encoder and decoder. As expected, the spectral characteristics of both the desired encoder and decoder are almost the same. The isolation between  $\lambda_6$  and  $\lambda_7$  is 21 dB, and that between  $\lambda_1$  and  $\lambda_3$  is 35 dB.

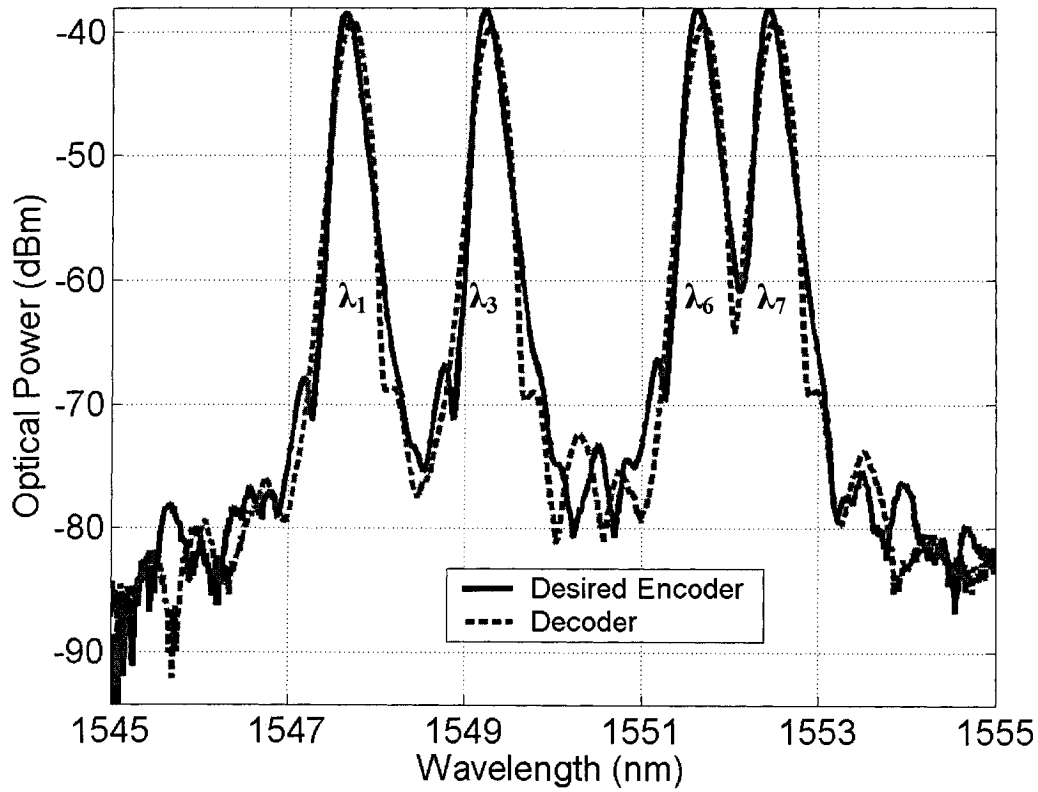
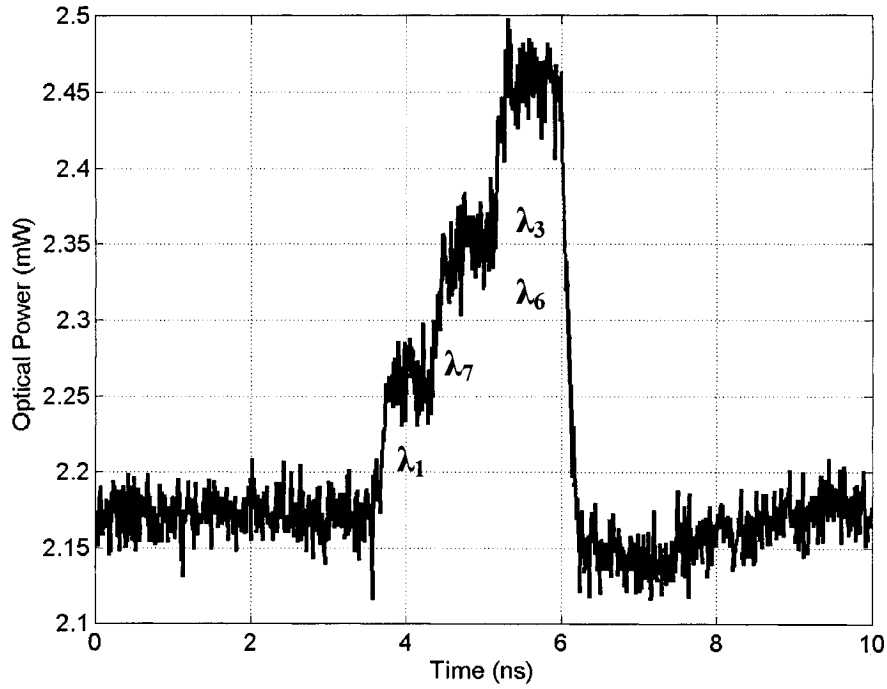
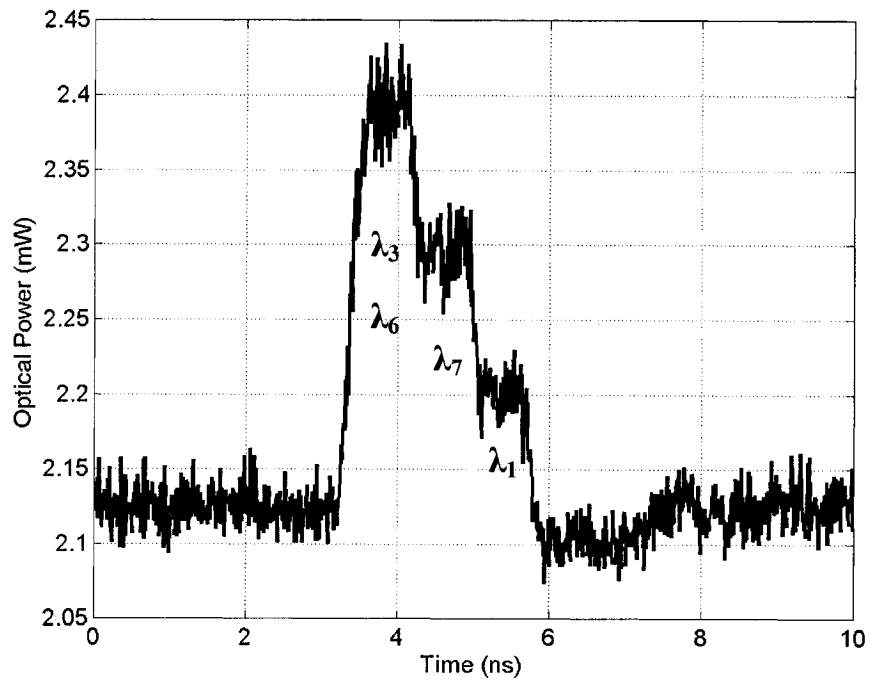


Fig. 4.8 Wavelength characteristics of desired encoder and decoder

Fig. 4.9 illustrates the time characteristics of (a) the desired user, and (b) the decoder.



(a)



(b)

Fig. 4.9 Time characteristics of (a) the desired user, and (b) the decoder

Clearly time chip misalignments are present. In Fig. 4.9 (a), we notice that the  $\lambda_1$  and  $\lambda_7$  peaks of optical power are not of equal value, as they should be according to Fig. 4.4 (a). This is due to  $\lambda_1$  having a positive time misalignment and  $\lambda_3$  and  $\lambda_6$  having both negative time misalignments (refer to Appendix B). This results in having optical power from time chips 1 and 3 leaking into time chip 2. This is further exemplified in Fig. 4.10, where illustrations of the desired encoded signal with missing wavelength components are presented.

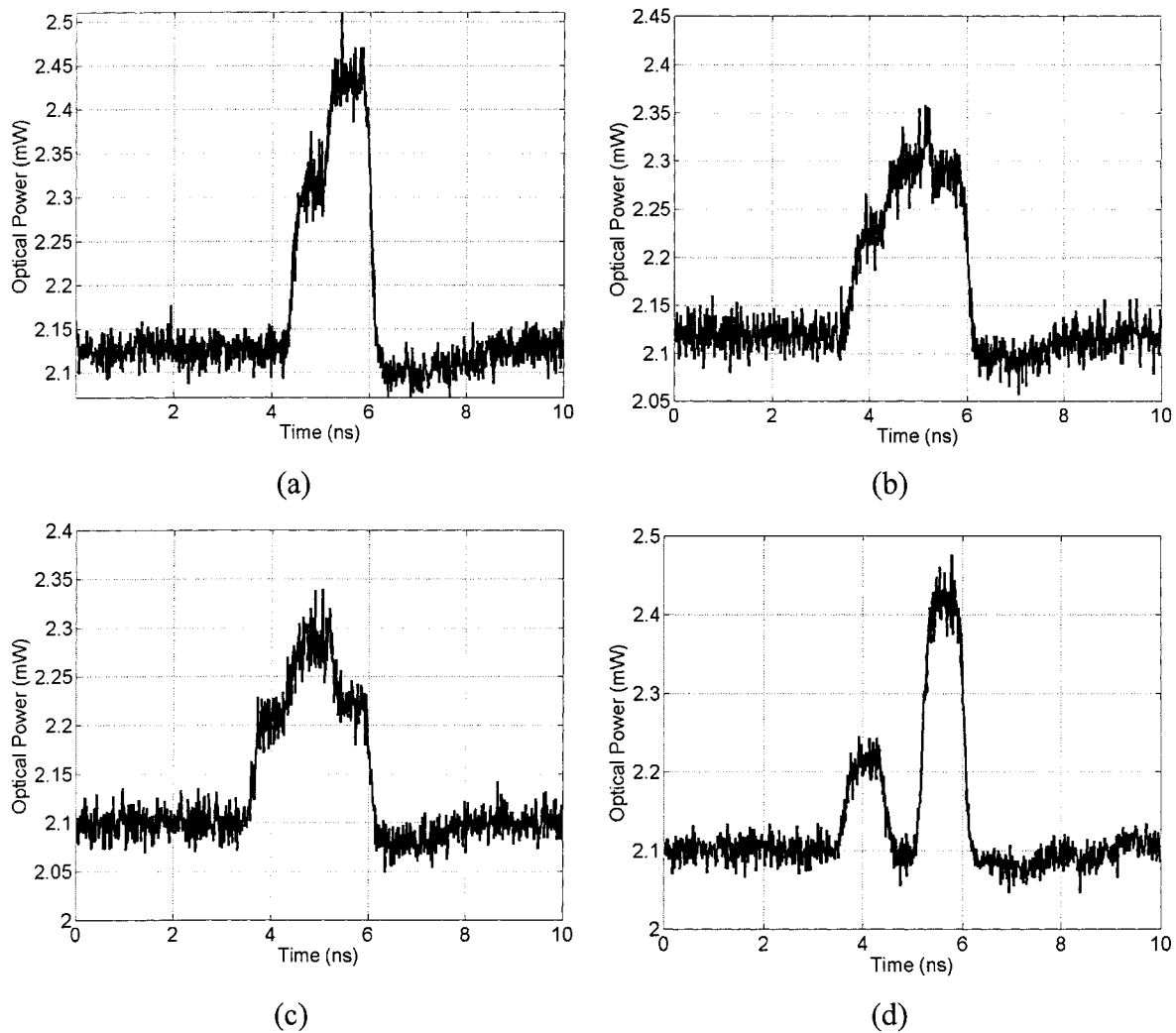
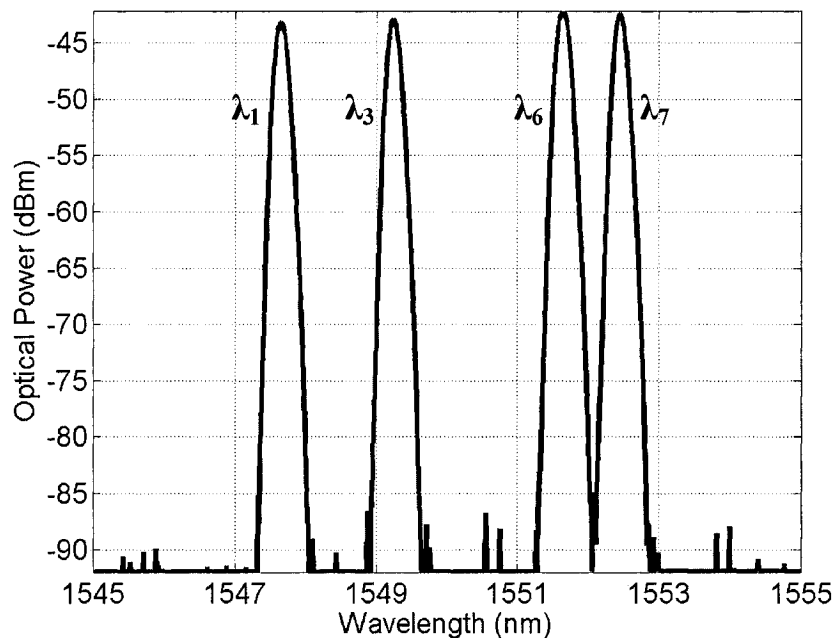


**Fig. 4.10** The desired encoded code with (a)  $\lambda_1$ ; (b)  $\lambda_3$ ; (c)  $\lambda_6$ ; (d)  $\lambda_7$  missing

By chance, the time misalignments present in the decoder are opposite to those of the desired encoder. That is,  $\lambda_1$  suffers from a negative time misalignment, while  $\lambda_3$  and

$\lambda_6$  both suffer positive time misalignments. The end result is that the total time misalignment of the desired encoder and decoder pair for each of the 4 wavelengths is between -5 ps and 10 ps, which is -0.625% and 1.25% off target. The wavelength and time characteristics of the decoded signal are presented in Fig. 4.11. The reconstructed auto-correlation peak is shown in Fig. 4.11 (b). The measured FWHM is 810 ps and the extinction is 3.17 dB. Note that, compared to the input pulse, the reconstructed pulse has the same FWHM duration, its amplitude is decreased and there is more noise present. The added noise is due to the use of EDFAs to compensate for losses. Note that the plot in Fig. 4.11 (a) is sensitivity limited.



(a)

Fig. 4.11 (a) Wavelength characteristics and (b) time characteristics of the desired decoded signal

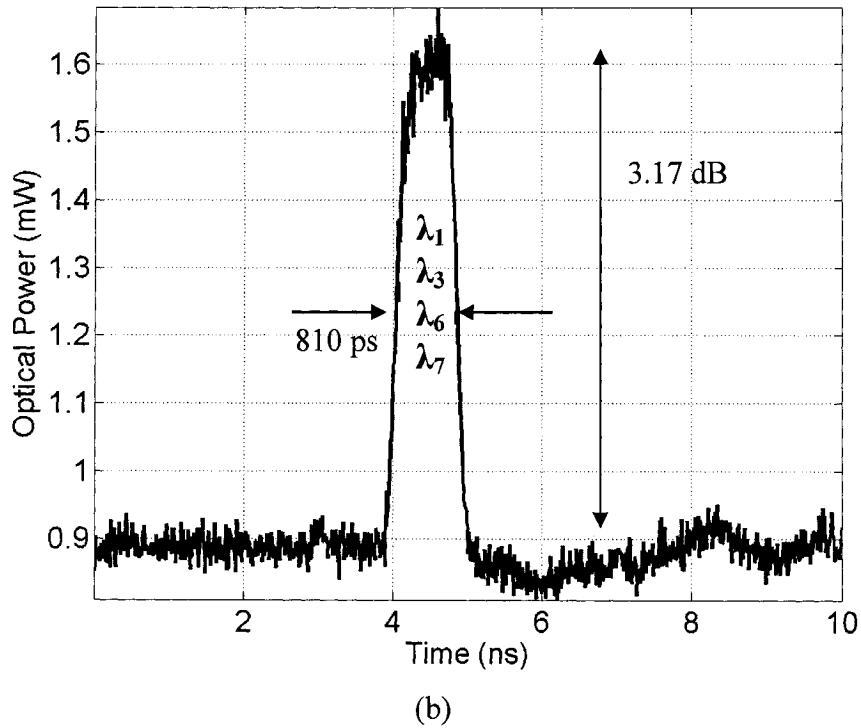
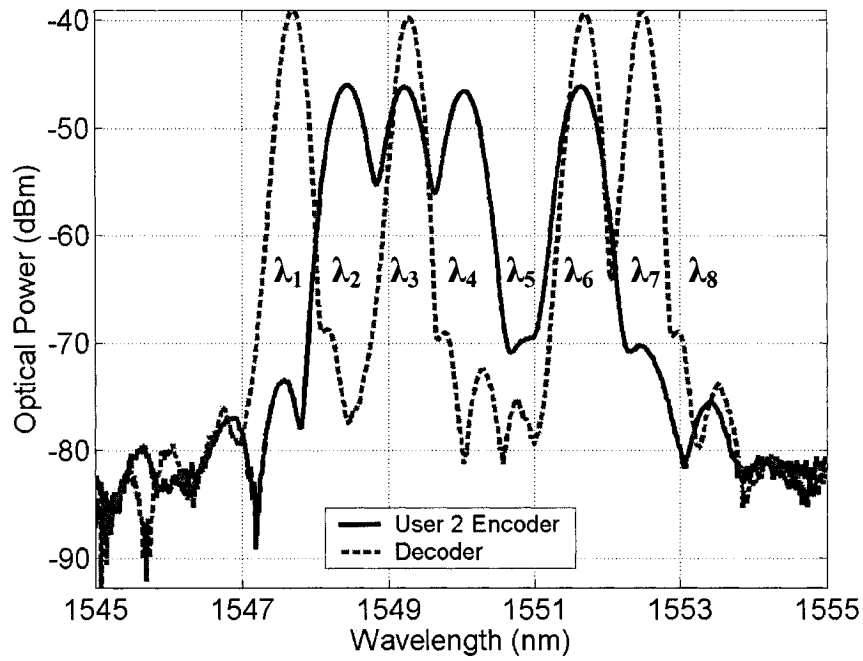


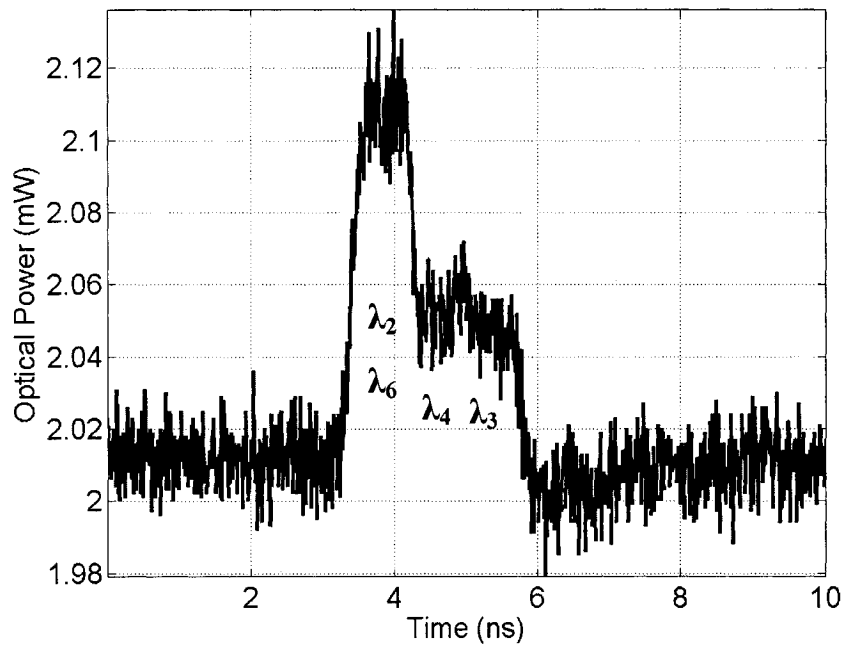
Fig 4.11 (cont.) (a) Wavelength characteristics and (b) time characteristics of the desired decoded signal

#### 4.2.3.2 User 2 encoder

The first interferer we examine is user 2. Its wavelength characteristics are displayed in Fig. 4.12 (a) and its time characteristics in Fig. 4.12 (b).



(a)



(b)

Fig. 4.12 (a) Wavelength characteristics and (b) time characteristics of user 2

The spectral characteristics of user 2 is as anticipated, however the power levels of the peaks are 7 - 8 dB lower than user 1. From Fig. 4.12 (b), we also note that the

noise floor of the signal is lower than the noise floor of user 1 (Fig. 4.9 (a)). As a result, an EDFA dedicated to user 2 was used to ensure that its power level is similar to those of the other users.

As for time misalignments,  $\lambda_6$  suffers from a positive time misalignment and  $\lambda_3$  suffers from a negative time misalignment, resulting in having power from time chips 1 and 3 leaking into time chip 2. Fig. 4.13 presents the temporal signal of user 2 with missing wavelength components. Finally, Fig. 4.14 depicts the waveform after decoding is performed. Due to unmatched filtering, both  $\lambda_2$  and  $\lambda_4$  are rejected and  $\lambda_3$  and  $\lambda_6$  are spread.

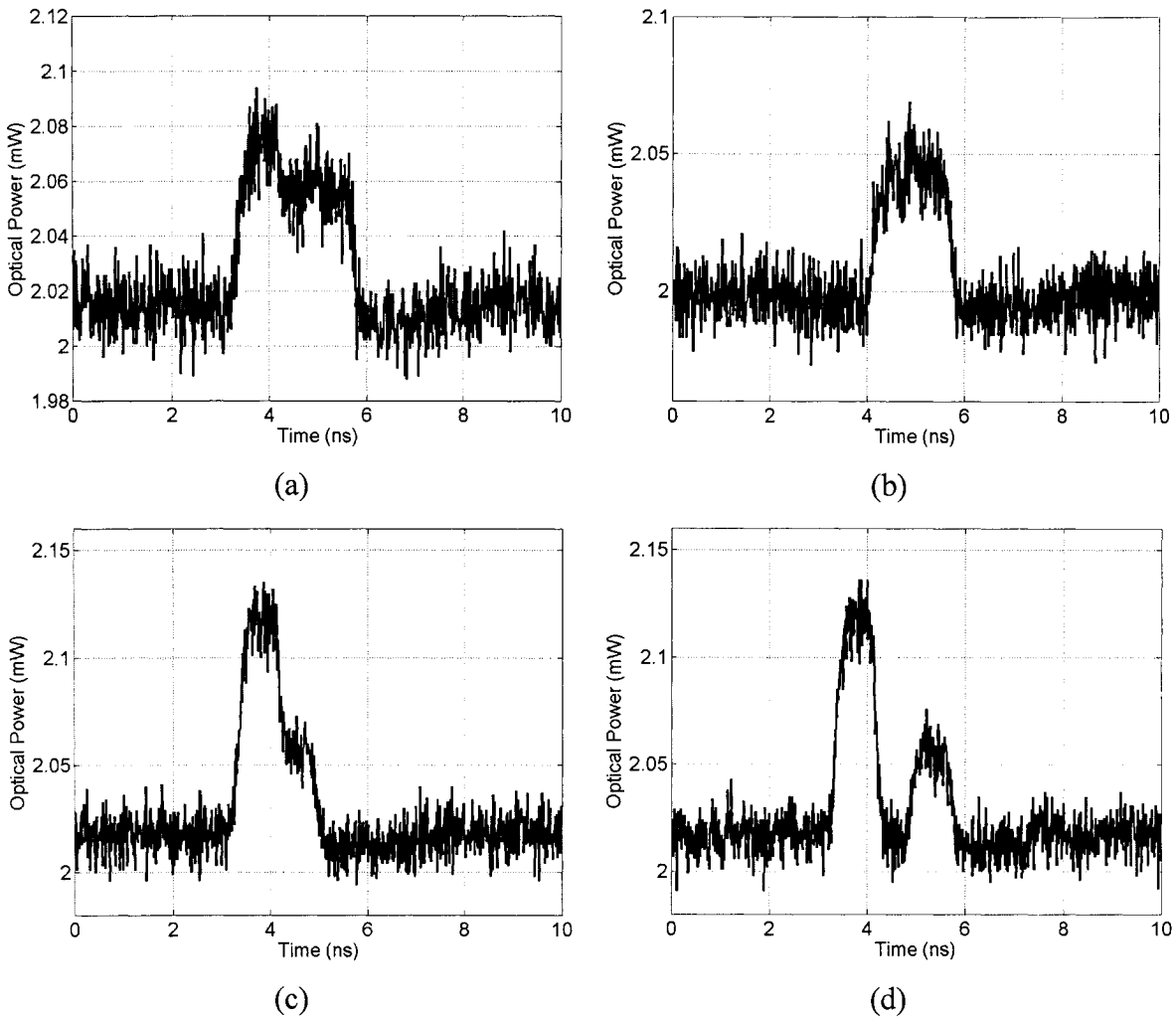
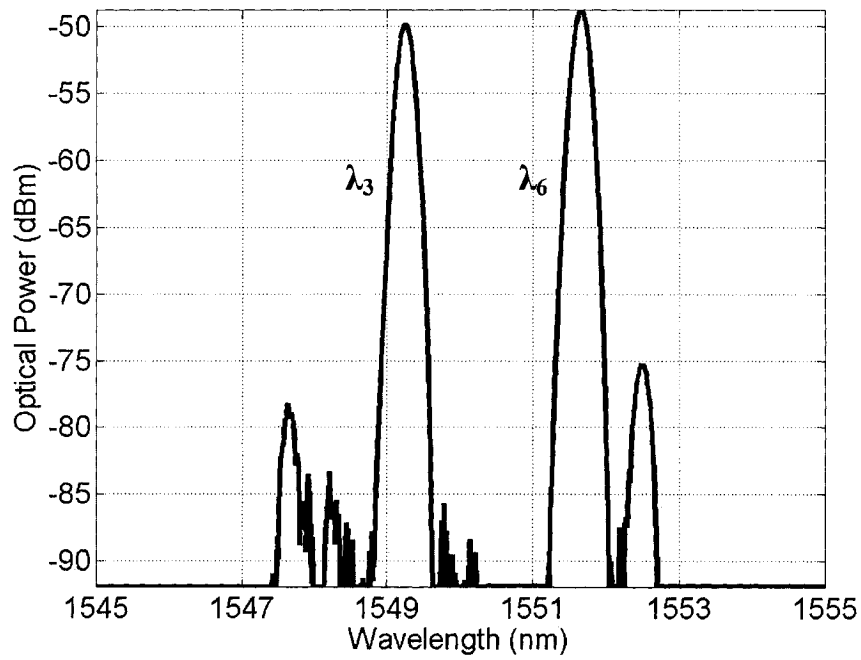
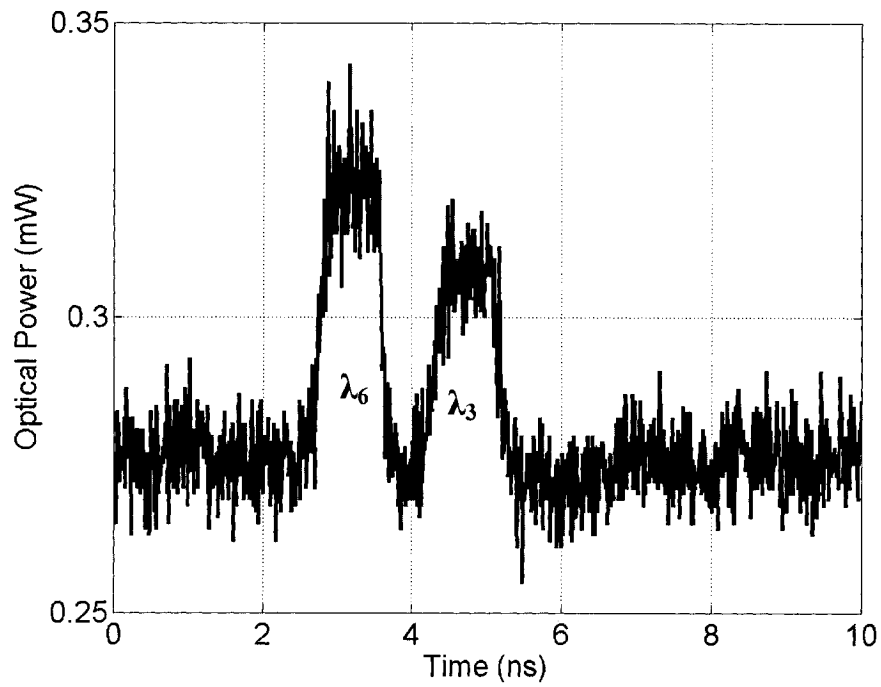


Fig. 4.13 User 2 encoded code with (a)  $\lambda_2$ ; (b)  $\lambda_2$  and  $\lambda_6$ ; (c)  $\lambda_3$ ; (d)  $\lambda_4$  missing



(a)

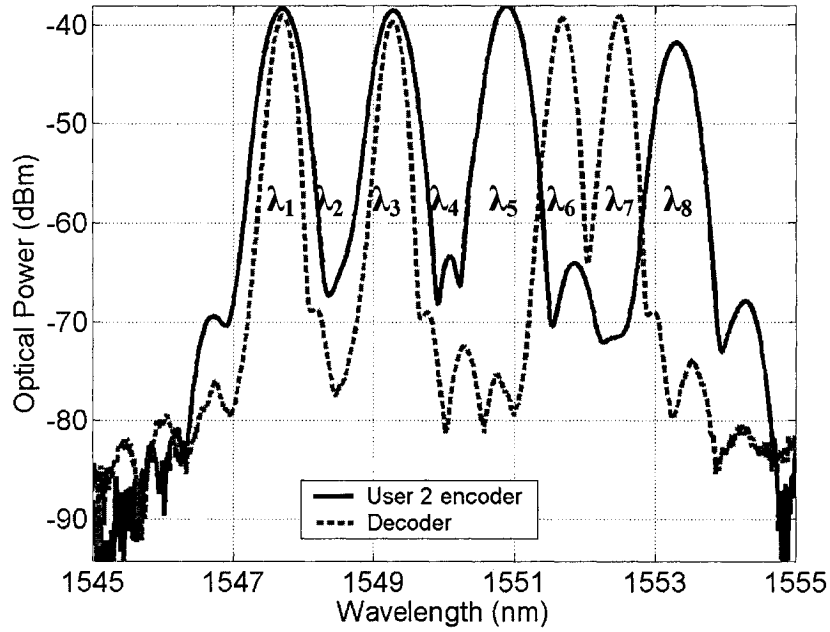


(b)

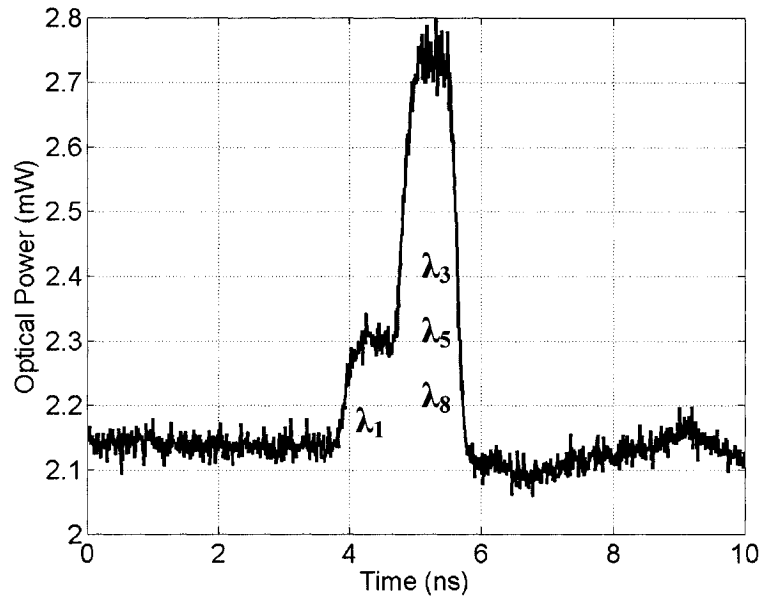
Fig. 4.14 (a) Wavelength characteristics and (b) time characteristics of the user 2 decoded signal

### 4.2.3.3 User 3 encoder

User 3 is the second interferer to be investigated. Its wavelength characteristics are presented in Fig. 4.15 (a) and its time characteristics in Fig. 4.15 (b).



(a)



(b)

Fig. 4.15 (a) Wavelength characteristics and (b) time characteristics of user 3

The spectral response for user 3 is as expected and with the exception of  $\lambda_8$ , its power level is consistent with that of user 1. The  $\lambda_8$  component of user 3 is 3.6 dB lower than  $\lambda_1$ ,  $\lambda_3$ , and  $\lambda_5$ , and will be left as is.

Regarding time misalignments, only  $\lambda_1$  is misaligned with respect to  $\lambda_3$ ,  $\lambda_5$ , and  $\lambda_8$ . It suffers from a negative misalignment, resulting in some power of time chip 1 leaking into time chip 0. This is better illustrated in Fig. 4.16 where the temporal waveform is shown with  $\lambda_3$  and  $\lambda_5$  missing. The misalignment is also visible in Fig. 4.17 (b), which presents the wavelength and time characteristics of the user 3 decoded signal. The decoder rejects  $\lambda_5$  and  $\lambda_8$ , and spreads  $\lambda_1$  by 3 time chips and  $\lambda_3$  by 1 time chip, see Fig. 4.17. As a result, the decoded signal has the  $\lambda_1$  component after  $\lambda_3$  in time. Due to the negative misalignment of  $\lambda_1$ , there should be a narrow peak in the middle of the  $\lambda_1$  and  $\lambda_3$  components, and this is indeed visible in Fig. 4.17 (b).

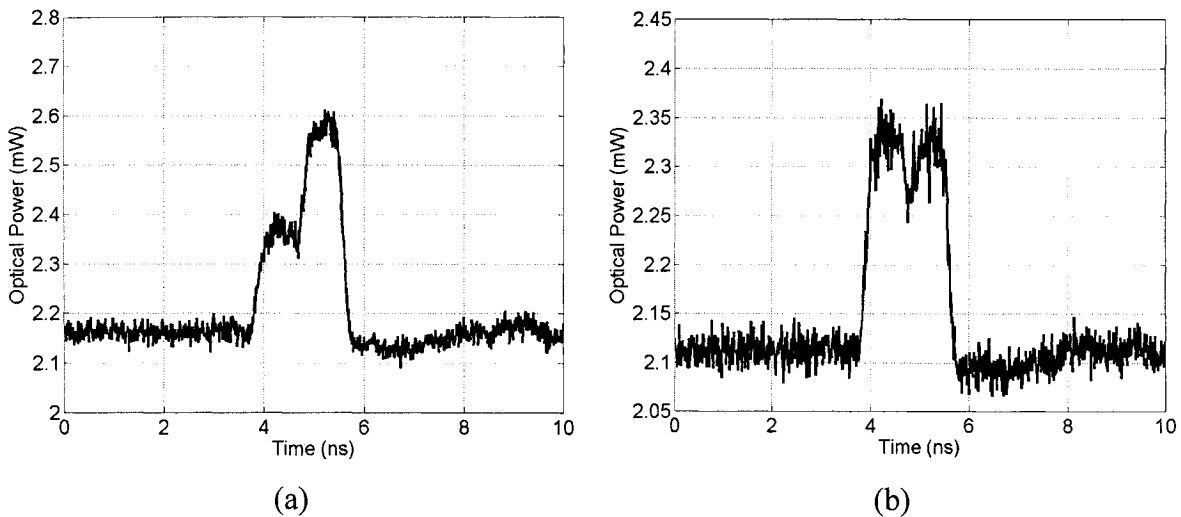
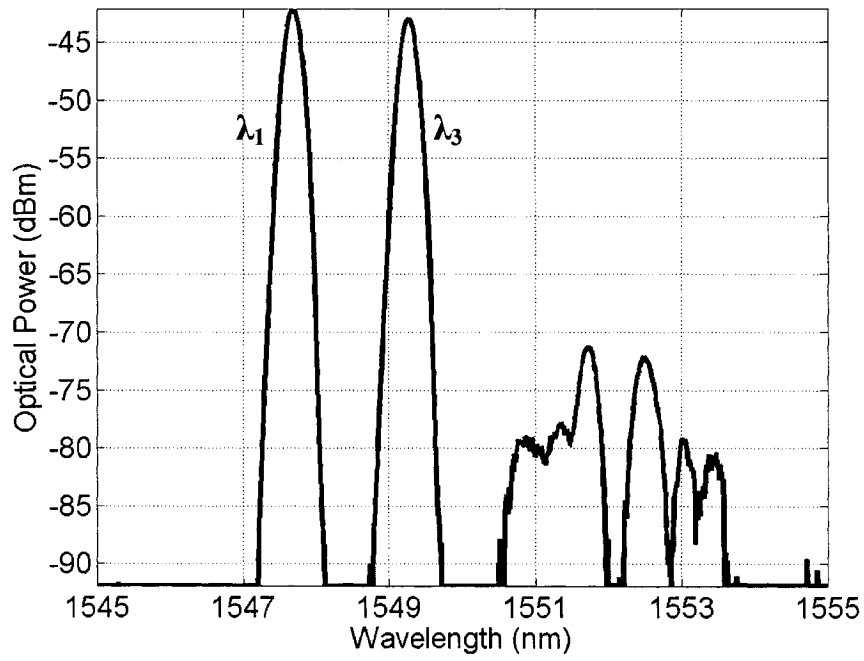
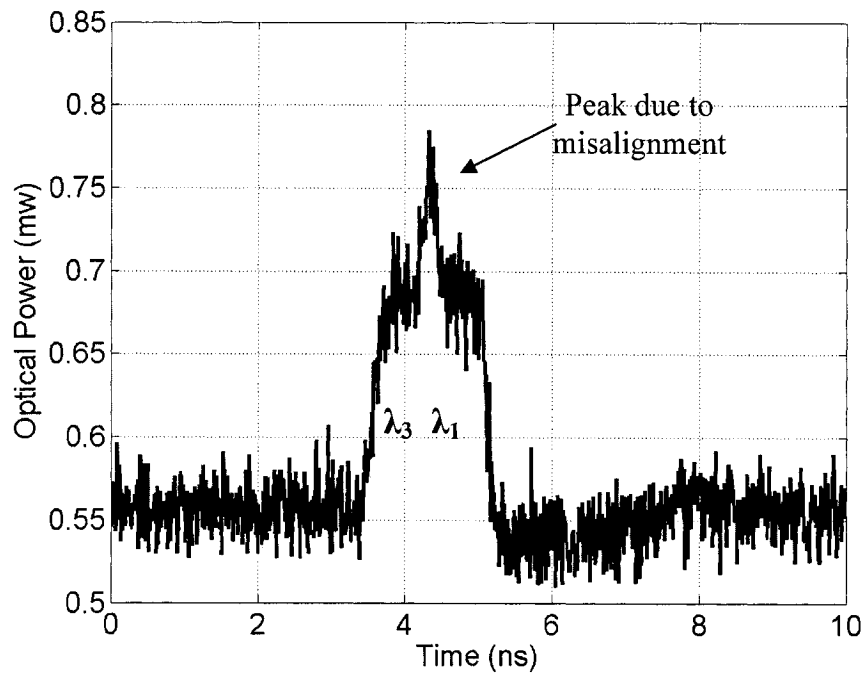


Fig. 4.16 User 3 encoded code with (a)  $\lambda_3$ ; (b)  $\lambda_3$  and  $\lambda_5$  missing



(a)

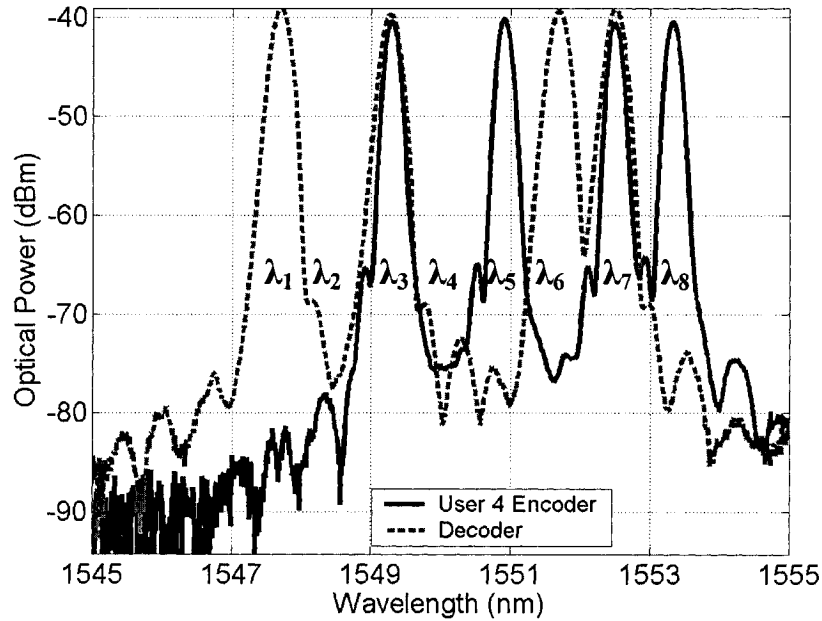


(b)

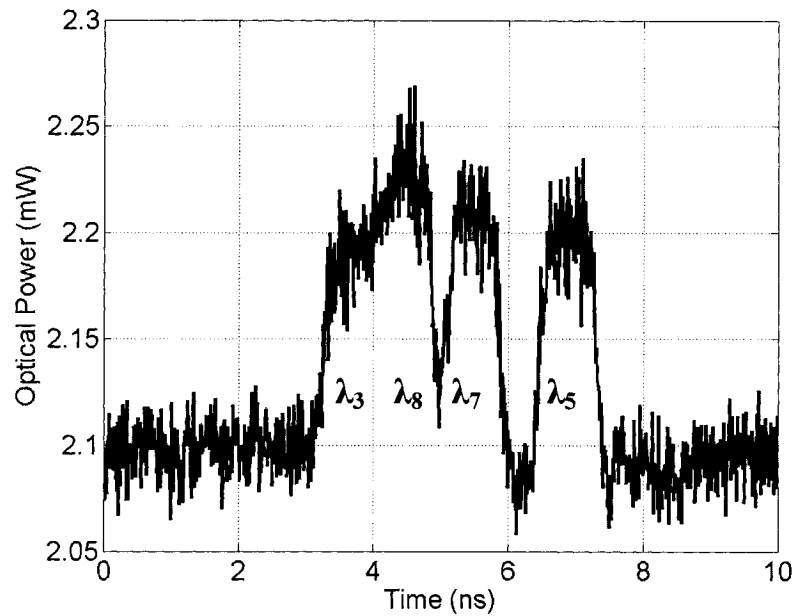
Fig. 4.17 (a) Wavelength characteristics and (b) time characteristics of the user 3 decoded signal

#### 4.2.3.4 User 4 encoder

The third and last interferer to scrutinize is user 3. Its wavelength characteristics are presented in Fig. 4.18 (a) and its time characteristics in Fig. 4.18 (b).



(a)



(b)

Fig. 4.18 (a) Wavelength characteristics and (b) time characteristics of user 4

The spectral response for user 4 is as projected and its power level is consistent with that of user 1.

Regarding time misalignments, only  $\lambda_8$  is misaligned with respect to  $\lambda_3$ ,  $\lambda_5$ , and  $\lambda_7$ ; it suffers from a negative misalignment, resulting in some power of time chip 2 leaking into time chip 1. This is better understood in Fig. 4.19 where the temporal waveform is shown with  $\lambda_3$ ,  $\lambda_5$ ,  $\lambda_7$  and  $\lambda_8$  missing. Finally, Fig. 4.20 presents the decoded signal of user 4. The decoder rejects  $\lambda_5$  and  $\lambda_8$ , and spreads  $\lambda_3$  and  $\lambda_7$ .

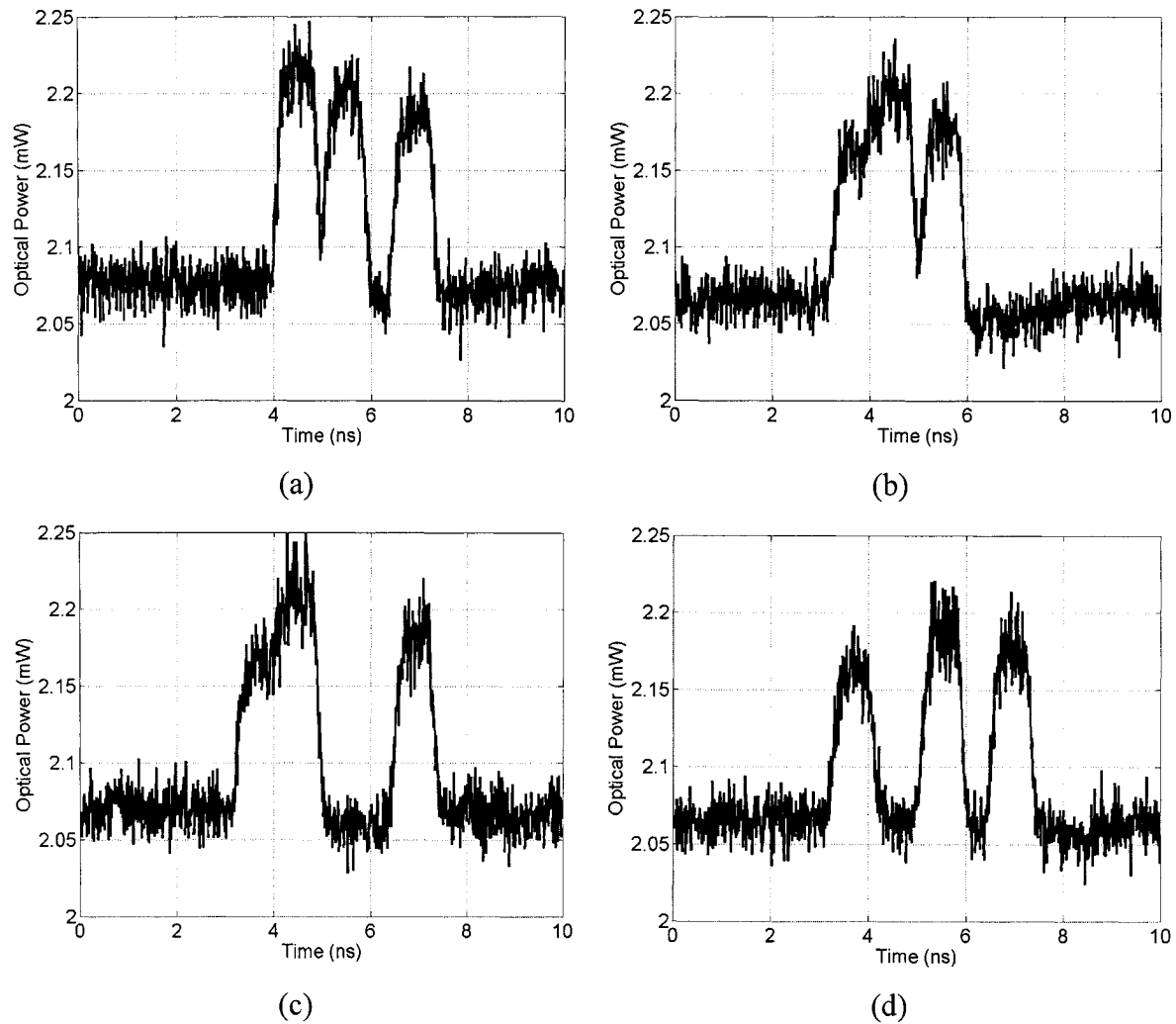
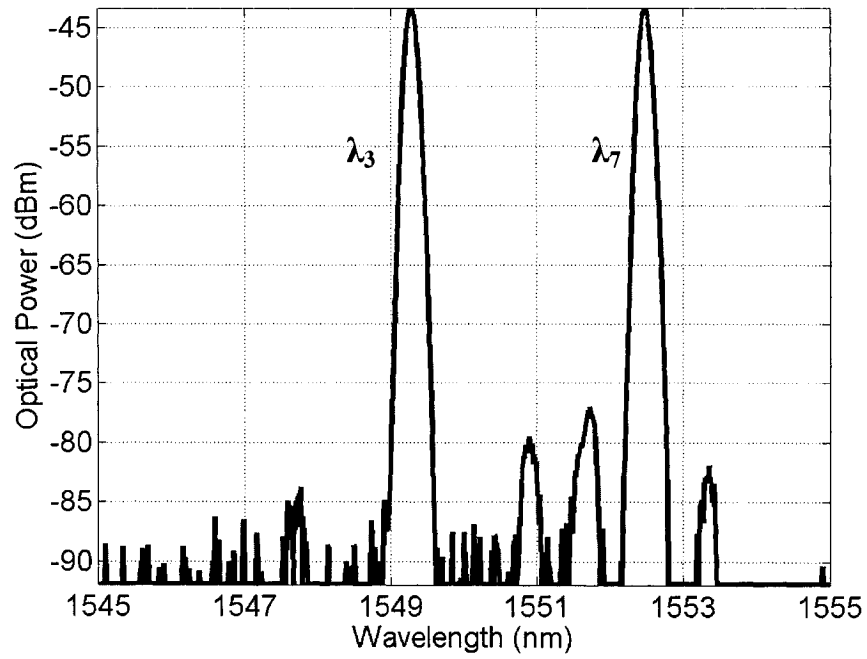
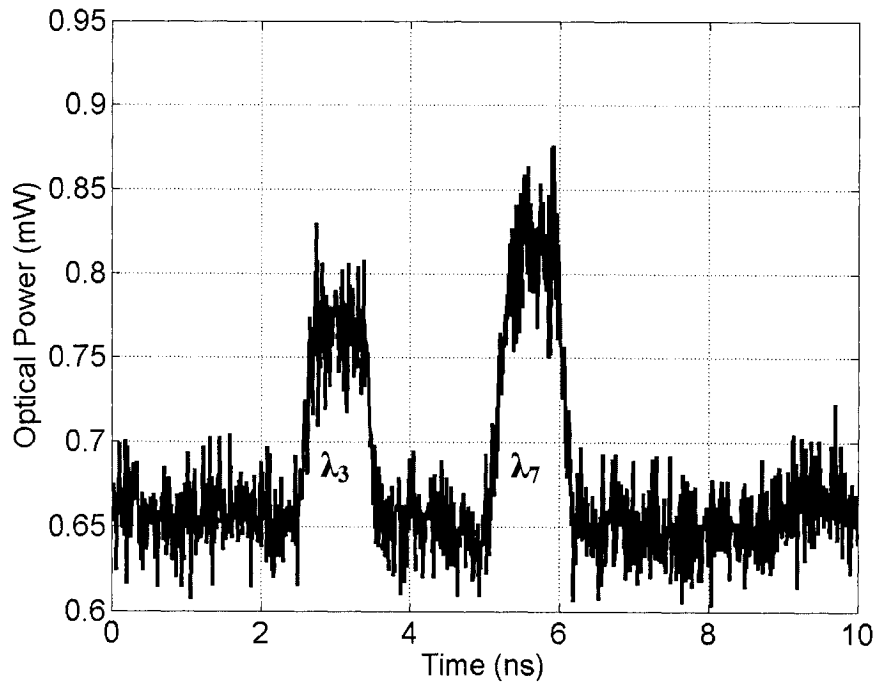


**Fig. 4.19** User 4 encoded code with (a)  $\lambda_3$ ; (b)  $\lambda_5$ ; (c)  $\lambda_7$ ; (d)  $\lambda_8$  missing



(a)



(b)

Fig. 4.20 (a) Wavelength characteristics and (b) time characteristics of the user 4 decoded signal

This concludes the testing of each individual encoder and decoder. The wavelength characteristics are as expected and the time misalignments are all within our set limits. Thus, we deem the implementation of the encoders and decoder to be a success.

### **4.3 Testing of full system**

#### **4.3.1 Sending a “1” bit and an arbitrary bit pattern**

The first full system test is to send a “1” bit and examine the encoding and decoding of the four separate “1” bits. Since the BBS is modulated at the chip rate and each bit is divided into 8 time chips, a “1” bit at the data rate is represented by a “10000000” pattern modulated at the chip rate. This will cause obvious complications when BER measurements are to be done at the data rate. The second test involves a repeated “11010011” bit pattern sent simultaneously by all encoders.

Fig. 4.21 illustrates the wavelength characteristics of the 4 codes multiplexed together before and after the decoder. The high noise level is due to the EDFA used to compensate the losses of encoder 2 (see 4.2.3.2). Fig. 4.22 (a) and (b) respectively show the encoded waveforms of the four “1” bits multiplexed together and the output signal from the decoder; the same plots for “11010011” bit patterns are presented in Fig. 4.23.

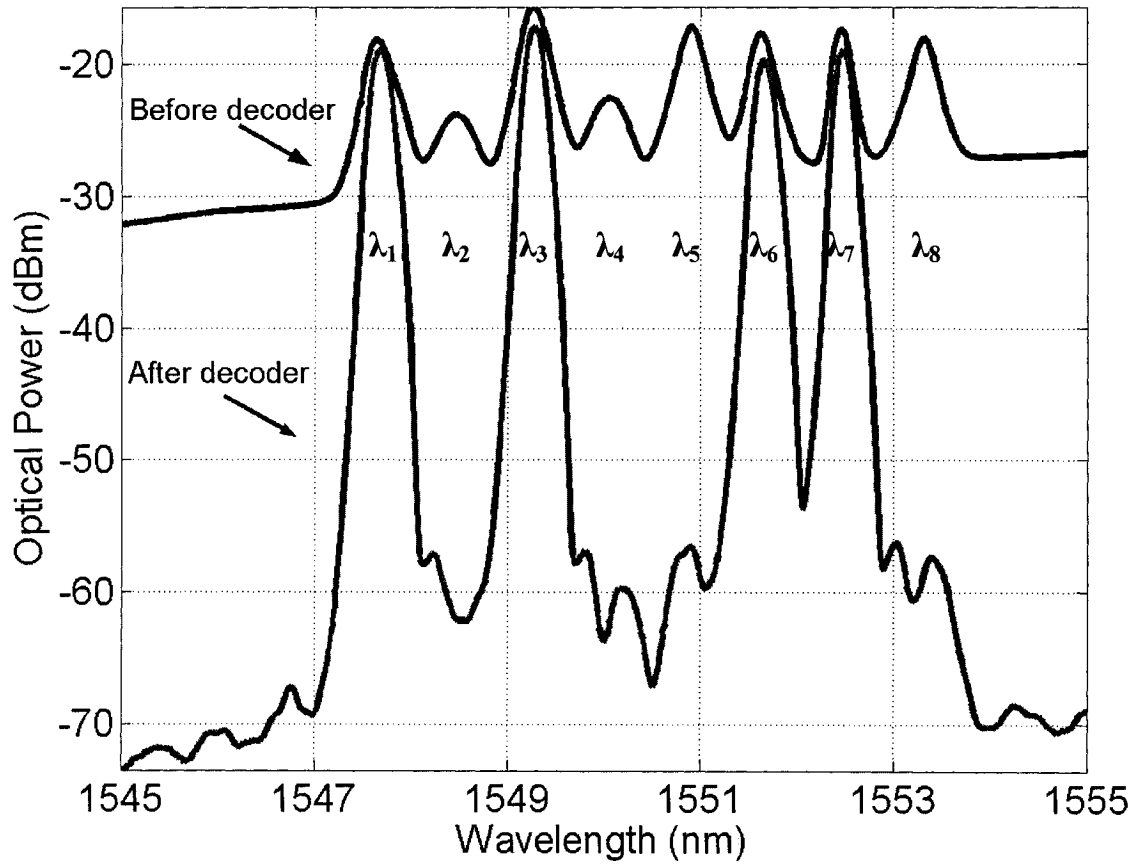
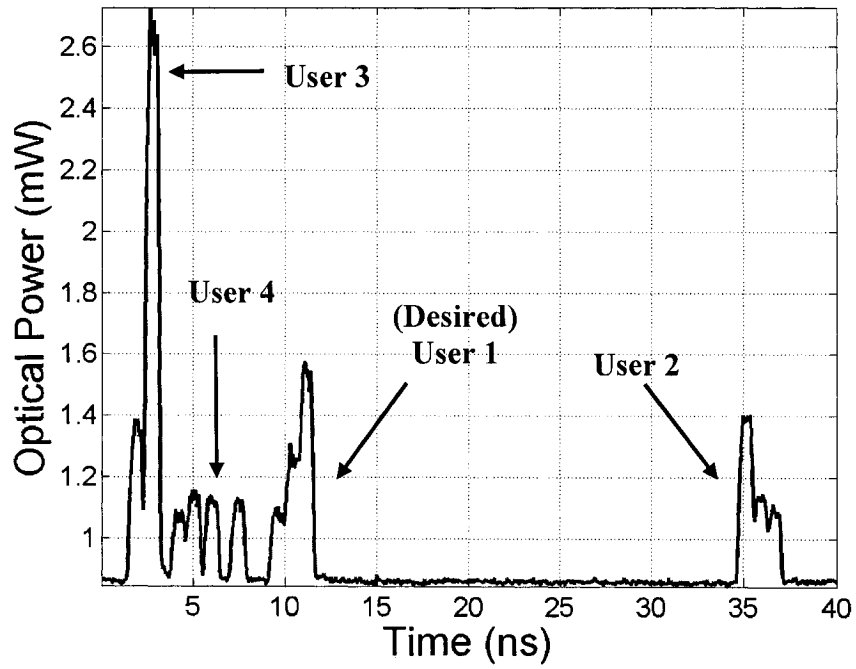
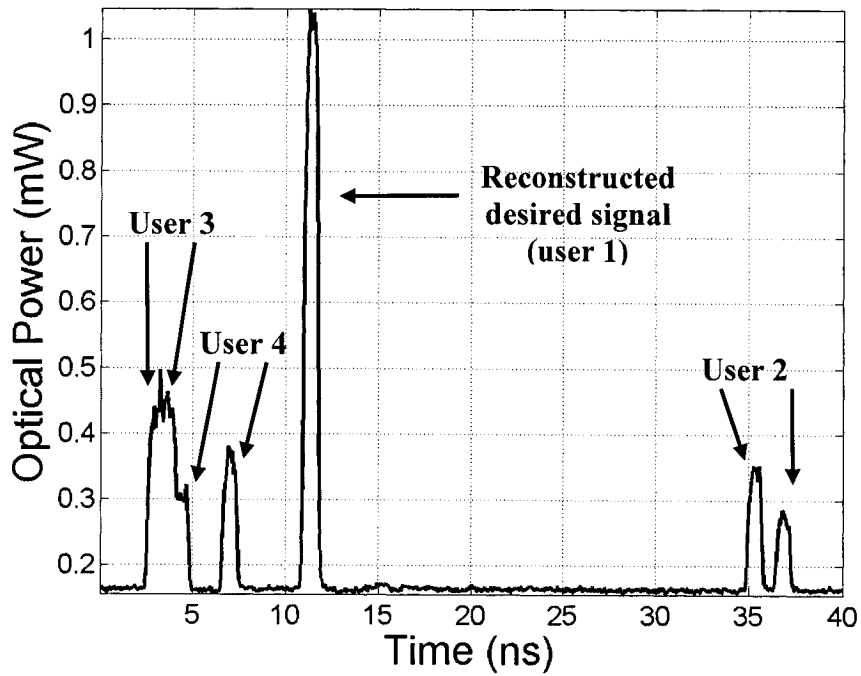


Fig. 4.21 Wavelength characteristics of all codes multiplexed together (top) before and (bottom) after the decoder

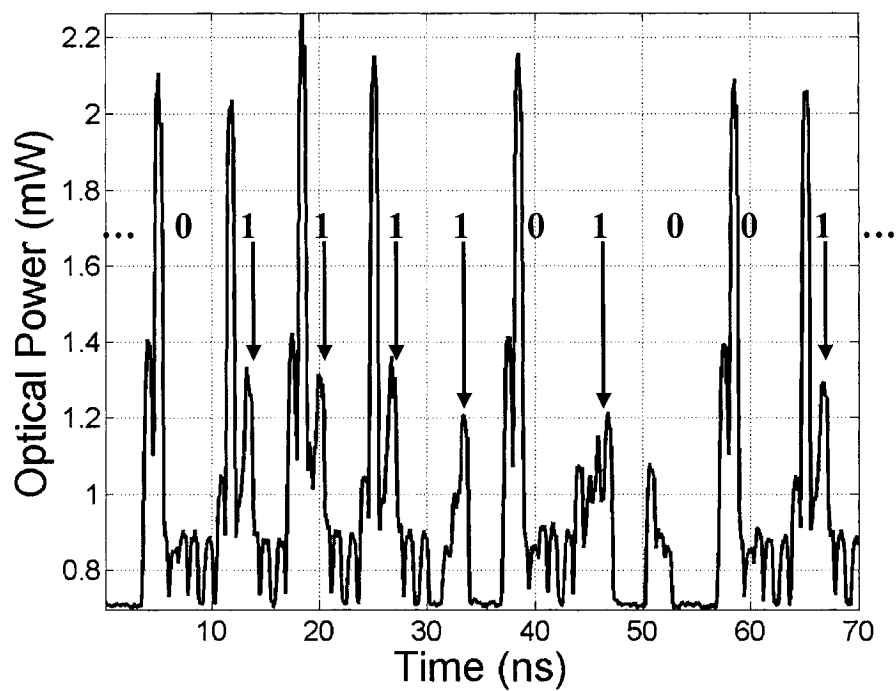


(a)

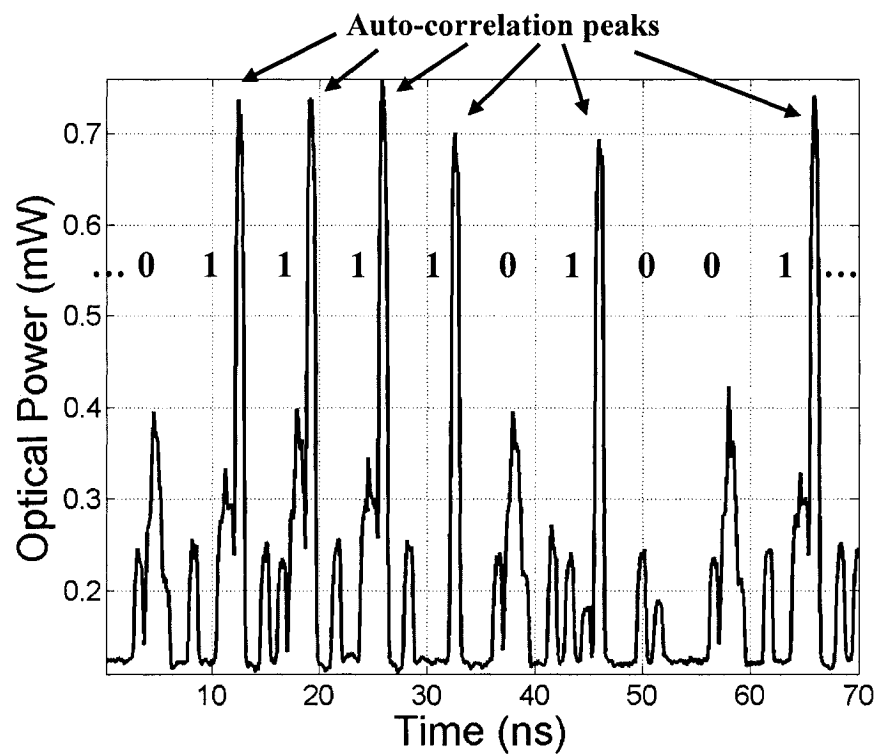


(b)

Fig. 4.22 Time characteristics of all codes multiplexed together (a) before and (b) after the decoder for a "1" bit



(a)



(b)

Fig. 4.23 Time characteristics of all codes multiplexed together (a) before and (b) after the decoder for a repeated "11010011" bit pattern

From the multiplexed signal spectrum plot in Fig. 4.21, we see that the wavelength components have different power levels. This is explained by noting that between the four codes,  $\lambda_2$  and  $\lambda_4$  are present only once (with user 2);  $\lambda_1$ ,  $\lambda_5$ ,  $\lambda_6$ ,  $\lambda_7$ , and  $\lambda_8$  are present twice, while  $\lambda_3$  is common to all four codes. Furthermore, even though an EDFA is used to boost the power of user 2, its power level is still about 1 dB less than the three other users, hence contributing to  $\lambda_2$  and  $\lambda_4$  having less power. Due to the coarse setting available on the EDFA, if we were to boost further the power of user 2, its power would have been too high. Also note that the widths of all wavelengths are not constant. This is a consequence of the WDMs not all having the exact same spectral responses.

The decoded signal spectrum in Fig. 4.21 confirms that only the four wavelengths of the desired user are kept. Note that two wavelengths of each of the remaining four users ( $\lambda_3$  and  $\lambda_6$  of user 2;  $\lambda_1$  and  $\lambda_3$  of user 3;  $\lambda_3$  and  $\lambda_7$  of user 4) are also retained and contribute to the optical power and MAI. An EDFA was used after the decoder to make up the insertion loss of the decoder. The rejection of each unwanted wavelength is 38 dB for  $\lambda_2$ , 37 dB for  $\lambda_4$ , 48 dB for  $\lambda_5$ , and 42 dB for  $\lambda_8$ .

We can clearly identify each of the four encoders in Fig. 4.22 (a); Fig. 4.22 (b) confirms that the reconstructed desired signal (auto-correlation peak) is indeed distinguishable from the MAI. The cross-correlation pulses in the decoded waveform correspond to the interfering wavelengths that are picked up by the decoder. Even when many bits are sent, as illustrated in Fig. 4.23, the auto-correlation peaks remain clearly distinguishable. Note however, that in a worst case scenario where cross-correlation pulses of many interferers superimpose in a time chip, the auto-correlation peak will be less distinguishable from the MAI and errors can occur.

### 4.3.2 Effects of chromatic dispersion

It is also of importance to examine the effects of dispersion on our OCDMA system. Since multiple wavelengths are used for encoding, we expect that our OCDMA system is sensitive to chromatic dispersion. Fig. 4.24 (a) presents all four encoded “1”

bits after propagating through 7.4 km of single-mode fiber, and Fig. 4.24 (b) shows the decoded waveform.

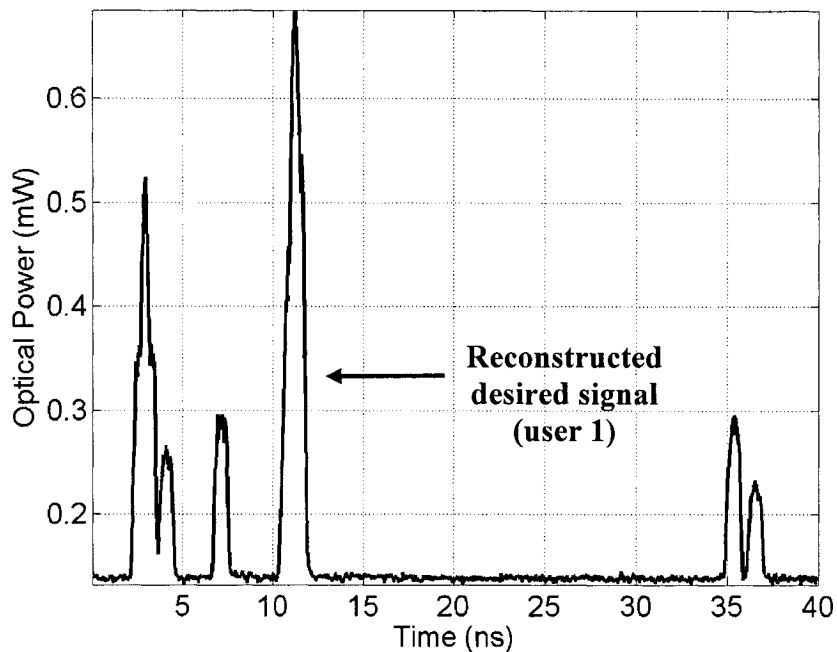
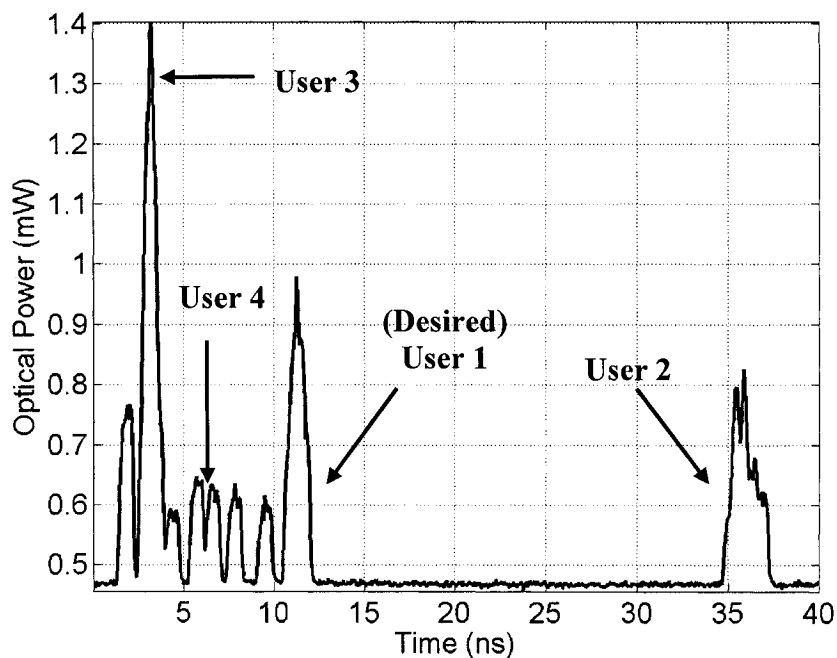


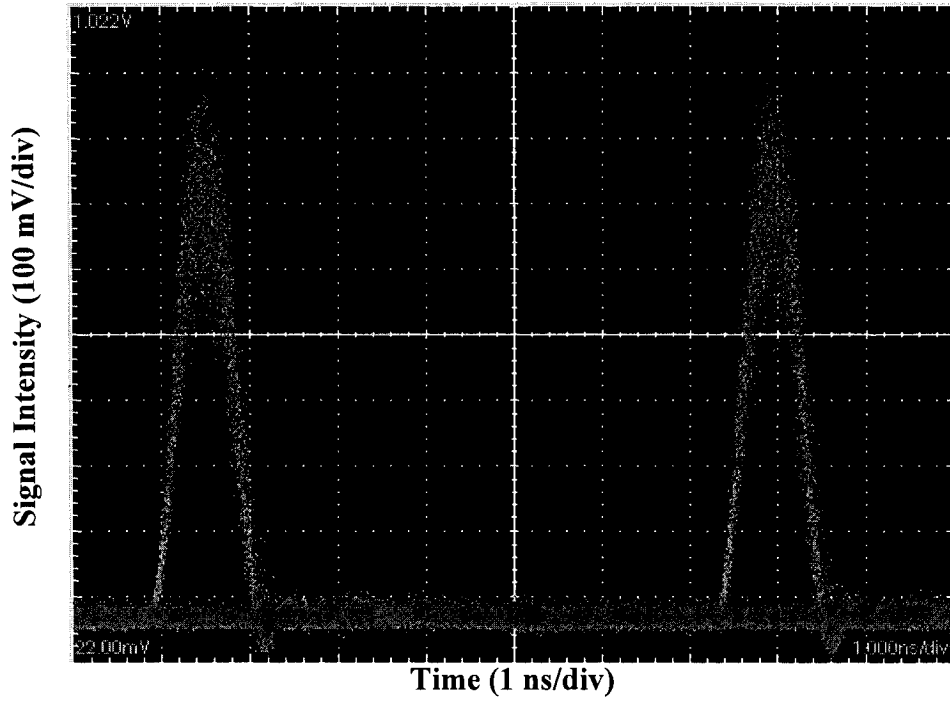
Fig. 4.24 Time characteristics of all codes multiplexed together after propagating through 7.4 km of single-mode fiber (a) before and (b) after the decoder for a "1" bit

As expected, chromatic dispersion deteriorates the performance of the OCDMA system since the wavelength components of the codes are no longer well aligned in their appropriate time chips. This causes time misalignments between the encoders and the decoder. As a result, the auto-correlation peak has a lower power level and the signal width is approximately 1000 ps, which is 180 ps more than the non-dispersed signal duration. Another result is that the cross-correlation pulse from user 3 has a higher power level since its two wavelength components become superimposed instead of being spread. This makes the task of distinguishing the auto-correlation peak among the MAI even more difficult.

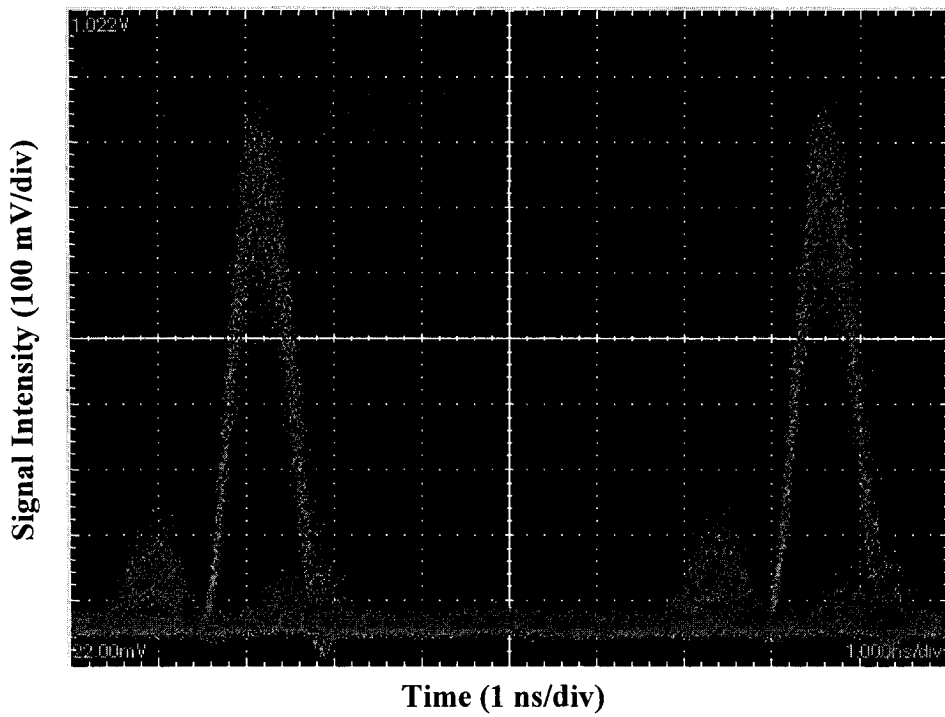
If the pulses were to propagate through more fiber, the auto-correlation peak would further worsen while cross-correlation pulses of other users could complicate the distinguishing of the auto-correlation peak. Consequently, chromatic dispersion has to be managed. Dispersion compensation fiber (DCF) can be used to perform dispersion compensation before the decoder. Pre-compensation can also be used whereby the decoder time delays are readjusted to account for dispersion [48]. Another alternative is to operate at the zero dispersion wavelength near 1300 nm.

### 4.3.3 Eye diagrams and BER measurements

We now investigate our OCDMA signal using a 1.5 GHz photo-detector. Fig. 4.25 presents eye diagrams of the decoded waveforms for: (a) only the desired signal; (b) the desired signal and user 2; (c) the desired signal and user 3; (d) the desired signal and user 4; and (e) all users. All eye diagrams are measured at the data rate using a pseudo random bit sequence (PRBS) of  $2^7-1$  (128) bits. They are all of 10 ns span and use sample mode with 10 second persistence. Due to the subtle issue of each “1” bit being represented by a “10000000” pattern at the chip rate, the PRBS was manually entered in both the pattern generator and error detector. It is realized that using a PRBS of 128 bits does not stress a system to the standards that are typically done today; however, for the purpose of preliminary testing and due to the data/chip rate issue, it is satisfactory.

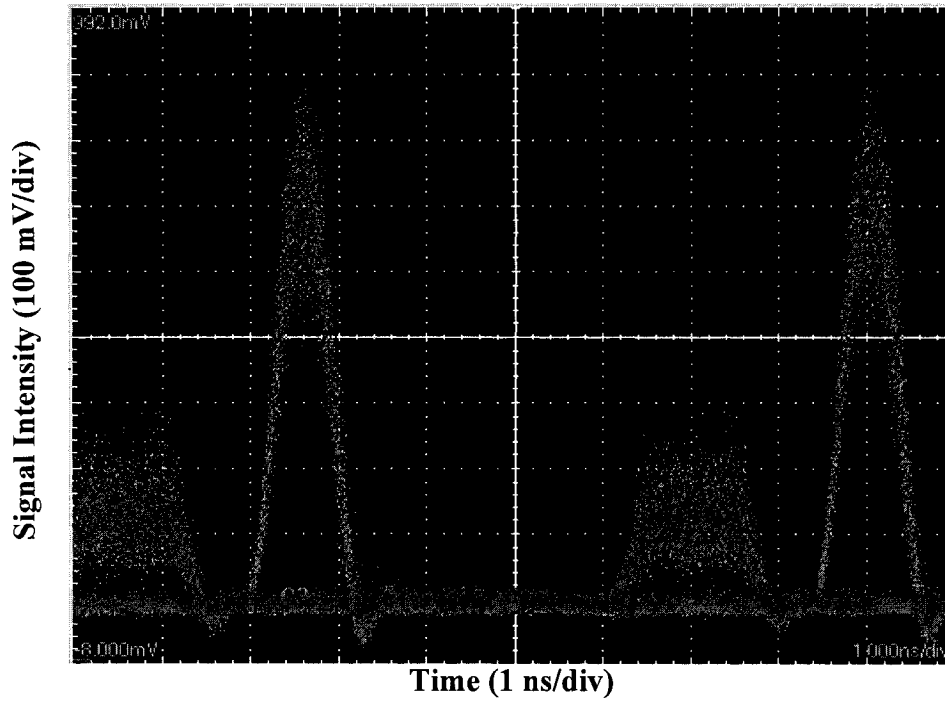


(a)

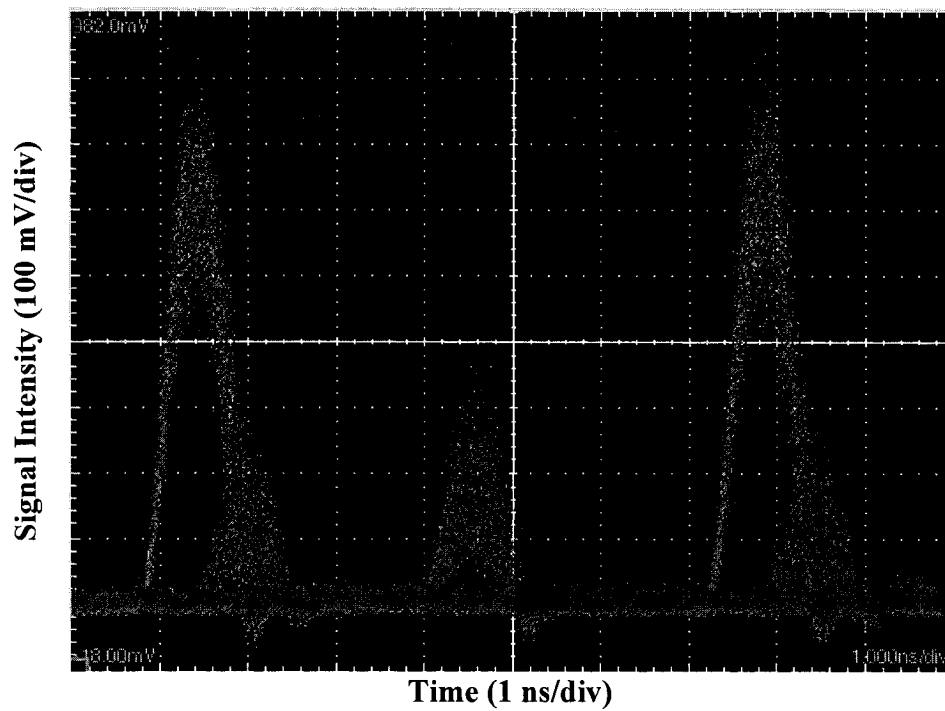


(b)

Fig. 4.25 Eye diagram of decoded waveform of: (a) only the desired signal; (b) the desired signal and user 2; (c) the desired signal and user 3; (d) the desired signal and user 4; and (e) all users



(c)



(d)

Fig. 4.25 (cont.) Eye diagram of decoded waveform of: (a) only the desired signal; (b) the desired signal and user 2; (c) the desired signal and user 3; (d) the desired signal and user 4; and (e) all users

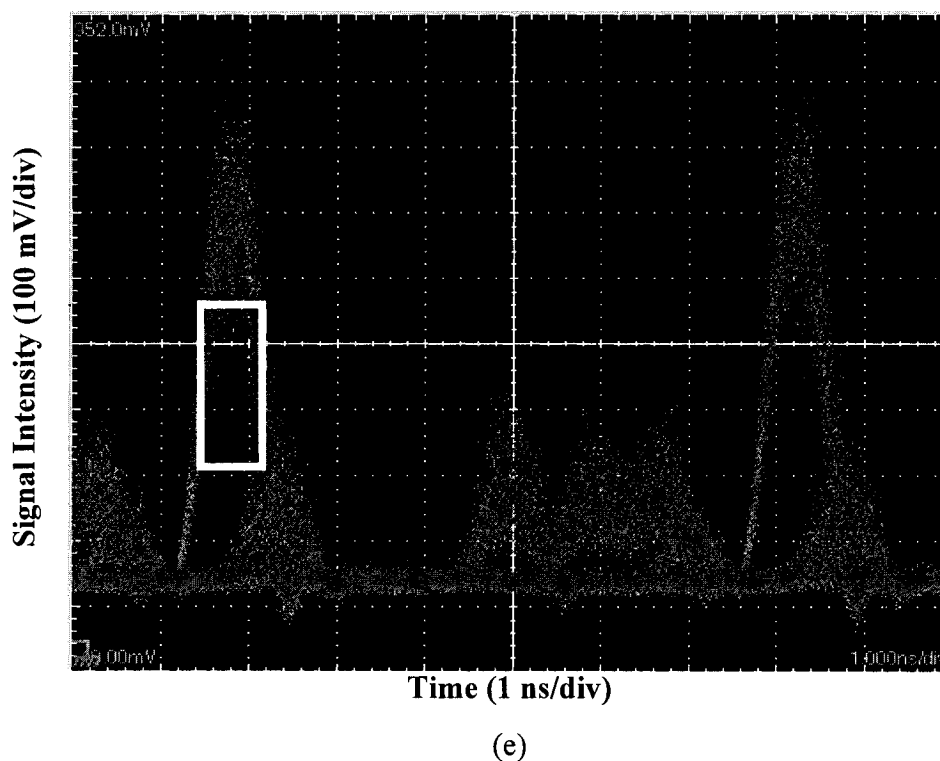


**Fig. 4.25 (cont.)** Eye diagram of decoded waveform of: (a) only the desired signal; (b) the desired signal and user 2; (c) the desired signal and user 3; (d) the desired signal and user 4; and (e) all users (the square box illustrates the eye opening of the desired signal)

The eye diagrams show a desired user with a clear eye opening. With only the desired user present, the eye has a vertical opening of approximately 500 mV (measured from base to bottom of “1” rail), while its width at the half maximum is 810 ps and 1000 ps at the base. When all interferers are present, the eye of the desired user closes slightly and has a vertical opening of approximately 400 mV. Since cross-correlation peaks are present in the same time chip as the auto-correlation peak, the opening of the desired eye is in fact, roughly 200 mV.

A BER measurement at the data rate was taken at all five instances. The measurements were made with the global clock from the PPG (at the chip rate) that was connected to a “divide-by-8” circuit in order to obtain the data rate. Fig. 4.26 presents the BER as a function of the received average optical power for all five different cases. The output of the O/E converter is directly connected to the error detector. For each separate case, the detection level is set at a constant value for all optical power levels launched in the O/E converter.

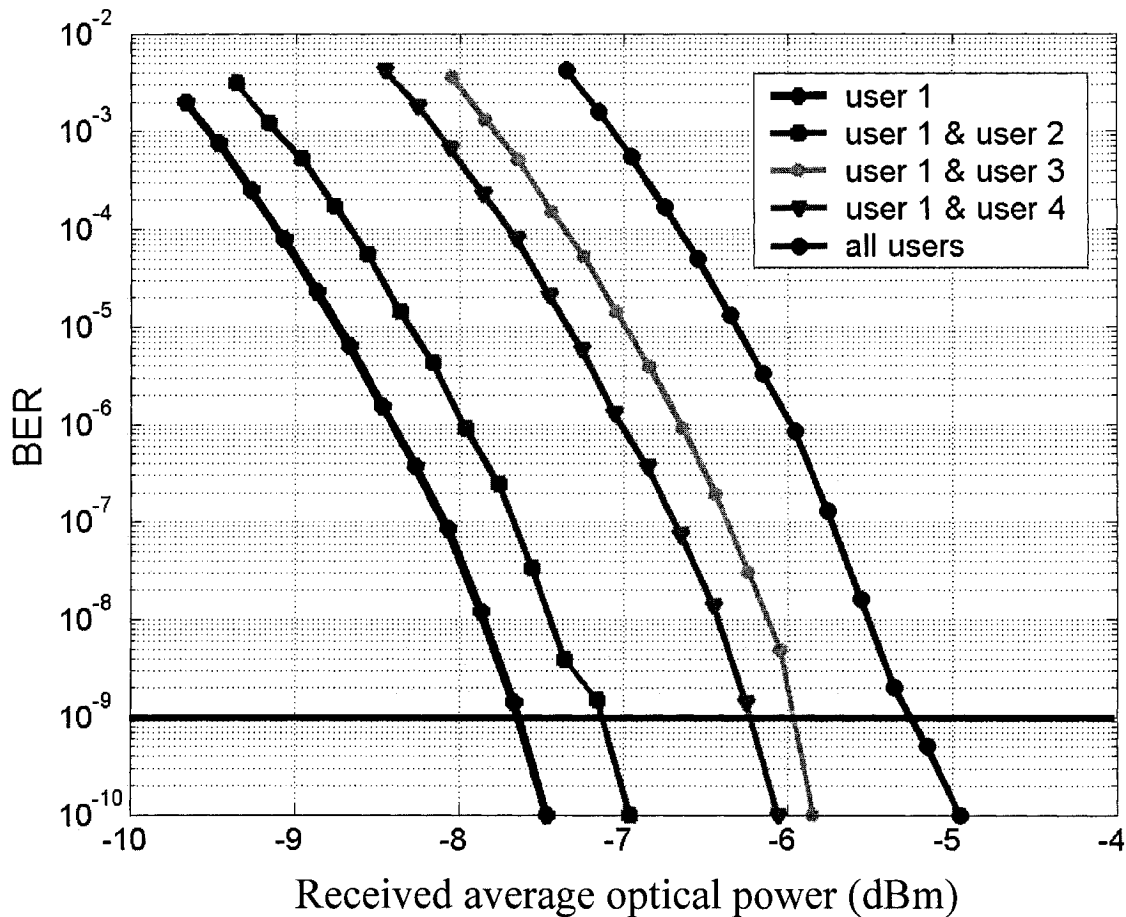


Fig. 4.26 BER as a function of the average optical power launched in the O/E converter; from left to right: user 1 alone; users 1 and 2; users 1 and 4; users 1 and 3; all users

The BER results are consistent with the eye diagrams, and power penalties are increased as interferers are added. At a BER of  $10^{-9}$ , the power penalty of only user 2 is 0.5 dB, only user 3 is 1.6 dB, only user 4 is 1.4 dB, and 2.3 dB when all users are present. We expect additional power penalties if longer PRBS are used. However, for this preliminary measurement, it is encouraging that a BER of  $10^{-9}$  with all users present can be obtained without the use of FEC and that no error floors are observed.

#### 4.3.4 Clock and data recovery

The previous section qualitatively revealed that our OCDMA signal is of good quality. One goal of OCDMA is to exploit it as an optical transport system. To

accomplish this, it is important to be able to perform CDR. Achieving CDR is of great significance; for example, if internet data from a central office was sent to a home user 5 km away via OCDMA, it is not feasible to also send a global clock signal. At the home, an OCDMA receiver that accepts the OCDMA signal should be able to recover both data and clock signals at the data rate, and then be able to process the data.

Julien Faucher designed an OCDMA receiver using commercially available components. Details pertaining to the design and testing of OCDMA receiver are given in [8, 9]. One key point is that the OCDMA receiver converts return-to-zero (RZ) data to non-return-to-zero (NRZ) data, facilitating the interfacing with electronics that operate with digital NRZ logic. Fig. 4.27 presents the recovered data and clock signals (in sample mode) when only the desired user is transmitting using a PRBS of 128 bits.

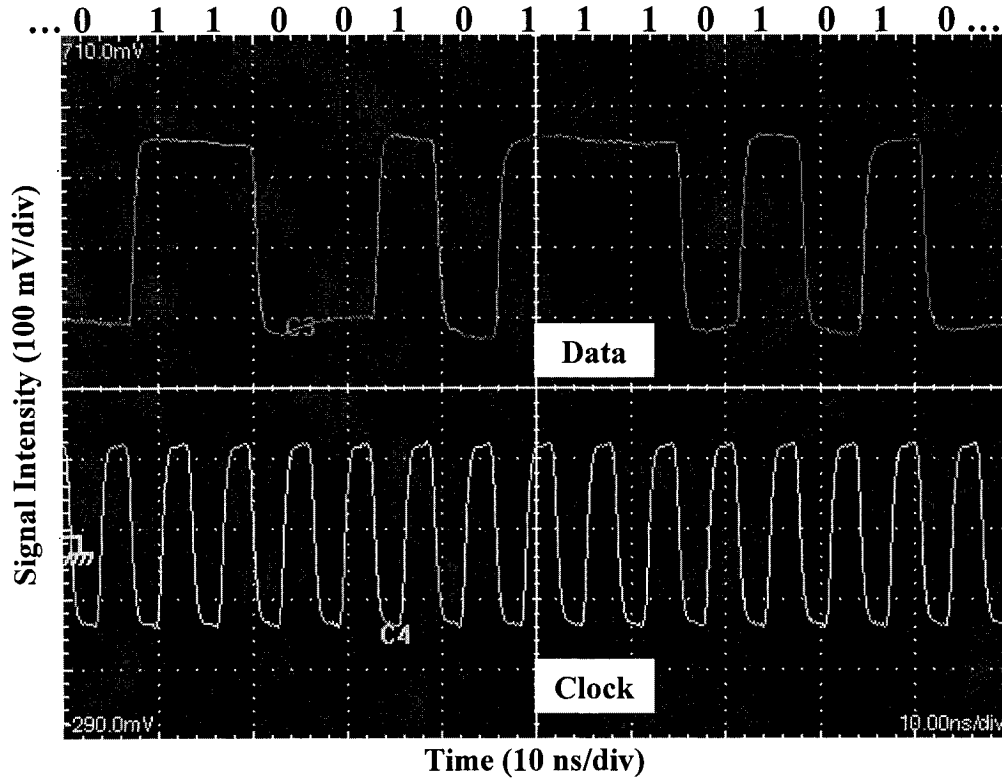
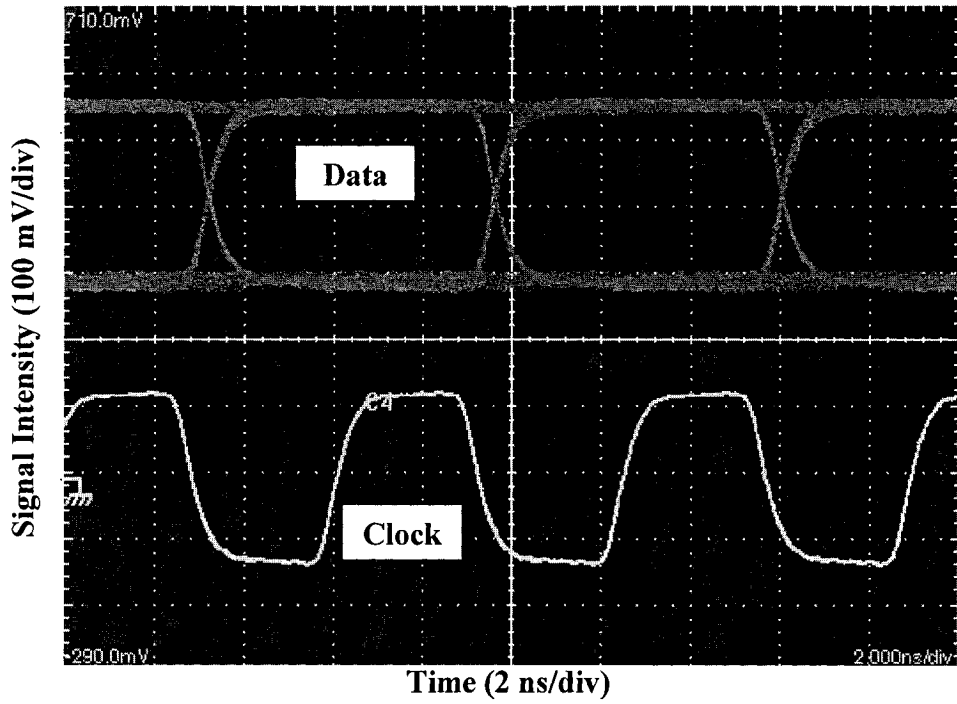
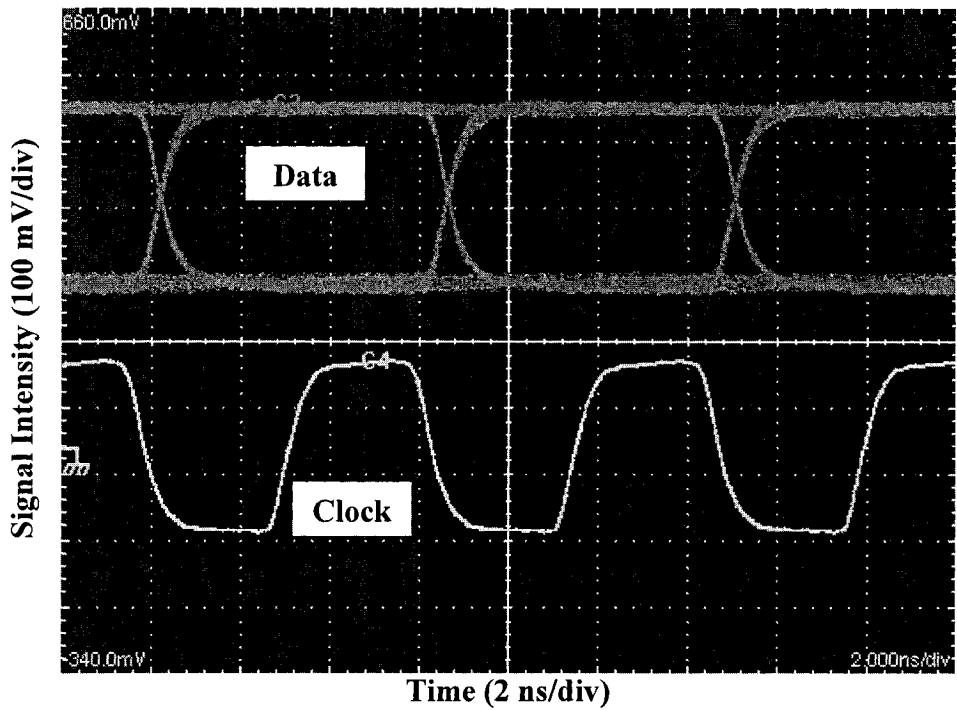


Fig. 4.27 CDR signals when only desired user is present

The bit duration is measured to be 6.4 ns and the clock rate is 155.52 Mb/s, as specified for the demonstration setup. Fig. 4.28 illustrates the eye diagrams of both CDR signals for 1, 2 and 3 simultaneous users.

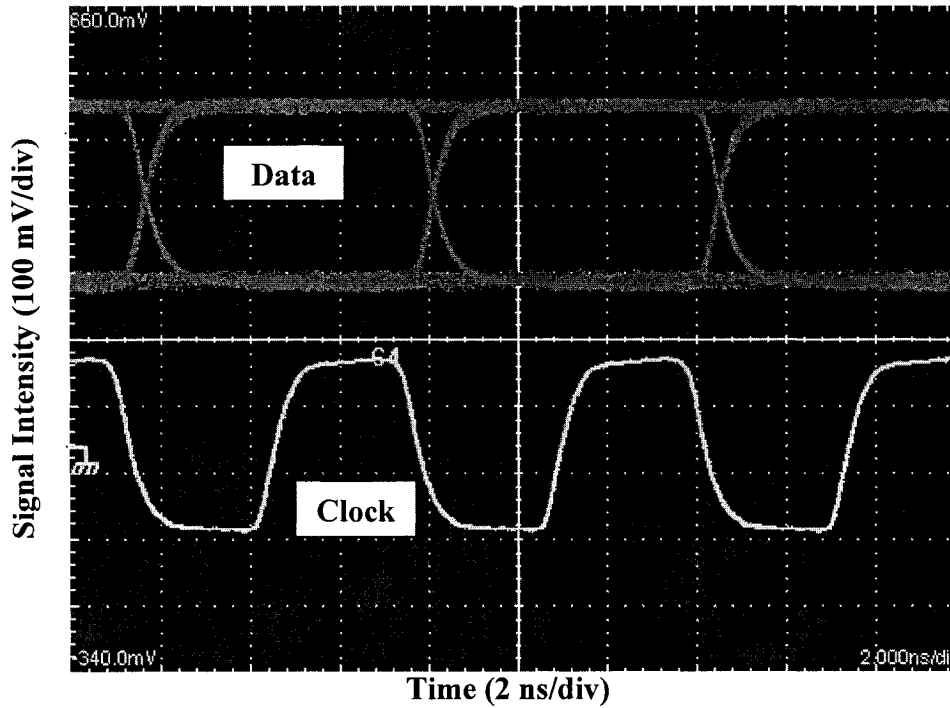


(a)



(b)

Fig. 4.28 Eye diagram of CDR signals (a) desired user only; (b) desired user and user 3; (c) desired user and users 3 and 4



(c)

Fig. 4.28 (cont.) Eye diagram of CDR signals (a) desired user only; (b) desired user and user 3; (c) desired user and users 3 and 4

We see that as the number of users increase, the quality of the data signal eye diagram remains relatively the same. Even though full BER measurements were not yet taken at this time, it is encouraging to see that the eye quality remains constant as the number of users increase.

#### 4.4 Summary

In this chapter, we presented the successful encoding and decoding of 2D  $\lambda$ -t DFSCs, and the successful implementation of a 4-user system. All encoders and decoder were built using commercially available optical components and can be easily integrated into the system since the input of each encoder only requires a BBS. The disadvantage is that the encoders and decoder cannot be tuned; each is set for only one specific code.

With careful design, wavelength and time misalignments are minimal, hence reducing encoder/decoder mismatch. Once all four encoded signals are decoded, the auto-correlation peak is clearly distinguishable from the MAI. Even when many bits are sent, the auto-correlation peak remains clearly distinguishable from the MAI. BER measurements showed that error free operation can be achieved, and furthermore, CDR was accomplished with up to 3 simultaneous users.

It is important to emphasize the significance of CDR for OCDMA. The designed OCDMA receiver not only recovers the clock from the OCDMA signal, but also converts the multi-level RZ signal with a duty cycle of  $1/8$  to a NRZ signal at the data rate. The receiver thus allows digital circuits to process OCDMA data in the same way as if TDMA or WDMA had been used in the transport network.

Note that it is difficult to validate that the theoretical analysis of chapter 3 mirrors with the implementation of a 4-user system. The code dimensions used in chapter 3 reflect a more probable approach for possible future OCDMA systems, whereas the code dimensions used for the 4-user system are of more modest size. Also, to properly validate the theoretical analysis of chapter 3, we would need well-controlled wavelength and time chip misalignments, which poses a challenge with the commercially available off-the-shelf optical components used. Lastly, experimental BER measurements take into account real sources of noise; not just MAI as in the simulation model in chapter 3.

Given the advantages of the DFSCs used, and the success of the 4-user implementation and CDR, we believe this should be a promising approach for realizing OCDMA systems.

## 5. Conclusion

### 5.1 Summary and conclusions

This thesis is concerned with: 1) the effects of encoder/decoder mismatch on BER performance for 2D  $\lambda$ -t OCDMA, and 2) the demonstration of a 4-user 2D  $\lambda$ -t OCDMA direct detection system. Additionally, this thesis focused on the use of 2D  $\lambda$ -t DFSCs.

In chapter 1, we motivated OCDMA, and articulated the objectives of the thesis. This was followed by a brief review of OCDMA in chapter 2. Fundamentals of OCDMA were discussed, additional details of the DFSCs were given, and challenges involved with OCDMA were put forward.

In chapter 3, we examined the effects of having wavelength and time misalignments between the encoders and decoder. We presented the simulation procedure used to investigate the effects of encoder/decoder mismatch on the BER performance; these simulations tested all different scenarios of the desired encoder, interfering encoders and decoder being ideal or non-ideal. The simulation model created can accommodate all 2D  $\lambda$ -t OCDMA codes, but the focus was on DFSCs. We investigated the effects with codes having more wavelengths than time chips and vice versa for both 8 and 12 simultaneous users. The misalignments are modeled as Gaussian probability distributions with variable variances.

The two main conclusions of chapter 3 are the following: 1) for the most probable scenario (“III”), the variance of the wavelength and/or time misalignments must remain below 0.01 if the BER penalty is to be less than one order of magnitude; and 2) the results are almost identical for (32, 16, 6) and (16, 32, 6) DFSCs, hence it is better to create codes using more wavelengths than time chips in order to achieve higher data rates and to generate a greater number of codes. These results are of much importance as they provide us with implementation tolerances that must be considered if encoding and decoding of 2D  $\lambda$ -t OCDMA is to be successful.

In chapter 4, we present the demonstration of a 4-user 2D  $\lambda$ -t OCDMA system employing (8, 8, 4) DFSCs. Each encoder and decoder was carefully built using

commercially available optical components, characterized and tested. Once fully implemented, a “1” bit and then a repeated arbitrary bit pattern are encoded by all 4 encoders, multiplexed together, and finally decoded. The reconstructed auto-correlation peak is indeed distinguishable from the MAI, and even when many bits are sent, the auto-correlation peaks remain clearly distinguishable. Effects of chromatic dispersion were examined and we concluded that dispersion compensation is necessary for transmission of more than a few kilometers. We also presented eye diagrams and BER plots. The eye diagrams showed a clear eye opening when using a 128 bit PRBS and the BER plots revealed that no error floor exists. A power penalty of 2.3 dB is incurred when all 4 users are present. Finally, we showed that CDR can be achieved and illustrated both the recovered clock and data signals.

This is the first 2D  $\lambda$ -t OCDMA demonstration system employing DFSCs. DFSCs provide many advantages over other 2D  $\lambda$ -t OCDMA code families, so its implementation is of great significance. Not only have we succeeded in encoding and decoding DFSCs and succeeded in implementing a 4-user system, but we did so in a cost effective way by utilizing standard commercially available off-the-shelf optical components. Keeping costs low is imperative if this approach is to be considered promising. Furthermore, their applicability with CDR makes DFSCs even more attractive for future OCDMA systems. We believe that the results presented will have an impact when future OCDMA systems are realized.

## **5.2 Future directions**

OCDMA is an exciting research area that has been attracting increasingly more attention. In this thesis, we have explored 2D  $\lambda$ -t OCDMA, specifically with DFSCs, and presented results that show much potential for realizing future OCDMA systems. Yet, there is opportunity for future work.

The 2D  $\lambda$ -t OCDMA simulation model can be made more complex to take into account non-idealities such as: channel noise, receiver noise, non-rectangular-shaped temporal pulses and spectral slices for the encoded and decoded signals. Furthermore,

---

simulating the use of a BBS or distributed feedback (DFB) lasers can lead to interesting comparisons of the two light sources and a better understanding of the consequential noise that would be present within the OCDMA system.

Concerning the demonstration setup, the modulator is driven by a pulse with a 2 volt peak-to-peak. However, the transfer function of the modulator reveals that it can be driven with a 4 volt signal, which would result in a better extinction ratio of the pulses, and improve the signal-to-noise ratio. To achieve 4 volts, a modulator amplifier that is capable of amplifying a PRBS is needed. Also, the modulator modulates the entire spectrum of the BBS, of most is unnecessary for us. A 10 nm (1545 nm – 1555 nm) pass band filter could be used to filter the unnecessary spectrum before modulation to reduce some noise. Finally, identical WDMs and more accurate ODLs could be used to decrease the existing misalignments.

If we had the infrastructure and more time, it would be interesting to implement more active users and even a second decoder. In addition, increased code sizes that enable more users could be implemented and tested. Different architectures for encoders and decoders, and with possible tunability, can also be examined. A thorough analysis of the noise present in the system (e.g. beat noise present from using a BBS) and an attempt to minimize the noise would be beneficial.

Testing wise, the eye diagrams and BER plots would have to be completed using a PRBS of at least  $2^{23}-1$  or  $2^{32}-1$ . Testing with such a PRBS would conform to what seems to be standard among the most recent publications that discuss BER performance. It is also of great interest to perform BER testing with the CDR signals from the OCDMA receiver and compare them to the results presented in section 4.3.3.

Also of much interest is OCDMA that makes use of bipolar codes and differential detection [56-63]. The use of differential detection can bring the average MAI to zero and improve the BER compared to direct detection systems.

Another consideration is OCDMA code conversion [64]. Once implemented in a lightwave network, two different data streams, each using the same code, can collide at a node. It is hence important to investigate OCDMA code conversion, especially mechanisms compatible with 2D  $\lambda$ -t OCDMA.

This is a sample of future work and directions that interest us now. Given the renewed interest in OCDMA within the scientific community and the advancements in photonic components, we are bound to witness key advancements in OCDMA in the near future. This will trigger chain reactions of research ideas and innovations. We believe that today's results are significant as OCDMA matures.

## 6. References

- [1] A. Stok and E. H. Sargent, "Lighting the Local Area: Optical Code-Division Multiple Access and Quality of Service Provisioning," *IEEE Network*, November/December 2000, pp. 42-46.
- [2] A. Stok and E. H. Sargent, "The Role of Optical CDMA in Access Networks," *IEEE Communications Magazine*, September 2002, pp. 83-87.
- [3] R. M. H. Yim, "New Approaches to Optical Code-Division Multiple Access," Masters Thesis, Department of Electrical and Computer Engineering, McGill University, Montréal, Québec, Canada, 2002.
- [4] R. M. H. Yim, L. R. Chen, and J. Bajcsy, "Design and performance of 2-D codes for wavelength-time optical CDMA," *IEEE Photon Technology Letters*, vol. 14, no. 5, May 2002, pp. 714-716.
- [5] R. Adams and L. R. Chen, "Effects of encoder/decoder mismatch on BER performance for 2-D wavelength-time OCDMA," *Conference Proceedings CLEO/IQEC '04*, San Francisco, CA, USA, paper CWA13, 2004.
- [6] R. Adams and L. R. Chen, "Impact of encoder/decoder mismatch due to wavelength and time misalignments on system performance of 2D wavelength-time optical CDMA systems," submitted to *Applied Optics (Lasers, Photonics, and Environmental Optics division)*, November 2004.
- [7] R. Adams and L. R. Chen, "Demonstration of a 4-user 2-D wavelength-time OCDMA system employing depth-first search codes," *Conference Proceedings LEOS '04*, San Juan, Puerto Rico, paper TuJ2, 2004.

- 
- [8] J. Faucher, R. Adams, L. R. Chen, and D. V. Plant, "Multi-user OCDMA system demonstrator with full CDR using a novel OCDMA receiver," submitted to IEEE Photonics Technology Letters, November 2004.
- [9] J. Faucher, R. Adams, L. R. Chen, and D. V. Plant, "Performance of a multi-user OCDMA system demonstrator with full clock and data recovery," submitted for CLEO/IQEC '05, November 2004.
- [10] A. Leon-Garcia and I. Widjaja, *Communication Networks: Fundamental Concepts and Key Architectures*, 1<sup>st</sup> ed. Chapter 6, McGraw-Hill, 2000.
- [11] G. Keiser, *Optical Fiber Communications*, 3<sup>rd</sup> ed. Chapter 12, McGraw-Hill, 2000.
- [12] J. A. Salehi, "Emerging Optical Code-Division Multiple Access Communications Systems," IEEE Network, March 1989, pp. 31-39.
- [13] J. A. Salehi, "Code Division Multiple-Access Techniques in Optical Fiber Networks – Part 1: Fundamental Principles," IEEE Transactions on Communications, vol. 37, no. 8, August 1989, pp. 824-833.
- [14] M. E. Marhic, "Coherent Optical CDMA Networks," IEEE Journal of Lightwave Technology, vol. 11, no. 5/6, May/June 1993, pp. 854-864.
- [15] F. R. K. Chung, J. A. Salehi, and V. K. Wei, "Optical Orthogonal Codes: Design, Analysis, and Applications," IEEE Transactions on Information Theory, vol. 35, no. 3, May 1989, pp. 595-604.
- [16] K. Iversen and D. Hampicke, "Comparison and classification of all-optical CDMA systems for future telecommunication networks," Proceedings SPIE, vol. 2614, December 1995, pp. 110-121.

- 
- [17] L. R. Chen, Course notes for *ESCE 596 Optical Waveguides*, McGill University, 2002.
- [18] P. R. Prucnal, M. A. Santoro, and T. R. Fan, "Spread Spectrum Fiber-Optic Local Area Network Using Optical Processing," *IEEE Journal of Lightwave Technology*, vol. 4, no. 5, May 1986, pp. 547-554.
- [19] A. M. Weiner, J. P. Heritage, and J. A. Salehi, "Encoding and Decoding of femtosecond pulses," *Optics Letters*, vol. 13, no. 4, April 1988, pp. 300-302.
- [20] J. A. Salehi, A. M. Weiner, and J. P. Heritage, "Coherent ultrashort light pulse code-division multiple access communication systems," *IEEE Journal of Lightwave Technology*, vol. 8, no. 3, March 1990, pp. 478-491.
- [21] R. P. Scott, W. Cong, K. Li, V. J. Hernandez, B. H. Kolner, J. P. Heritage, and S. J. Ben Yoo, "Demonstration of an Error-Free 4 x 10 Gb/s Multiuser SPECTS O-CDMA Network Testbed," *IEEE Photonics Technology Letters*, vol. 16, no. 9, September 2004, pp. 2186-2188.
- [22] M. Kavehrad and D. Zaccarin, "Optical code-division-multiplexed systems based on spectral encoding of noncoherent sources," *IEEE Journal of Lightwave Technology*, vol. 13, no. 3, March 1995, pp. 534-545.
- [23] K. Kitayama, "Novel spatial spread spectrum based fiber optic CDMA networks for image transmission," *IEEE Journal of Selected Areas in Communications*, vol. 12, no. 4, May 1994, pp. 762-772.
- [24] G.-C. Yang and W. C. Kwong, "Two-dimensional spatial signature patterns," *IEEE Transactions on Communications*, vol. 44, no. 2, February 1996, pp. 184-191.

- 
- [25] A. J. Mendez, V. J. Hernandez, C. V. Bennett, W. J. Lennon, and R. M. Gagliardi, "Optical CDMA (O-CDMA) Technology Demonstrator (TD) for 2D Codes," Conference Proceedings LEOS '03, Tucson, AZ, USA, paper ThEE3, 2003.
- [26] L. R. Chen, S. D. Benjamin, P. W. E. Smith, and J. E. Sipe, "Applications of Ultrashort Pulse Propagation in Bragg Gratings for Wavelength-Division multiplexing and Code-Division Multiple Access," *IEEE Journal of Quantum Electronics*, vol. 34, no. 11, November 1998, pp. 2117-2129.
- [27] E. Park, A. J. Mendez, and E. M. Garmin, "Temporal / Spatial Optical CDMA Networks-Design, Demonstration, and Comparison with Temporal Networks," *IEEE Photonics Technology Letters*, vol. 4, no. 10, October 1992, pp. 1160-1162.
- [28] A. J. Mendez, J. L. Lambert, J.-M. Morookian, and R. M. Gagliardi, "Synthesis and Demonstration of High Speed, Bandwidth Efficient Optical Code Division Multiple Access (CDMA) Tested at 1Gb/s Throughput," *IEEE Photonics Technology Letters*, vol. 6, no. 9, September 1994, pp. 1146-1149.
- [29] Conference Proceedings CLEO/IQEC '04, San Francisco, CA, USA, session CWH: *Optical CDMA*, 2004.
- [30] C.-C. Yang and J.-F. Huang, "Two-Dimensional M-Matrices Coding in Spatial / Frequency Optical CDMA Networks," *IEEE Photonics Technology Letters*, vol. 15, no. 1, January 2003, pp. 168-170.
- [31] S. Kim, K. Yu, and N. Park, "A New Family of Space / Wavelength / Time Spread Three-Dimensional Optical Code for OCDMA Networks," *IEEE Journal of Lightwave Technology*, vol. 18, no. 4, April 2000, pp. 502-511.

- 
- [32] L. Tancevski and I. Andonovic, "Wavelength hopping / time spreading code division multiple access systems," *Electronics Letters*, vol. 30, no. 17, August 1994, pp. 1388-1390.
- [33] L. Tancevski and I. Andonovic, "Hybrid Wavelength Hopping / Time Spreading Schemes for Use in Massive Optical Networks with Increased Security," *IEEE Journal of Lightwave Technology*, vol. 14, no. 12, December 1996, pp. 2636-2647.
- [34] H. Fathallah, L. A. Rusch, and S. LaRochelle, "Passive Optical Fast Frequency-Hop CDMA Communications Systems," *IEEE Journal of Lightwave Technology*, vol. 17, no. 3, March 1999, pp. 397-405.
- [35] E. Inaty, H. M. H. Shalaby, P. Fortier, and L. A. Rusch, "Multirate Optical Fast Frequency Hopping CDMA System Using Power Control," *IEEE Journal of Lightwave Technology*, vol. 20, no. 2, February 2002, pp. 166-177.
- [36] K. Yu and N. Park, "Design of new family of two-dimensional wavelength-time spreading codes for optical code division multiple access networks," *Electronics Letters*, vol. 35, no. 10, May 1999, pp. 830-831.
- [37] A. J. Mendez, R. M. Gagliardi, H. X. C. Feng, J. P. Heritage, and J.-M. Morookian, "Strategies for Realizing Optical CDMA for Dense, High-Speed, Long Span, Optical Network Applications," *IEEE Journal of Lightwave Technology*, vol. 18, no. 12, December 2000, pp. 1685-1696.
- [38] A. J. Mendez, R. M. Gagliardi, V. J. Hernandez, C. V. Bennett, and W. J. Lennon, "Design and Performance Analysis of Wavelength / Time (W/T) Matrix Codes for Optical CDMA," *IEEE Journal of Lightwave Technology*, vol. 21, no. 11, November 2003, pp. 2524-2533.

- 
- [39] S. P. Wan and Y. Hu, "Two-Dimensional Optical CDMA Differential System with Prime / OOC Codes," *IEEE Photonics Technology Letters*, vol. 13, no. 12, December 2001, pp. 1373-1375.
- [40] V. Baby, C.-S. Bres, L. Xu, I. Glesk, and P. R. Prucnal, "Demonstration of a differentiated service provisioning with 4-node 253 Gchip/s fast frequency-hopping time-spreading OCDMA," *Electronic Letters*, vol. 40, no. 12, June 2004, pp. 755-756.
- [41] I. Glesk, V. Baby, C.-S. Bres, L. Xu, D. Rand, and P. R. Prucnal, "Experimental demonstration of a 2.5Gbps incoherent 2D OCDMA system," *Conference Proceedings CLEO/IQEC '04*, San Francisco, CA, USA, paper CWH5, 2004.
- [42] K. Yu, J. Shin, and N. Park, "Wavelength-Time Spreading Optical CDMA System Using Wavelength Multiplexers and Mirrored Fiber Delay Lines," *IEEE Photonics Technology Letters*, vol. 12, no. 9, September 2000, pp. 1278-1280.
- [43] L. R. Chen, "Flexible Fiber Bragg Grating Encoder/Decoder for Hybrid Wavelength-Time Optical CDMA," *IEEE Photonics Technology Letters*, vol. 13, no. 11, November 2001, pp. 1233-1235.
- [44] L. R. Chen, P. W. E. Smith, and C. Martijn de Sterke, "Wavelength-encoding/temporal-spreading optical code division multiple-access system with in-fiber chirped moire gratings," *Applied Optics*, vol. 38, no. 21, July 1999, pp. 4500-4508.
- [45] L. R. Chen and P. W. E. Smith, "Demonstration of Incoherent Wavelength-Encoding/Time-Spreading Optical CDMA Using Chirped Moire Gratings," *IEEE Photonics Technology Letters*, vol. 12, no. 9, September 2000, pp. 1281-1283.

- 
- [46] S. Kutsuzawa, N. Minato, S. Oshiba, A. Nishiki, and K. Kitayama, "10 Gb/s x 2 ch Signal Unrepeated Transmission Over 100 km of Data Rate Enhanced Time-Spread / Wavelength-Hopping OCDM Using 2.5-Gb/s-FBG En/Decoder," *IEEE Photonics Technology Letters*, vol. 15, no. 2, February 2003, pp. 317-319.
- [47] P. C. Teh, M. Ibsen, and D. J. Richardson, "Demonstration of a Full-Duplex Bidirectional Spectrally Interleaved OCDMA / DWDM System," *IEEE Photonics Technology Letters*, vol. 15, no. 3, March 2003, pp. 482-484.
- [48] H. Tamai, H. Iwamura, N. Minato, and S. Oshiba, "Experimental Study on Time-Spread/Wavelength-Hop Optical Code Division Multiplexing with Group Delay Compensating En/Decoder," *IEEE Photonics Technology Letters*, vol. 16, no. 1, January 2004, pp. 335-337.
- [49] H. B. Jaafar, S. LaRochelle, P.-Y. Cortes, and H. Fathallah, "1.25 Gbit/s transmission of optical FFH-OCDMA signals over 80 km with 16 users," *Conference Proceedings OFC '01, Los Angeles, CA, USA, paper TuV3-1, 2001.*
- [50] J. Y. Kim and H. V. Poor, "Turbo-Coded Optical Direct-Detection CDMA System with PPM Modulation," *IEEE Journal of Lightwave Technology*, vol. 19, no. 3, March 2001, pp. 312-323.
- [51] C. Zuo, W. M. Hongtu, and J. Lin, "The Impact of Group Velocity on Frequency-Hopping Optical Code Division Multiple Access System," *IEEE Journal of Lightwave Technology*, vol. 19, no. 10, October 2001, pp. 1416-1419.
- [52] X. Wang and K. T. Chan, "The effect of grating-position deviation and fiber dispersion in the fiber-optic-CDMA network with the FBG encoder/decoder for incoherent 2D coding," *Microwave and Optical Technology Letters*, vol. 35, no. 1, October 2002, pp. 16-19.

- 
- [53] E. K. H. Ng, G. E. Weichenberg, and E. H. Sargent, "Dispersion in Multiwavelength Optical Code-Division-Multiple-Access Systems: Impacts and Remedies," *IEEE Transactions on Communications*, vol. 50, no. 11, November 2002, pp. 1811-1816.
- [54] A. Sahin and A. E. Willner, "System limitations due to chromatic dispersion and receiver bandwidth for 2-D time-wavelength OCDMA systems," *Conference Proceedings LEOS '03*, Tucson, AZ, USA, paper W15, 2003.
- [55] L. Tancevski and L. A. Rusch, "Impact of the Beat Noise on the Performance of 2-D Optical CDMA Systems," *IEEE Communications Letters*, vol. 4, no. 8, August 2000, pp. 264-266.
- [56] D. Zaccarin and M. Kavehrad, "Performance Evaluation of Optical CDMA Systems Using Non-Coherent Detection and Bipolar Codes," *IEEE Journal of Lightwave Technology*, vol. 12, no. 1, January 1994, pp. 96-105.
- [57] G. J. Pendock and D. D. Sampson, "Increasing the Transmission Capacity of Coherence Multiplexed Communication Systems by Using Differential Detection," *IEEE Photonics Technology Letters*, vol. 7, no. 12, December 1995, pp. 1504-1506.
- [58] L. Nguyen, T. Dennis, B. Aazhang, and J. F. Young, "Experimental Demonstration of Bipolar Codes for Optical Spectral Amplitude CDMA Communication," *IEEE Journal of Lightwave Technology*, vol. 15, no. 9, September 1997, pp. 1647-1653.
- [59] T. Dennis and J. F. Young, "Optical Implementation of Bipolar Codes," *IEEE Journal of Quantum Electronics*, vol. 35, no. 3, March 1999, pp. 287-291.
- [60] C. F. Lam, D. T. K. Tong, M. C. Wu, and E. Yablonovitch, "Experimental Demonstration of Bipolar Optical CDMA System Using a Balanced Transmitter and Complementary Spectral Encoding," *IEEE Photonics Technology Letters*, vol. 10, no. 10, October 1998, pp. 1504-1506.

[61] R. M. H. Yim, J. Bajcsy, and L. R. Chen, "A New Family of 2-D Wavelength-Time Codes for Optical CDMA with Differential Detection," *IEEE Photonics Technology Letters*, vol. 15, no. 1, January 2003, pp. 165-167.

[62] U. N. Griner and S. Arnon, "A Novel Bipolar Wavelength-Time Coding Scheme for Optical CDMA Systems," *IEEE Photonics Technology Letters*, vol. 16, no. 1, January 2004, pp. 332-334.

[63] H. Heo, S. Min, Y. H. Won, Y. Yeon, B. K. Kim, and B. W. Kim, "A New Family of 2-D Wavelength-Time Spreading Code for Optical Code-Division Multiple-Access System with Balanced Detection," *IEEE Photonics Technology Letters*, vol. 16, no. 9, September 2004, pp. 2189-2191.

[64] K. Kitayama, "Code Division Multiplexing Lightwave Networks Based upon Optical Code Conversion," *IEEE Journal on Selected Areas in Communication*, vol. 16, no. 7, September 1998, pp. 1309-1319.

## Appendix A: Results of encoder/decoder mismatch simulations

**Table A.1 Average BER and the standard deviation for simulating wavelength misalignment; (32, 16, 6) DFSCs; K = 8 active users**

Variance of Gaussian	<u>PPP</u> Average BER	Standard deviation of BER	<u>IPP</u> Average BER	Standard deviation of BER
0	2.4500E-09	2.9711E-08	2.4500E-09	2.9711E-08
0.001	2.4500E-09	2.9711E-08	5.0394E-09	2.6107E-15
0.005	2.4500E-09	2.9711E-08	1.2283E-08	1.0491E-14
0.01	2.4500E-09	2.9711E-08	2.3900E-08	3.0529E-14
0.05	2.4500E-09	2.9711E-08	3.7964E-07	3.0827E-12
0.1	2.4500E-09	2.9711E-08	2.7639E-06	9.5767E-11
Variance of Gaussian	<u>PIP</u> Average BER	Standard deviation of BER	<u>IIP</u> Average BER	Standard deviation of BER
0	2.4500E-09	2.9711E-08	2.4500E-09	2.9711E-08
0.001	1.2330E-09	1.7938E-08	2.5766E-09	3.0463E-08
0.005	5.3178E-10	9.8520E-09	2.9298E-09	3.2968E-08
0.01	2.8705E-10	6.4322E-09	3.4075E-09	3.6518E-08
0.05	2.8471E-11	1.3178E-09	1.2138E-08	1.0000E-07
0.1	8.4582E-12	4.8319E-10	6.6533E-08	4.3253E-07
Variance of Gaussian	<u>PPI</u> Average BER	Standard deviation of BER	<u>IPI</u> Average BER	Standard deviation of BER
0	2.4500E-09	2.9711E-08	2.4500E-09	2.9711E-08
0.001	2.5634E-09	2.9613E-08	3.4996E-09	3.9009E-08
0.005	2.8702E-09	3.0751E-08	5.9365E-09	5.8639E-08
0.01	3.2777E-09	3.2859E-08	9.4490E-09	8.4670E-08
0.05	1.0405E-08	7.6770E-08	1.3736E-07	8.2559E-07
0.1	5.5020E-08	3.3523E-07	1.8295E-06	8.3948E-06
Variance of Gaussian	<u>PII</u> Average BER	Standard deviation of BER	<u>III</u> Average BER	Standard deviation of BER
0	2.4500E-09	2.9711E-08	2.4500E-09	2.9711E-08
0.001	1.9604E-09	2.4933E-08	2.6809E-09	3.3047E-08
0.005	1.4920E-09	1.4121E-08	3.1788E-09	2.6703E-08
0.01	1.5929E-09	1.9184E-08	4.6020E-09	4.4253E-08
0.05	4.7924E-09	5.4067E-08	6.7648E-08	5.2578E-07
0.1	3.9698E-08	3.0051E-07	1.3234E-06	6.7602E-06

**Table A.2 Average BER and the standard deviation for simulating wavelength misalignment; (32, 16, 6) DFSCs; K = 12 active users**

Variance of Gaussian	<b>PPP</b> Average BER	Standard deviation of BER	<b>IPP</b> Average BER	Standard deviation of BER
0	3.6184E-07	7.4752E-07	3.6184E-07	7.4752E-07
0.001	3.6184E-07	7.4752E-07	6.5013E-07	1.2278E-06
0.005	3.6184E-07	7.4752E-07	1.3258E-06	2.2617E-06
0.01	3.6184E-07	7.4752E-07	2.2410E-06	3.5644E-06
0.05	3.6184E-07	7.4752E-07	1.8601E-05	2.3247E-05
0.1	3.6184E-07	7.4752E-07	8.0271E-05	8.8157E-05

Variance of Gaussian	<b>PIP</b> Average BER	Standard deviation of BER	<b>IIP</b> Average BER	Standard deviation of BER
0	3.6184E-07	7.4752E-07	3.6184E-07	7.4752E-07
0.001	2.0533E-07	4.6330E-07	3.7736E-07	7.7661E-07
0.005	1.0225E-07	2.5734E-07	4.1969E-07	8.5481E-07
0.01	6.1219E-08	1.6701E-07	4.7510E-07	9.5591E-07
0.05	8.9998E-09	3.3148E-08	1.3103E-06	2.4060E-06
0.1	3.4782E-09	1.4813E-08	4.8126E-06	8.0463E-06

Variance of Gaussian	<b>PPI</b> Average BER	Standard deviation of BER	<b>IPI</b> Average BER	Standard deviation of BER
0	3.6184E-07	7.4752E-07	3.6184E-07	7.4752E-07
0.001	3.7676E-07	7.7210E-07	4.8484E-07	9.6688E-07
0.005	4.1612E-07	8.3726E-07	7.4334E-07	1.4119E-06
0.01	4.6691E-07	9.2085E-07	1.0766E-06	1.9644E-06
0.05	1.2164E-06	2.0967E-06	8.3334E-06	1.2736E-05
0.1	4.3907E-06	6.8109E-06	5.4539E-05	7.5347E-05

Variance of Gaussian	<b>PII</b> Average BER	Standard deviation of BER	<b>III</b> Average BER	Standard deviation of BER
0	3.6184E-07	7.4752E-07	3.6184E-07	7.4752E-07
0.001	3.0123E-07	6.3851E-07	3.9204E-07	7.9060E-07
0.005	2.6270E-07	5.5563E-07	4.7971E-07	9.5618E-07
0.01	2.5743E-07	5.5901E-07	6.0427E-07	1.1712E-06
0.05	6.4607E-07	1.2597E-06	4.7680E-06	7.8534E-06
0.1	3.3782E-06	5.9610E-06	4.2773E-05	6.2954E-05

**Table A.3 Average BER and the standard deviation for simulating wavelength misalignment; (16, 32, 6) DFSCs; K = 8 active users**

Variance of Gaussian	<u>PPP</u> Average BER	Standard deviation of BER	<u>IPP</u> Average BER	Standard deviation of BER
0	1.2928E-09	8.7854E-09	1.2928E-09	8.7854E-09
0.001	1.2928E-09	8.7854E-09	2.8669E-09	1.6841E-08
0.005	1.2928E-09	8.7854E-09	7.6510E-09	3.7921E-08
0.01	1.2928E-09	8.7854E-09	1.5905E-08	7.0021E-08
0.05	1.2928E-09	8.7854E-09	3.2581E-07	9.6116E-07
0.1	1.2928E-09	8.7854E-09	2.7548E-06	6.7247E-06
Variance of Gaussian	<u>PIP</u> Average BER	Standard deviation of BER	<u>IIP</u> Average BER	Standard deviation of BER
0	1.2928E-09	8.7854E-09	1.2928E-09	8.7854E-09
0.001	5.9846E-10	4.6976E-09	1.3683E-09	9.4190E-09
0.005	2.3221E-10	2.1863E-09	1.5857E-09	1.0984E-08
0.01	1.1573E-10	1.2507E-09	1.8866E-09	1.3010E-08
0.05	8.4924E-12	1.6093E-10	8.0162E-09	4.8587E-08
0.1	2.2556E-12	5.6986E-11	5.3301E-08	2.6578E-07
Variance of Gaussian	<u>PPI</u> Average BER	Standard deviation of BER	<u>IPI</u> Average BER	Standard deviation of BER
0	1.2928E-09	8.7854E-09	1.2928E-09	8.7854E-09
0.001	1.3538E-09	8.9033E-09	1.9249E-09	1.2312E-08
0.005	1.5248E-09	9.5445E-09	3.4797E-09	2.0592E-08
0.01	1.7562E-09	1.0516E-08	5.8571E-09	3.2659E-08
0.05	6.1250E-09	2.8170E-08	1.1383E-07	4.9758E-07
0.1	3.8582E-08	1.5294E-07	1.8493E-06	7.1428E-06
Variance of Gaussian	<u>PII</u> Average BER	Standard deviation of BER	<u>III</u> Average BER	Standard deviation of BER
0	1.2928E-09	8.7854E-09	1.2928E-09	8.7854E-09
0.001	9.9933E-10	3.7648E-05	1.4174E-09	9.5671E-09
0.005	8.1123E-10	4.2775E-05	1.8297E-09	1.1559E-08
0.01	7.7017E-10	5.0708E-05	2.5713E-09	1.4185E-08
0.05	2.6219E-09	2.2519E-04	5.0709E-08	2.7204E-07
0.1	2.8781E-08	1.1483E-03	1.3186E-06	5.5505E-06

**Table A.4 Average BER and the standard deviation for simulating wavelength misalignment; (16, 32, 6) DFSCs;  $K = 12$  active users**

Variance of Gaussian	<u>PPP</u>		<u>IPP</u>	
	Average BER	Standard deviation of BER	Average BER	Standard deviation of BER
0	4.2923E-07	5.3483E-07	4.2923E-07	5.3483E-07
0.001	4.2923E-07	5.3483E-07	7.8155E-07	9.0309E-07
0.005	4.2923E-07	5.3483E-07	1.6162E-06	1.7173E-06
0.01	4.2923E-07	5.3483E-07	2.7550E-06	2.7697E-06
0.05	4.2923E-07	5.3483E-07	2.3284E-05	1.9997E-05
0.1	4.2923E-07	5.3483E-07	1.0000E-04	8.2135E-05
<hr/>				
Variance of Gaussian	<u>PIP</u>		<u>IIP</u>	
	Average BER	Standard deviation of BER	Average BER	Standard deviation of BER
0	4.2923E-07	5.3483E-07	4.2923E-07	5.3483E-07
0.001	2.3910E-07	3.2201E-07	4.4690E-07	5.5556E-07
0.005	1.1593E-07	1.7185E-07	4.9624E-07	6.1478E-07
0.01	6.7874E-08	1.0796E-07	5.6126E-07	6.9330E-07
0.05	8.9625E-09	1.8498E-08	1.5437E-06	1.8894E-06
0.1	3.2171E-09	7.5205E-09	5.6342E-06	6.9505E-06
<hr/>				
Variance of Gaussian	<u>PPI</u>		<u>IPI</u>	
	Average BER	Standard deviation of BER	Average BER	Standard deviation of BER
0	4.2923E-07	5.3483E-07	4.2923E-07	5.3483E-07
0.001	4.4568E-07	5.5354E-07	5.7575E-07	6.9175E-07
0.005	4.9031E-07	6.0268E-07	8.8408E-07	1.0209E-06
0.01	5.4839E-07	6.6551E-07	1.2817E-06	1.4442E-06
0.05	1.4079E-06	1.5692E-06	9.8688E-06	1.0810E-05
0.1	5.0341E-06	5.5365E-06	6.3104E-05	7.1931E-05
<hr/>				
Variance of Gaussian	<u>PII</u>		<u>III</u>	
	Average BER	Standard deviation of BER	Average BER	Standard deviation of BER
0	4.2923E-07	5.3483E-07	4.2923E-07	5.3483E-07
0.001	3.5334E-07	4.4775E-07	4.5878E-07	5.6664E-07
0.005	3.0385E-07	3.9501E-07	5.5898E-07	6.8329E-07
0.01	2.9214E-07	3.8209E-07	7.1372E-07	8.6390E-07
0.05	7.1495E-07	9.2211E-07	5.5025E-06	6.7287E-06
0.1	3.7487E-06	4.9141E-06	4.7987E-05	5.8511E-05

**Table A.5 Average BER and the standard deviation for simulating time misalignment; (32, 16, 6) DFSCs; K = 8 active users**

Variance of Gaussian	<b>PPP</b> Average BER	Standard deviation of BER	<b>IPP</b> Average BER	Standard deviation of BER
0	2.4500E-09	2.9711E-08	2.4500E-09	2.9711E-08
0.001	2.4500E-09	2.9711E-08	5.0347E-09	5.2144E-08
0.005	2.4500E-09	2.9711E-08	1.1559E-08	8.1832E-08
0.01	2.4500E-09	2.9711E-08	2.3811E-08	1.7724E-07
0.05	2.4500E-09	2.9711E-08	3.7707E-07	1.8496E-06
0.1	2.4500E-09	2.9711E-08	2.6096E-06	8.7014E-06
<hr/>				
Variance of Gaussian	<b>PIP</b> Average BER	Standard deviation of BER	<b>IIP</b> Average BER	Standard deviation of BER
0	2.4500E-09	2.9711E-08	2.4500E-09	2.9711E-08
0.001	1.2112E-09	1.7042E-08	2.5431E-09	3.0312E-08
0.005	4.5827E-10	5.7690E-09	2.6256E-09	2.3896E-08
0.01	2.8267E-10	5.3058E-09	3.3779E-09	4.0165E-08
0.05	3.4181E-11	1.2999E-09	1.2051E-08	1.3335E-07
0.1	8.4552E-12	2.8501E-10	5.6540E-08	4.1321E-07
<hr/>				
Variance of Gaussian	<b>PPI</b> Average BER	Standard deviation of BER	<b>IPI</b> Average BER	Standard deviation of BER
0	2.4500E-09	2.9711E-08	2.4500E-09	2.9711E-08
0.001	2.5315E-09	2.9899E-08	3.4541E-09	4.0434E-08
0.005	2.6015E-09	2.4477E-08	5.4250E-09	4.5612E-08
0.01	3.2539E-09	3.7798E-08	9.3246E-09	8.9689E-08
0.05	1.0454E-08	1.1798E-07	1.3284E-07	1.4074E-06
0.1	4.6643E-08	3.4825E-07	1.5079E-06	7.0345E-06
<hr/>				
Variance of Gaussian	<b>PII</b> Average BER	Standard deviation of BER	<b>III</b> Average BER	Standard deviation of BER
0	2.4500E-09	2.9711E-08	2.4500E-09	2.9711E-08
0.001	1.9299E-09	2.4003E-08	2.6343E-09	2.9690E-08
0.005	1.4660E-09	1.5467E-08	3.1249E-09	3.2134E-08
0.01	1.6457E-09	2.2906E-08	4.6358E-09	6.0104E-08
0.05	5.6217E-09	6.5862E-08	7.0440E-08	6.2443E-07
0.1	4.9009E-08	4.5370E-07	1.5114E-06	8.2351E-06

**Table A.6 Average BER and the standard deviation for simulating time misalignment; (32, 16, 6) DFSCs; K = 12 active users**

Variance of Gaussian	<u>PPP</u> Average BER	Standard deviation of BER	<u>IPP</u> Average BER	Standard deviation of BER
0	3.6184E-07	7.4752E-07	3.6184E-07	7.4752E-07
0.001	3.6184E-07	7.4752E-07	6.5051E-07	1.2308E-06
0.005	3.6184E-07	7.4752E-07	1.3276E-06	2.2508E-06
0.01	3.6184E-07	7.4752E-07	2.2482E-06	3.6067E-06
0.05	3.6184E-07	7.4752E-07	1.8573E-05	2.3116E-05
0.1	3.6184E-07	7.4752E-07	7.9790E-05	8.5681E-05
<hr/>				
Variance of Gaussian	<u>PIP</u> Average BER	Standard deviation of BER	<u>IIP</u> Average BER	Standard deviation of BER
0	3.6184E-07	7.4752E-07	3.6184E-07	7.4752E-07
0.001	2.0096E-07	4.5568E-07	3.6976E-07	7.6407E-07
0.005	9.7001E-08	2.4120E-07	3.9948E-07	8.2440E-07
0.01	5.6671E-08	1.5666E-07	4.4283E-07	9.0335E-07
0.05	7.2252E-09	2.8230E-08	1.0860E-06	2.1615E-06
0.1	2.5043E-09	1.1823E-08	3.7030E-06	6.9116E-06
<hr/>				
Variance of Gaussian	<u>PPI</u> Average BER	Standard deviation of BER	<u>IPI</u> Average BER	Standard deviation of BER
0	3.6184E-07	7.4752E-07	3.6184E-07	7.4752E-07
0.001	3.6906E-07	7.6267E-07	4.7478E-07	9.4890E-07
0.005	3.9707E-07	8.0532E-07	7.0843E-07	1.3414E-06
0.01	4.3649E-07	8.9499E-07	1.0040E-06	1.8776E-06
0.05	1.0143E-06	1.9493E-06	7.0027E-06	1.1530E-05
0.1	3.4300E-06	6.2025E-06	4.3663E-05	6.4754E-05
<hr/>				
Variance of Gaussian	<u>PII</u> Average BER	Standard deviation of BER	<u>III</u> Average BER	Standard deviation of BER
0	3.6184E-07	7.4752E-07	3.6184E-07	7.4752E-07
0.001	2.9577E-07	6.3028E-07	3.7951E-07	7.8745E-07
0.005	2.4589E-07	5.5354E-07	4.4692E-07	9.1365E-07
0.01	2.3454E-07	5.3556E-07	5.5752E-07	1.1551E-06
0.05	5.5291E-07	1.3056E-06	4.0253E-06	7.7682E-06
0.1	2.8722E-06	6.1948E-06	3.9038E-05	6.7046E-05

**Table A.7 Average BER and the standard deviation for simulating time misalignment; (16, 32, 6) DFSCs; K = 8 active users**

Variance of Gaussian	<u>PPP</u> Average BER	Standard deviation of BER	<u>IPP</u> Average BER	Standard deviation of BER
0	1.2928E-09	8.7854E-09	1.2928E-09	8.7854E-09
0.001	1.2928E-09	8.7854E-09	2.8630E-09	1.6771E-08
0.005	1.2928E-09	8.7854E-09	7.6066E-09	3.8127E-08
0.01	1.2928E-09	8.7854E-09	1.5643E-08	6.1633E-08
0.05	1.2928E-09	8.7854E-09	3.1313E-07	8.9589E-07
0.1	1.2928E-09	8.7854E-09	2.6029E-06	5.9126E-06
<hr/>				
Variance of Gaussian	<u>PIP</u> Average BER	Standard deviation of BER	<u>IIP</u> Average BER	Standard deviation of BER
0	1.2928E-09	8.7854E-09	1.2928E-09	8.7854E-09
0.001	5.7534E-10	4.0846E-09	1.3611E-09	9.3606E-09
0.005	2.3456E-10	2.3887E-09	1.5653E-09	1.1541E-08
0.01	1.0798E-10	9.2907E-10	1.7904E-09	1.0487E-08
0.05	8.2167E-12	1.6099E-10	7.4123E-09	3.8341E-08
0.1	2.1862E-12	3.4021E-11	4.7608E-08	2.3091E-07
<hr/>				
Variance of Gaussian	<u>PPI</u> Average BER	Standard deviation of BER	<u>IPI</u> Average BER	Standard deviation of BER
0	1.2928E-09	8.7854E-09	1.2928E-09	8.7854E-09
0.001	1.3528E-09	9.1852E-09	1.9163E-09	1.2796E-08
0.005	1.5307E-09	1.0744E-08	3.4344E-09	2.2326E-08
0.01	1.7210E-09	9.8010E-09	5.5559E-09	2.6570E-08
0.05	6.1349E-09	3.0454E-08	1.0394E-07	4.5115E-07
0.1	3.8244E-08	1.7092E-07	1.5711E-06	5.2678E-06
<hr/>				
Variance of Gaussian	<u>PII</u> Average BER	Standard deviation of BER	<u>III</u> Average BER	Standard deviation of BER
0	1.2928E-09	8.7854E-09	1.2928E-09	8.7854E-09
0.001	1.0239E-09	7.6179E-09	1.4430E-09	9.8830E-09
0.005	8.5606E-10	7.0558E-09	1.9168E-09	1.4633E-08
0.01	8.3742E-10	7.6704E-09	2.6607E-09	1.5645E-08
0.05	3.4391E-09	2.1420E-08	5.6684E-08	2.8190E-07
0.1	4.3112E-08	2.7208E-07	1.7165E-06	7.7364E-06

**Table A.8 Average BER and the standard deviation for simulating time misalignment; (16, 32, 6) DFSCs;  $K = 12$  active users**

Variance of Gaussian	<u>PPP</u>		<u>IPP</u>	
	Average BER	Standard deviation of BER	Average BER	Standard deviation of BER
0	4.2923E-07	5.3483E-07	4.2923E-07	5.3483E-07
0.001	4.2923E-07	5.3483E-07	7.8083E-07	8.9927E-07
0.005	4.2923E-07	5.3483E-07	1.6121E-06	1.6990E-06
0.01	4.2923E-07	5.3483E-07	2.7486E-06	2.7075E-06
0.05	4.2923E-07	5.3483E-07	2.3137E-05	1.9109E-05
0.1	4.2923E-07	5.3483E-07	9.9102E-05	7.6774E-05
<hr/>				
Variance of Gaussian	<u>PIP</u>		<u>IIP</u>	
	Average BER	Standard deviation of BER	Average BER	Standard deviation of BER
0	4.2923E-07	5.3483E-07	4.2923E-07	5.3483E-07
0.001	2.3925E-07	3.2168E-07	4.4269E-07	5.5338E-07
0.005	1.1326E-07	1.6571E-07	4.8470E-07	6.0915E-07
0.01	6.5717E-08	1.1105E-07	5.4207E-07	6.8758E-07
0.05	8.0293E-09	1.8188E-08	1.4098E-06	1.8032E-06
0.1	2.7419E-09	7.0776E-09	4.9577E-06	6.3291E-06
<hr/>				
Variance of Gaussian	<u>PPI</u>		<u>IPI</u>	
	Average BER	Standard deviation of BER	Average BER	Standard deviation of BER
0	4.2923E-07	5.3483E-07	4.2923E-07	5.3483E-07
0.001	4.4190E-07	5.5056E-07	5.7107E-07	6.9337E-07
0.005	4.8117E-07	5.8798E-07	8.6746E-07	1.0020E-06
0.01	5.3590E-07	6.5957E-07	1.2526E-06	1.4449E-06
0.05	1.3105E-06	1.5621E-06	9.1756E-06	1.0161E-05
0.1	4.5597E-06	5.2645E-06	5.7942E-05	6.3302E-05
<hr/>				
Variance of Gaussian	<u>PII</u>		<u>III</u>	
	Average BER	Standard deviation of BER	Average BER	Standard deviation of BER
0	4.2923E-07	5.3483E-07	4.2923E-07	5.3483E-07
0.001	3.5437E-07	4.5707E-07	4.5968E-07	5.7497E-07
0.005	3.0181E-07	4.0514E-07	5.5424E-07	6.8384E-07
0.01	2.9160E-07	3.9414E-07	7.0905E-07	8.8939E-07
0.05	7.5119E-07	1.0714E-06	5.5942E-06	7.1660E-06
0.1	4.2106E-06	5.9716E-06	5.5590E-05	6.9186E-05

Appendix B: Encoders and decoder measurements

Table A.9 Insertion loss, OPL and ODL measurements for all encoders and decoder

VDM					Interferer # 1					CODEWORD								ODL				
CH	V #	wavelength (nm)	IL (dBm)	length (m)	rel wrt V3 (m)	tc1	tc2	tc3	tc4	tc5	tc6	tc7	tc8	Offset wrt V3 (cm)	time delay added (cm)	physical length (cm)	measured length of 1X4-ODL (cm)	rel length diff (cm)	off target (cm)	off target wrt -0.3 (cm)		
29	1	1547.6	6.7	2.286	0.018	0	0	0	0	0	0	0	0	3.7	0.0	20.3	1113.1	0.0	0.0	0.3		
30	2	1548.4	7.2	2.267	0.037	1	0	0	0	0	0	0	0	0.0	32.0	51.8	1144.3	31.2	-0.8	-0.5		
31	3	1549.2	6.4	2.304	0.000	0	0	1	0	0	0	0	0	2.3	16.0	33.4	1128.8	15.7	-0.3	0.4		
32	4	1550.0	6.6	2.281	0.023	0	0	1	0	0	0	0	0	4.3	0.0	33.0	1113.3	0.2	0.2	0.5		
33	5	1550.8	--	--	--	0	0	0	0	0	0	0	0									
35	6	1551.6	6.4	2.261	0.043	1	0	0	0	0	0	0	0									
35	7	1552.4	6.5	2.231	0.073	0	0	0	0	0	0	0	0									
34	8	1553.2	6.4	2.287	0.017	0	0	0	0	0	0	0	0									

\* Insertion loss values have worsen since the original recording of the measurements

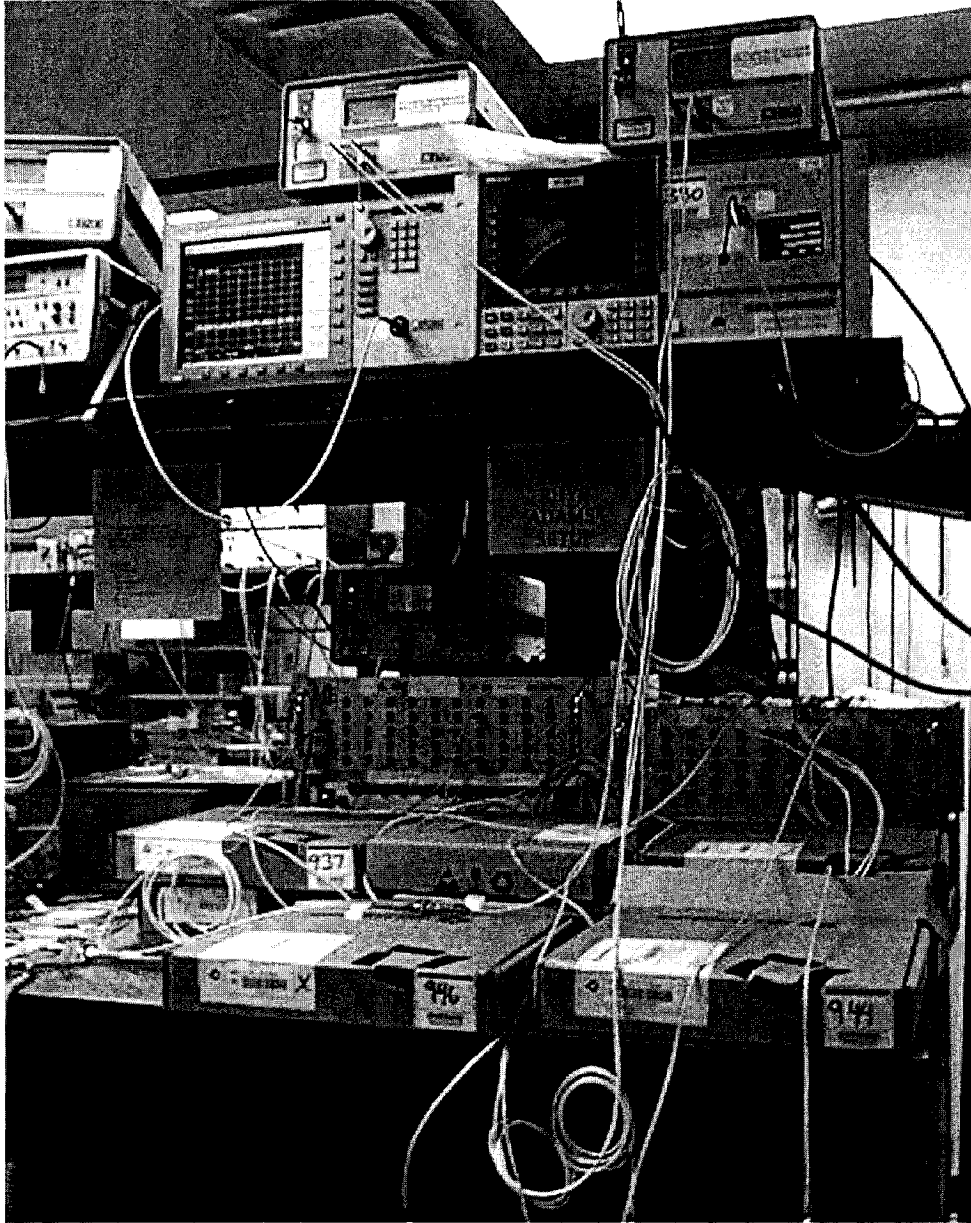
VDM					Interferer # 2					CODEWORD								ODL				
CH	V #	wavelength (nm)	IL (dBm)	length (m)	rel wrt V8 (m)	tc1	tc2	tc3	tc4	tc5	tc6	tc7	tc8	Offset wrt V8 (cm)	time delay added (cm)	physical length (cm)	measured length of 1X4-ODL (cm)	rel length diff (cm)	off target (cm)	off target wrt 0.8 (cm)		
29	1	1547.6	6.3	2.359	0.001	1	0	0	0	0	0	0	0	0.1	0.0	17.3	1106.2	0.0	0.0	0.6		
30	2	1548.4	6.4	2.364	-0.004	0	0	0	0	0	0	0	0									
31	3	1549.2	6.6	2.355	0.001	0	1	0	0	0	0	0	0	0.1	16.0	26.4	1123.5	17.3	1.3	0.5		
32	4	1550.0	--	--	--	0	0	0	0	0	0	0	0									
33	5	1550.8	6.3	2.356	0.004	0	1	0	0	0	0	0	0	0.4	16.0	31.1	1123.7	17.5	1.5	0.7		
34	6	1551.6	5.4	2.362	-0.002	0	0	0	0	0	0	0	0									
35	7	1552.4	5.3	2.367	0.003	0	0	0	0	0	0	0	0									
36	8	1553.2	6.6	2.360	0.000	0	1	0	0	0	0	0	0	0.0	16.0	30.7	1123.6	17.4	1.4	0.6		

VDM					Interferer # 3					CODEWORD								ODL				
CH	V #	wavelength (nm)	IL (dBm)	length (m)	rel wrt V8 (m)	tc1	tc2	tc3	tc4	tc5	tc6	tc7	tc8	Offset wrt V8 (cm)	time delay added (cm)	physical length (cm)	measured length of 1X4-ODL (cm)	rel length diff (cm)	off target (cm)	off target wrt -0.6 (cm)		
29	1	1547.6	7.3	3.233	0.013	0	0	0	0	0	0	0	0									
30	2	1548.4	--	--	--	0	0	0	0	0	0	0	0									
31	3	1549.2	6.4	3.241	0.005	1	0	0	0	0	0	0	0	0.5	0.0	31.7	1102.3	0.0	0.0	0.6		
32	4	1550.0	--	--	--	0	0	0	0	0	0	0	0									
33	5	1550.8	6.2	3.243	0.003	0	0	0	0	1	0	0	0	0.3	64.0	86.4	1166.3	64.0	0.0	0.1		
34	6	1551.6	--	--	--	0	0	0	0	0	0	0	0									
35	7	1552.4	6.6	3.179	0.067	0	0	1	0	0	0	0	0	6.7	32.0	61.1	1134.3	32.0	0.0	0.6		
36	8	1553.2	6.9	3.246	0.000	0	1	0	0	0	0	0	0	0.0	16.0	42.7	1117.1	14.8	-1.2	-0.6		

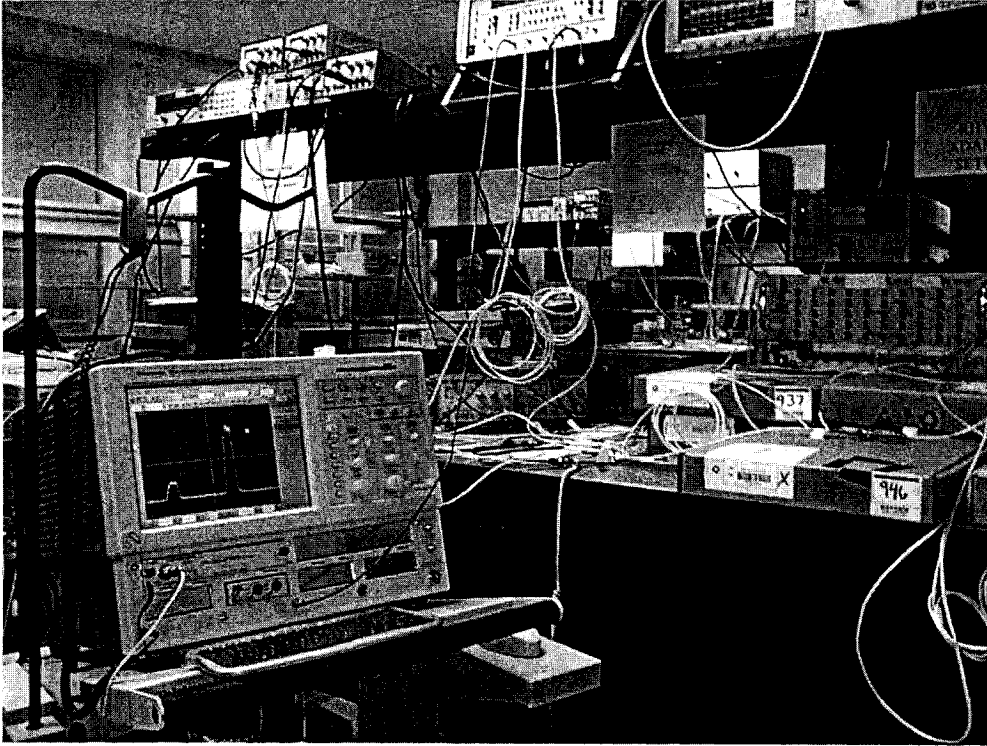
VDM					Desired Encoder					CODEWORD								ODL				
CH	V #	wavelength (nm)	IL (dBm)	length (m)	rel wrt V1 (m)	tc1	tc2	tc3	tc4	tc5	tc6	tc7	tc8	Offset wrt V1 (cm)	time delay added (cm)	physical length (cm)	measured length of 1X4-ODL (cm)	rel length diff (cm)	off target (cm)	off target wrt -0.4 (cm)		
27	1	1547.6	6.1	3.911	0.000	1	0	0	0	0	0	0	0	0.0	0.0	20.0	576.65	0.00	0.0	0.4		
28	2	1548.4	5.6	3.911	0.000	0	0	0	0	0	0	0	0									
29	3	1549.2	4.8	3.909	0.003	0	0	1	0	0	0	0	0	0.3	32.0	52.3	607.97	31.32	-0.7	-0.3		
30	4	1550.0	5.0	3.909	0.002	0	0	0	0	0	0	0	0									
31	5	1550.8	5.2	3.901	0.010	0	0	0	0	0	0	0	0									
32	6	1551.6	5.8	3.909	0.002	0	0	1	0	0	0	0	0	0.2	32.0	52.2	607.85	31.20	-0.9	-0.4		
33	7	1552.4	5.6	3.910	0.001	0	0	1	0	0	0	0	0	0.1	16.0	36.1	592.35	15.70	-0.3	0.1		
34	8	1553.2	5.7	3.911	0.000	0	0	0	0	0	0	0	0									

VDM					Desired Decoder					CODEWORD								ODL				
CH	V #	wavelength (nm)	IL (dBm)	length (m)	rel wrt V6 (m)	tc1	tc2	tc3	tc4	tc5	tc6	tc7	tc8	Offset wrt V6 (cm)	time delay added (cm)	physical length (cm)	measured length of 1X4-ODL (cm)	rel length diff (cm)	off target (cm)	off target wrt -0.4 (cm)	Encoder - Decoder	
27	1	1547.6	5.4	3.569	0.001	1	0	0	0	0	0	0	0	0.1	32.0	52.1	613.7	31.1	-0.9	-0.5	-0.1	
28	2	1548.4	5.5	3.569	0.001	0	0	0	0	0	0	0	0									
29	3	1549.2	5.8	3.562	0.007	0	0	1	0	0	0	0	0	0.7	0.0	22.9	582.6	0.0	0.0	0.4	0.1	
30	4	1550.0	6.4	3.565	0.005	0	0	0	0	0	0	0	0									
31	5	1550.8	5.7	3.572	-0.002	0	0	0	0	0	0	0	0									
32	6	1551.6	6.7	3.570	0.006	0	0	1	0	0	0	0	0	0.0	0.0	20.0	582.8	0.2	0.2	0.6	0.2	
33	7	1552.4	5.2	3.570	0.006	0	0	1	0	0	0	0	0	0.0	16.0	36.0	598.3	15.7	-0.3	0.1	0.2	
34	8	1553.2	5.8	3.573	-0.003	0	0	0	0	0	0	0	0									

## Appendix C: Pictures of the OCDMA setup



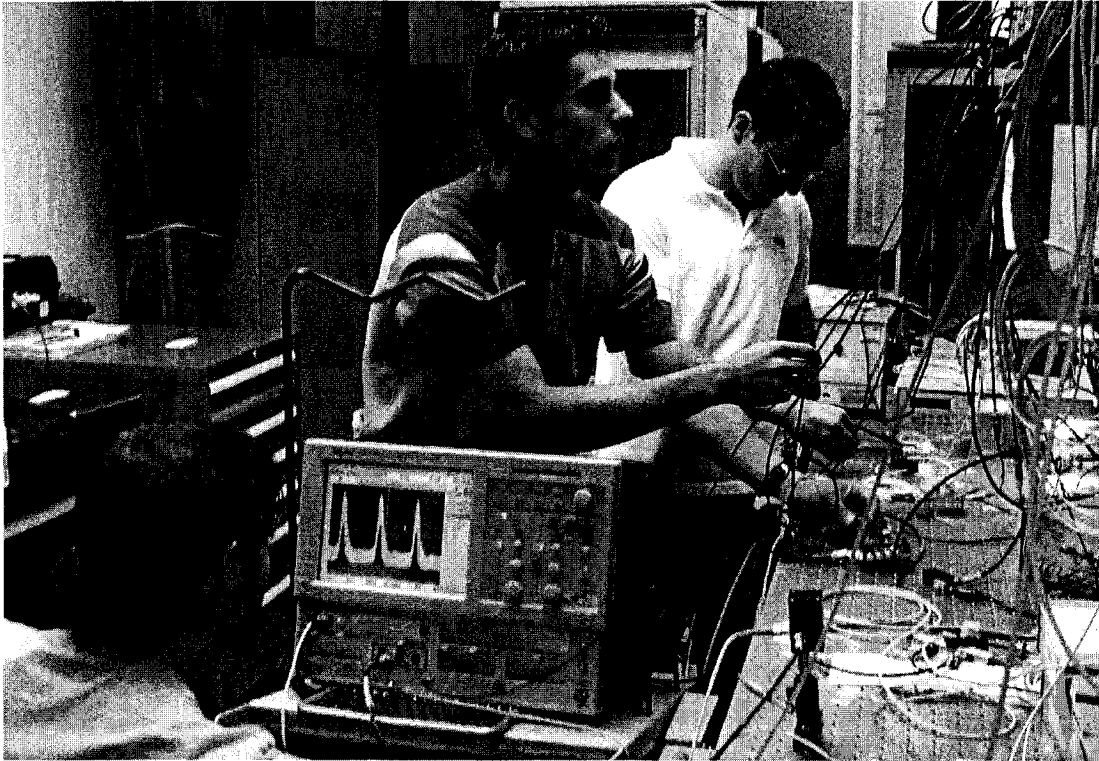
OCDMA demonstration setup



OCDMA demonstration setup



Rhys Adams setting the CSA



**Rhys Adams setting the CSA; Julien Faucher and Paul Kamel setting the OCDMA receiver**

## Appendix D: Publications accepted for conferences

The following are the two publications that have been accepted for conference presentations.

- Rhys Adams and Lawrence R. Chen, “Effects of encoder/decoder mismatch on BER performance for 2-D wavelength-time OCDMA,” Presented at the conference on lasers and electro-optics (CLEO '04), San Francisco, CA, USA, paper CWA13, Wednesday May 19, 2004. [5]
- Rhys Adams and Lawrence R. Chen, “Demonstration of a 4-user 2-D wavelength-time OCDMA system employing depth-first search codes,” Presented at the annual meeting of the IEEE laser and electro-optics society (LEOS '04), San Juan, Puerto Rico, paper TuJ2, Tuesday November 9, 2004. [7]

# Effects of encoder/decoder mismatch on BER performance for 2-D wavelength-time OCDMA

Rhys Adams and Lawrence R. Chen

Photonic Systems Group, Department of Electrical and Computer Engineering, McGill University  
3480 University Street, Montréal, Québec, Canada, H3A 2A7

Tel: +1 514 398 5483, Fax: +1 514 398 5208, E-mail: radams@photonics.ece.mcgill.ca

**Abstract:** We investigate the impact of encoder/decoder mismatch, caused by wavelength and/or time misalignment, on the bit error rate (BER) performance of 2-D wavelength-time OCDMA systems.

©2004 Optical Society of America

OCIS codes: (060.2330) fiber optics communication, (060.4510) optical communications

## 1. Introduction

The BER performance of optical code-division-multiple-access (OCDMA) systems is vital to assess its viability as an optical transport technology [1]. Moreover, system limitations must be determined. Within the context of 2-D wavelength-time ( $\lambda$ - $t$ ) OCDMA, in which each bit is subdivided into time chips and wavelength slots, limitations due to chromatic dispersion have been studied [2]. However, there have been no studies on the limitations imposed by encoder/decoder mismatch. In 2-D  $\lambda$ - $t$  OCDMA, the optically encoded signals comprise pulses at different wavelengths positioned in specific time chips. In the encoding/decoding process, these pulses can extend beyond their desired time chip (time misalignment) and because of laser drift or filter mismatch, the pulses may also exhibit wavelength misalignment. These misalignments impact the desired user signal power, the level of multi-access interference (MAI), and ultimately the BER. In this paper, we examine the impact of wavelength, time, and combined wavelength-time misalignments on BER performance.

We consider the 2-D  $\lambda$ - $t$  codes developed in [3]. Fig. 1 illustrates a typical 2-D code and the possible misalignment scenarios. For example, Fig. 1 (b) shows a code with a time misalignment: the pulse at position  $(\lambda_2, t_4)$  is distributed across time chips 4 and 5.

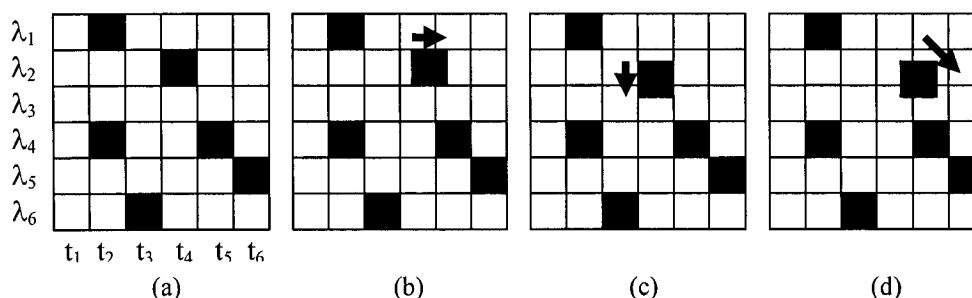


Fig.1. Examples of codes using 6 wavelengths, 6 time chips, and weight 6. (a) Ideal situation, (b) pulse at position  $(\lambda_2, t_4)$  suffers a time misalignment, (c) pulse at position  $(\lambda_2, t_4)$  suffers a wavelength misalignment, (d) pulse at position  $(\lambda_2, t_4)$  suffers from both time and wavelength misalignments.

## 2. Simulations

Each simulation is described by a 3 letter set indicating whether the desired user encoder, interferer encoders, and desired user decoder are perfect (ideal) “P” or imperfect (non-ideal) “I”. For example, “PPP” describes the situation when the three components are perfect, where as “PPI” describes the situation when only the desired user decoder is imperfect.

We assume that the probability distribution of misalignment in wavelength or time is Gaussian with zero mean (i.e. no misalignment) and variances  $\sigma^2 = 0.001, 0.005, 0.01, 0.05,$  or  $0.1$  in units of a time chip or wavelength slot. We use codes with 32 wavelengths, 16 time chips, and weight 6 (yielding a total of 350 codes). For  $K$  active users, BER performance is evaluated [3] and accounts only for MAI. We illustrate our results for  $K = 12$  (1 desired user and 11 interferers). For a given set (e.g. “IPP”) and variance in the misalignment probability distribution, we perform Monte Carlo-type simulations in which all 6 pulses in a

code can exhibit different time and/or wavelength misalignments. 100,000 simulations are performed; in each, 12 of 350 codes are chosen randomly.

### 3. Results

Fig. 2(a) illustrates a typical BER histogram of 100,000 trials for “IPP” with only wavelength misalignment ( $\sigma^2 = 0.05$ ). Fig. 2(b) shows the average BER of the histogram as a function of the variance on the wavelength misalignment distribution. The worst case occurs when only the desired encoder is imperfect (“IPP”), since the desired user signal power is degraded. When only the desired decoder is imperfect (“PPP”), the decrease in desired user signal power is offset by a greater decrease in power from the interferers, thus resulting in a smaller BER penalty. The results for time misalignment are similar.

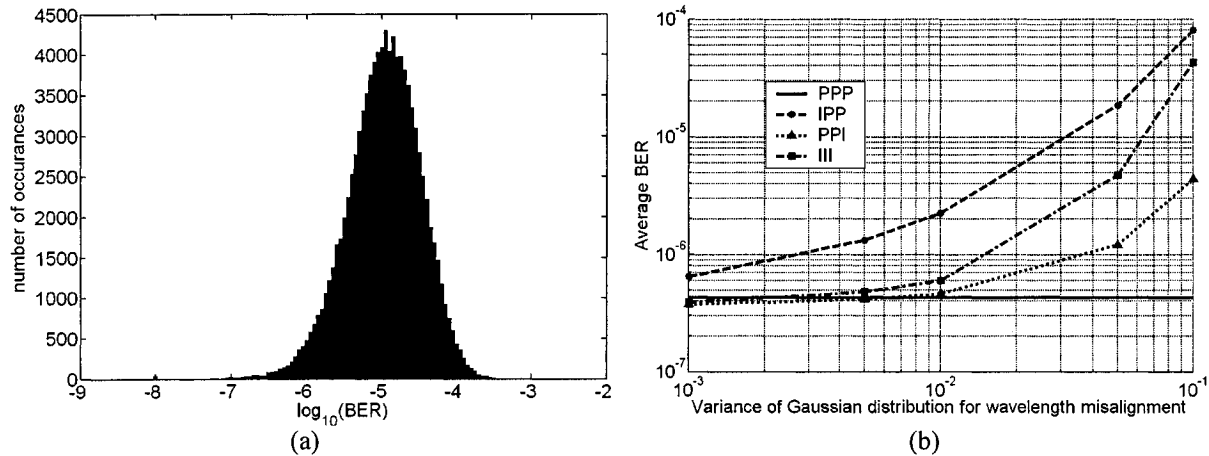


Fig. 2. (a) Histogram of a 100,000 trial IPP simulation with a variance of 0.05 and 12 active users. (b) Average BER of histogram vs. variance of the wavelength misalignment distribution. All sets were simulated, only PPP, IPP, PPI, and III are shown.

We conclude that in order to keep the BER penalty below one order of magnitude, the variance of the wavelength or time misalignment distribution must remain below 0.01. Further results on other sets (i.e. PIP, PII, IIP, and IPI) and combined wavelength/time misalignment will be presented.

### References

- [1] A. Stok and E. H. Sargent, “The role of optical CDMA in access networks,” *IEEE Comm. Mag.*, Sept. 2002, pp.83-87.
- [2] A. Sahin and A. E. Willner, “System limitations due to chromatic dispersion and receiver bandwidth for 2-D time-wavelength OCDMA systems,” in *LEOS 2003*, (IEEE, Tucson, AZ, USA, 2003), pp.551-552.
- [3] R. M. H. Yim, L. R. Chen, and J. Bajcsy, “Design and performance of 2-D codes for wavelength-time optical CDMA,” *Photon. Technol. Lett.*, vol. 14, no. 5, May 2002, pp.714-716.

## Demonstration of a 4-user 2-D wavelength-time OCDMA system employing depth-first search codes

**Rhys Adams and Lawrence R. Chen**

Photonic Systems Group, Department of Electrical and Computer Engineering, McGill University  
3480 University Street, Montréal, Québec, Canada, H3A 2A7

**Abstract:** We present a technology demonstrator for a 4-user 2-D wavelength-time OCDMA system based on depth-first search codes which have previously been shown to be attractive in OCDMA applications.

### 1. Introduction

Optical code-division-multiple-access (OCDMA) is a promising technology for use in local area or access optical networks carrying bursty and asynchronous traffic [1, 2]. Furthermore, 2-D wavelength-time ( $\lambda$ - $t$ ) OCDMA has been explored as a means to improve system performance by reducing the overall code dimension and providing flexibility in code design [1, 2]. Many different 2-D  $\lambda$ - $t$  codes have been proposed and technology demonstrators have been presented [3, 4]. Recently it has been shown that 2-D  $\lambda$ - $t$  depth first search codes (DFSCs) described in [2] provide several key advantages: the codes can be designed using fewer time chips and thus are able to support higher data rates; and since for a given code dimension a greater number of codes can be generated, they can fully exploit the gain provided by forward error correction to allow for a large number of simultaneous users operating with good BER performance [2]. In this paper, we demonstrate successful encoding and decoding of 2-D  $\lambda$ - $t$  DFSCs as well as a successful implementation of a 4-user system.

### 2. Demonstration set-up

The codes are based on 8 wavelengths (1547.6nm – 1553.2nm with 100GHz channel spacing), 8 time chips, and a weight of 4, resulting in 31 possible codes. The four codes used are illustrated in Fig. 1 (a). Users 2-4 are interferers and have been chosen such that they each have 2 wavelengths in common with the desired user (User 1) thereby making the task of identifying the auto-correlation peak more difficult. The data rate is 155.52 Mb/s and the chip rate is 1.244 Gb/s (corresponding to a chip window of 800ps). A block diagram of the set-up is shown in Fig. 1 (b).

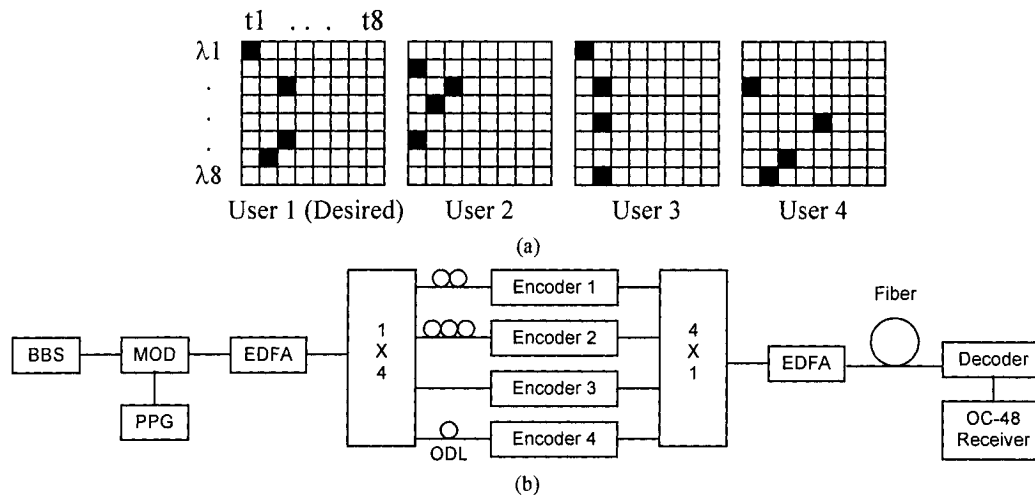


Fig. 1. (a) The four codes used in the demonstration set-up. (b) Block diagram of 4-user demonstration setup. OD L: Optical Delay Line.

An electro-optic modulator (MOD), which is driven by a pulse pattern generator (PPG), generates a pulse at the chip rate from the broadband source (BBS). The pulse is split into four paths of different lengths and encoded by the four encoders before being recombined and propagated through fiber. The decoder performs matched filtering before detection. Erbium doped fiber amplifiers (EDFAs) are used to amplify the signals. The encoders and decoder are constructed using commercially available wavelength multiplexers/demultiplexers, power splitters/combiners, and the time delays are obtained by splicing

appropriate lengths of fiber. Each delay line is carefully measured and has less than  $\pm 5\%$  of a time chip of error in order to minimize the effects of encoder/decoder mismatch [5]. We ensure that all encoded signals are launched with approximately the same power.

### 3. Results

The results of encoding and decoding are shown in Fig. 2. Fig. 2 (a) and (b) illustrates the wavelength characteristics of the 4 codes multiplexed together before and after the decoder, respectively. Fig. 2 (b) confirms that only the 4 wavelengths of the desired user are kept. Note that 2 wavelengths of each of the remaining 3 users are also retained and contribute to the optical power and multi-access interference (MAI). Fig. 2 (c) shows the time characteristics of the 4 codes multiplexed together before the decoder. Fig. 2 (d) confirms that the reconstructed desired signal (auto-correlation peak) is indeed distinguishable from the MAI. The cross-correlation pulses in the decoded waveform correspond to the interfering wavelengths that are picked up by the decoder. The insets of parts (c) and (d) show the results when an arbitrary bit pattern is used rather than a single pulse. Note that the auto-correlation peaks are clearly distinguishable.

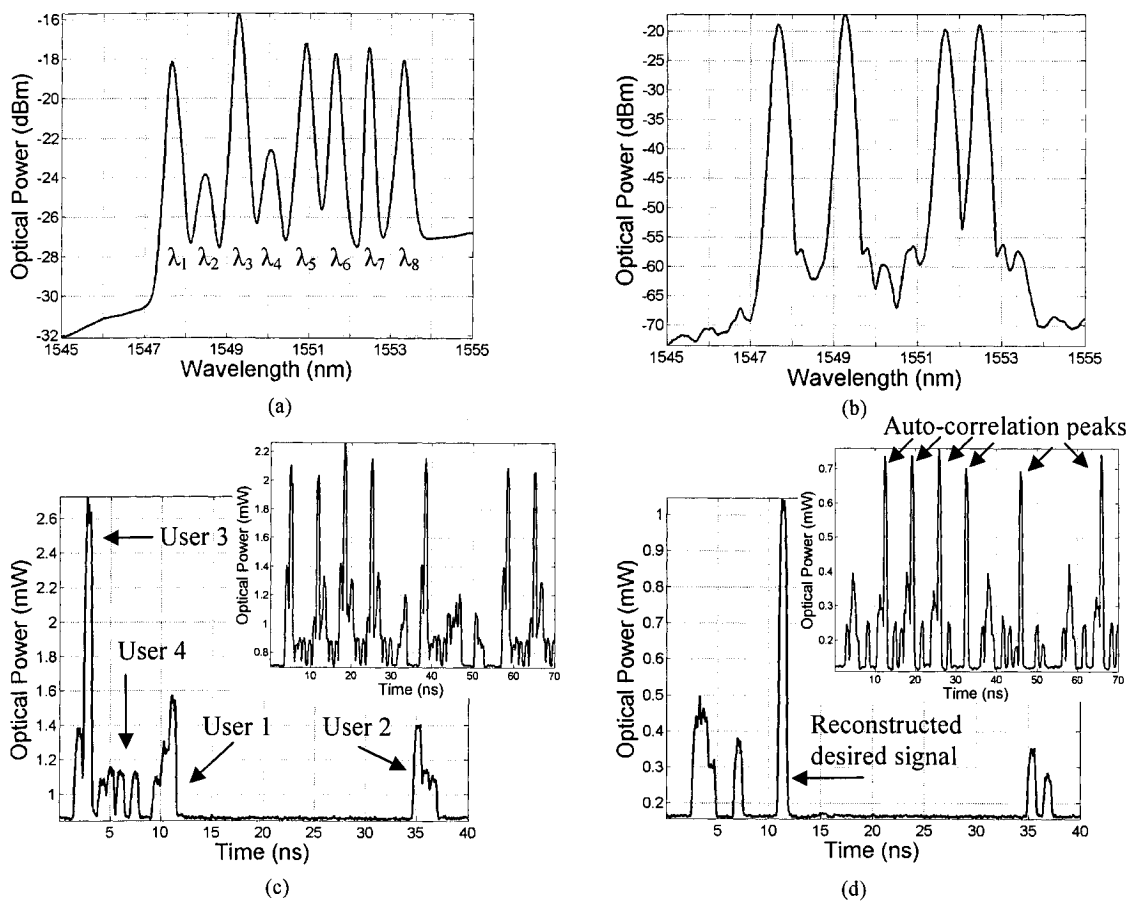


Fig. 2. Wavelength characteristics (a) before and (b) after decoder. Time characteristics (c) before and (d) after decoder.

In summary, we have demonstrated successful encoding and decoding of 2-D  $\lambda$ -t DFSCs and successful implementation of a 4-user system. Given the advantages of the DFSCs used, we believe this should be a promising approach for realizing OCDMA systems.

### References

- [1] A. Stok and E. H. Sargent, IEEE Networks, **14**, pp. 42-46, 2000.
- [2] R. M. H. Yim, L. R. Chen, and J. Bajcsy, Photon. Technol. Lett., **14**, pp. 714-716, 2002.
- [3] A. J. Mendez et al, Conf. Proc. LEOS '03, ThEE3, 2003.
- [4] V. Baby et al, Elec. Lett., **40**, pp.755-756, 2004.
- [5] R. Adams and L. R. Chen, Conf. Proc. CLEO/IQEC '04, CWA13, 2004.